Sub-50 nm Scale to Micrometer Scale Soft Lithographic Patterning of Functional Materials

Antony George

Committee members:

Chairman:

Prof. Paul Kelly (University of Twente)

Promotors:

Prof. J. E. ten Elshof (University of Twente)

Prof. D. H. A. Blank (University of Twente)

Members:

Prof. J. P. H. Benschop (University of Twente)

Prof. R.G.H. Lammertink (University of Twente)

Prof. Y. Lei (University of Münster)

Prof. J. Huskens (University of Twente)

The research work presented in this thesis was carried out in the Inorganic Materials Science group, MESA+ Institute for Nanotechnology, University of Twente, The Netherlands, and was financially supported by the Netherlands Organization for Scientific Research (NWO) and Netherlands Technology Foundation (STW) in the framework of the Innovational Research Incentives (VIDI Scheme, STW project number 07053).

ISBN: 978-90-365-3311-9

Printed by Koninklijke Wöhrmann B.V., Zutphen, the Netherlands

Copyright © Antony George, 2011

SUB-50 nm SCALE TO MICROMETER SCALE SOFT LITHOGRAPHIC PATTERNING OF FUNCTIONAL MATERIALS

DISSERTATION

to obtain
the doctor's degree at the University of Twente,
on the authority of the rector magnificus,
Prof. dr. H. Brinksma,
on the account of the decision of the graduation committee,
to be publicly defended
on Thursday, 15 December 2011 at 16.45 hrs.

by

Antony George

Born on 20th November 1981

in Kaipattoor, India

This dissertation is approved by the promotors
Prof. dr. ir. J.E. ten Elshof
Prof. dr. ing. D.H.A. Blank

TABLE OF CONTENTS

Page

CHAPTER 1
General Introduction

1.1. Introduction to Lithography 1
1.2. Soft Lithography 1
1.3. Scope of the Thesis 3
1.3. References 3

CHAPTER 2
Large area soft lithographic patterning of functional materials on sub-50 nanometer to micrometer length scale by transfer printing of metal-loaded water soluble polymers

2.1. Introduction 5
2.2. Experimental 7
2.3. Results and Discussion 8
2.4. Conclusions 14
2.5. References 14
2.6 Appendix to chapter 2 17

CHAPTER 3
Nanopatterning from the gas phase: High Resolution soft lithographic patterning of organosilane thin films

3.1. Introduction 18
3.2. Experimental 19
3.3. Results and Discussion 20
3.4. Conclusions 22
3.5. References 23

CHAPTER 4
Nanopatterning of functional materials by gas phase pattern deposition of self assembled molecular thin films in combination with electrodeposition

4.1. Introduction 24
4.2. Experimental section 25
4.3. Results and discussion 26
4.4. Conclusions 33
4.5. References 34

CHAPTER 5
Patterning of organosilane molecular thin films from gas phase and its applications: Large area thin molecular templates for site selective material deposition and fabrication of micro and nano scale multifunctional surfaces

5.1. Introduction 35
5.2. Experimental section 37
5.3. Results and Discussion 38
5.4. Conclusions 46
5.5. References 46

CHAPTER 6
Patterning functional materials using channel diffused plasma-etched self-assembled monolayer templates

6.1. Introduction 48
6.2. Experimental 49
6.3. Results and Discussion 51
6.4. Conclusions 57
6.5. References 58

CHAPTER 7
Micro- and nanopatterning of functional materials on flexible plastic substrates via site-selective surface modification using oxygen plasma
7.1 Introduction 60
7.2 Experimental 61
7.3 Results and Discussion 63
7.4. Conclusions 68
7.5. References 69

CHAPTER 8
Electrodeposition in capillaries: Bottom-up micro and nanopatterning of functional materials on conductive substrates
8.1. Introduction 71
8.2. Experimental 72
8.3. Results and Discussion 73
8.4. Conclusions 79
8.5. References 79
8.6. Appendix to Chapter 8 81

CHAPTER 9
General Conclusions 82

Samenvatting (summary in Dutch) 84

Acknowledgements 85

Chapter 1

General Introduction

1.1 Introduction to lithography

Patterning of functional materials such as metals, polymers, nanoparticles, biomaterials, semiconductors, etc. on the micro and nanometer scale with control over size, shape and position is a necessity to fabricate any type of device, e.g. computers, electronic equipment, sensors and data storage devices. For instance, to enable the fabrication of a simple electronic device, many components like interconnects, transistors, resistors, etc., which are made of various functional materials, have to be arranged in predetermined positions with precise control over quality, size shape and geometry. In simple words, lithography can be defined as “arranging materials on specific predetermined areas of a surface of interest”.

Traditionally, photolithography is used to enable fabrication of device structures. In photolithography light illuminates predetermined areas on a photosensitive polymer (photoresist) through a photomask that obstructs light to hit certain other predetermined areas [1]. Upon exposure to light the photoresist changes its properties, and is later developed in a developer solution to remove the exposed or non-exposed regions of the photoresist, depending on the type of photoresist used [1]. These photoresist structures have been used as templates for material deposition, etching and ion implantation processes to obtain the final device structures. Usually multiple photolithographic steps are used to enable complete device fabrication. Photolithography is the backbone of the all present device fabrication methods.

However, a trend for past 30 years in technology is the miniaturization of components used for fabrication of devices. Miniaturization helps to make smarter, lighter and faster devices in a cost-effective way. Miniaturization of functional materials can also be used to introduce novel interesting properties of materials due to the effect of size confinement on the nanometer scale [2]. These new/enhanced optical, mechanical, electronic and electrical properties open up more possibilities to use these functional materials, adding newer possible fields of application for these materials.

The resolution of photolithography is limited by the wavelength of the light used for patterning the photoresist. Patterning high resolution features of different functional materials on sub-micrometer length scales is difficult to achieve with conventional photolithography. Modified processes such as extreme UV light lithography [3] or laser interference lithography [4] have been introduced to overcome this problem. However, these technologies are expensive due to the use of complex equipment. Also the possibilities of functional materials and geometrical shapes are limited.

Other lithographic processes such as electron beam lithography (EBL) [5], focused ion beam lithography (FIB) [6] and scanning probe lithographic methods [7] are also widely used in research for fabricating high resolution features with high precision. In EBL processes a focused electron beam is used to write on an electron beam resist, typically PMMA. Later the resist is developed in a developer solution. Subsequent metal deposition or etching and resist stripping is performed to obtain the final pattern [5]. In the case of FIB, a focused ion beam of Gallium ions is used to directly mill the surfaces to be patterned [6]. In scanning probe lithographic methods an AFM tip is used as a pen to transfer molecular inks to the surface of interest [7]. Another approach is to use mechanical scratching to produce patterns on the surfaces of interest [7]. However these methods are serial in nature and slow, so that they can be used only in research as prototyping tools. Industrial use of these methods is not feasible.

1.2. Soft Lithography

In 1993, the Whitesides research group at Harvard University introduced a novel approach to pattern functional materials using a micropatterned polydimethylsiloxane (PDMS) mold [9]. The micropatterned PDMS mold or stamp inked with an alkanethiol ink is brought into conformal contact

with a gold surface. The alkanethiol molecules are transferred from the PDMS stamp to form a self-assembled monolayer (SAM) of alkanethiol molecules on the areas where the PDMS stamp contacts the substrate. This first process demonstrated in literature is known as microcontact printing. Afterwards many interesting variations of soft lithographic processes have been introduced, including micromolding in capillaries [10, 11, 12], microtransfer molding [11] and micromolding [12]. Due to the softness of the PDMS stamp, the method is called soft lithography. The method attracted considerable research interest due to the simplicity of the approach and its cost-effectiveness. Soft lithographic methods are parallel methods, so that large areas can be patterned in a relatively short time. It also avoids the use of complex processing equipment and multiple processing steps including resist patterning, development, etching, etc. Most of the soft lithographic processes are single step processes. Another major advantage of soft lithography is the patterning possibility of the functional materials directly on the substrates, where as other lithographic processes use multiple steps of resist patterning, deposition and etching.

Soft lithographic processes can be classified into two main categories, namely surface modification based methodologies and molding methodologies. A schematic diagram illustrating the main soft lithographic processes is shown in figure 1. In surface modification approaches an organic molecule is used to generate locally another chemistry on the surface, so that the chemical contrast can be used for area-selective binding of functional materials such as nanoparticles, polymers, biomaterials and molecules. Typically microcontact printing (D) of functional alkanethiols or organosilane molecules is used to create a chemical contrast on metallic or silicon/oxide surfaces [9, 11, 12, 13]. In molding-based approaches, the PDMS mold/stamp is used as mold to pattern typically sol-gels or polymeric precursors. In micro transfer molding (A) the precursor solution is applied on the PDMS mold first and then transferred to a receiving substrate [11, 12]. In micromolding process (B), first the precursor is applied onto the substrate to be patterned, and then the stamp is pressed on the substrate to mold the precursor [11, 12]. After solidification of the precursors by solvent drying, the mold is removed from the substrate. In the case of MIMIC (C), first a conformal contact is made between the substrate and the mold, and then the precursor is applied to the side openings of the channels formed between the substrate and the mold. The mold is then filled with the precursor by capillary force, dried inside by solvent evaporation through the PDMS mold/through the openings of the channels, after which the stamp is removed [10, 11, 12]. In the case of sol-gel precursors the substrates were heat-treated to obtain the final material pattern [14, 15].

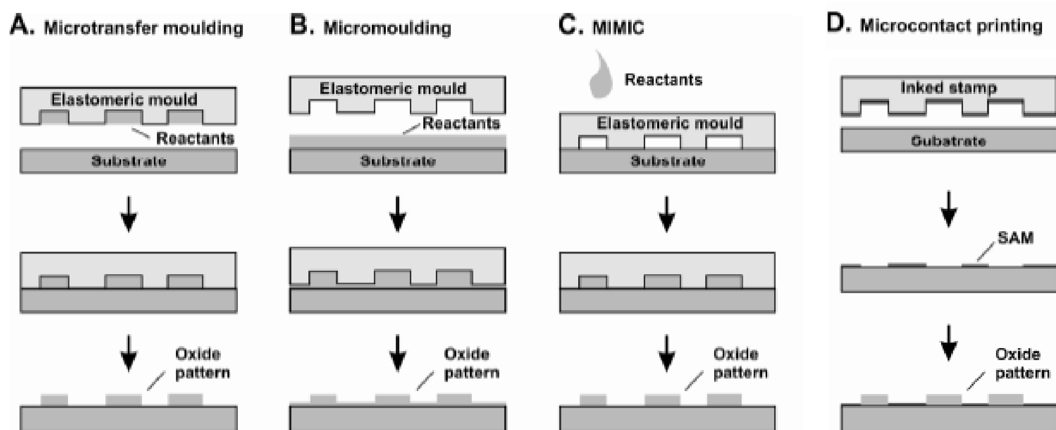

Figure 1: Schematic illustration of soft lithographic processes: a) Micro transfer molding, b) micromolding, c) Micromolding in capillaries (MIMIC), d) microcontact printing.

However the applicability of soft lithography on submicron length scale, and especially in the sub-100 nm scale remains challenging. In the case of micro contact printing, problems of ink diffusion may occur when stamp dimensions go down to the nanometer scale. This limits the lateral resolution of the dimensions of the pattern [16]. Micromolding processes require application of relatively large

pressure on the PDMS mold to avoid the formation of a thick residual layer between the patterned features. This may cause deformation or buckling of the PDMS mold, resulting in loss of pattern fidelity and limiting the use of this technique on sub micrometer dimensions. In the case of MIMIC processes the diffusion length of the precursor inside nanometer scale channels is limited due to the high viscosity of sol gel precursors.

1.3. Scope of the PhD thesis

This PhD thesis addresses two major issues:

1) Fabricating nanometer-scale patterns of functional materials,
2) Extending the applicability of soft lithographic processes to a wide range of functional materials on conventional silicon substrates and flexible plastic substrates.

This thesis describes novel soft lithographic processes, with which it is possible to fabricate sub-50 nanometer to micrometer length scale patterns of a wide range of functional materials, including metals, nanoparticles, organosilane molecules, nanowires, semiconducting materials and conducting polymers on silicon and flexible plastic substrates.

Chapter 2 describes the patterning of oxide materials in sub-50 nm scale to micrometer scale using transfer printing metal loaded water soluble polymers. The process is a simple and low cost approach to pattern a wide range of oxide materials on the sub -100 nanometer scale that have potential applications in the fabrication of device structures.

Chapter 3 introduces a method to pattern organosilane molecules on silicon substrates on the nanometer and micrometer scale. The process is a time-controlled approach which uses the phenomena of geometry dominated condensation of organosilane molecules from a vapor phase to generate high-resolution patterns. PDMS stamps of large dimensions can be used to fabricate patterns of much smaller dimensions.

Chapter 4 extends the application possibility of the process described in the previous chapter to pattern inorganic functional materials on the nanometer to micrometer scale. The chapter shows that the gas phase pattern deposition of organosilane molecules is fully controllable. Also self-assembled molecular thin films of mercaptosilane molecules were used as thin resists for the electrodeposition of metallic and semiconducting materials.

Chapter 5 further extends the application range of the process described in **chapter 3**. Sequential deposition of different organosilane molecules on silicon substrate is used to fabricate substrates with multiple chemical functionalities. Multifunctional multi-length scale surfaces have been realized on the micrometer and nanometer scale. The potential application of organosilane patterns as resists for atomic layer deposition (ALD) and as template for site-selective adsorption of nanoparticles has been demonstrated.

Chapter 6 describes a novel process to pattern octadecanethiol (ODT) SAMs on gold substrate by channel diffused plasma etching. The patterned SAMs were used as templates for electrodeposition, electroless deposition and solution phase deposition of a wide range of functional materials (Ni, Ag, ZnO, and ZnO nanowires) on the nanometer and micrometer scale.

Chapter 7 describes the potential application of channel diffused plasma surface modification of plastic substrates like polycarbonate (PC), PDMS and polyethylene terephthalate (PET) to create a hydrophilic-hydrophobic contrast on these surfaces. After surface modification, subsequent material deposition processes such as electroless deposition, solution phase deposition, site selective de-wetting and site selective adsorption were used to obtain patterns of functional materials such as ZnO, ZnO nanowires, Ag , TiO_2, conducting polymer (PEDOT:PSS) and Ag nanoparticles

Chapter 8 describes a novel process of electrodeposition in capillaries. The process enables bottom-up micro and nano patterning of metallic and semiconducting materials by electrodeposition of an electrolyte solution inside PDMS capillaries in contact with a substrate.

The thesis closes with conclusions and outlook in **chapter 9**.

1.4. References:

1. http://www.ece.gatech.edu/research/labs/vc/theory/photolith.html
2. http://en.wikipedia.org/wiki/Nanotechnology
3. Totzeck, M.; Ulrich, W.; Gohnermeier, A.; Kaiser, W., Semiconductor fabrication: Pushing deep ultraviolet lithography to its limits. *Nat Photon* **2007,** *1* (11), 629-631.
4. Hecht, J., Extreme-UV lithography struggles to shrink chip features. *Laser Focus World* **2009,** *45* (6), 64.
5. de Boor, J.; Geyer, N.; Wittemann, J. V.; Gosele, U.; Schmidt, V., Sub-100 nm silicon nanowires by laser interference lithography and metal-assisted etching. *Nanotechnology* **2010,** *21* (9), 095302.
6. Grigorescu, A. E.; Hagen, C. W., Resists for sub-20-nm electron beam lithography with a focus on HSQ: state of the art. *Nanotechnology* **2009,** *20* (29), 292001.
7. Matsui, S.; Ochiai, Y., Focused ion beam applications to solid state devices. *Nanotechnology* **1996,** *7* (3), 247-258.
8. Garcia, R.; Martinez, R. V.; Martinez, J., Nano-chemistry and scanning probe nanolithographies. *Chemical Society Reviews* **2006,** *35* (1), 29-38.
9. Kumar, A.; Whitesides, G. M., FEATURES OF GOLD HAVING MICROMETER TO CENTIMETER DIMENSIONS CAN BE FORMED THROUGH A COMBINATION OF STAMPING WITH AN ELASTOMERIC STAMP AND AN ALKANETHIOL INK FOLLOWED BY CHEMICAL ETCHING. *Applied Physics Letters* **1993,** *63* (14), 2002-2004.
10. Kim, E.; Xia, Y.; Whitesides, G. M., Micromolding in Capillaries: Applications in Materials Science. *Journal of the American Chemical Society* **1996,** *118* (24), 5722-5731.
11. Xia, Y. N.; Whitesides, G. M., Soft lithography. *Annual Review of Materials Science* **1998,** *28*, 153-184.
12. Xia, Y. N.; Whitesides, G. M., Soft lithography. *Angewandte Chemie-International Edition* **1998,** *37* (5), 551-575.
13. Onclin, S.; Ravoo, B. J.; Reinhoudt, D. N., Engineering Silicon Oxide Surfaces Using Self-Assembled Monolayers. *Angewandte Chemie International Edition* **2005**, 44, (39), 6282-6304.
14. Göbel, O. F.; Nedelcu, M.; Steiner, U., Soft Lithography of Ceramic Patterns. *Advanced Functional Materials* **2007,** *17* (7), 1131-1136.
15. ten Elshof, J. E.; Khan, S. U.; Göbel, O. F., Micrometer and nanometer-scale parallel patterning of ceramic and organic–inorganic hybrid materials. *Journal of the European Ceramic Society* **2010,** *30* (7), 1555-1577.
16. Jeon, N. L.; Finnie, K.; Branshaw, K.; Nuzzo, R. G., Structure and Stability of Patterned Self-Assembled Films of Octadecyltrichlorosilane Formed by Contact Printing. *Langmuir* **1997**, 13, (13), 3382-3391.

Chapter 2

Sub-50 nm to Micrometer Scale Patterning of Functional Materials by Transfer Printing of Water Soluble Polymers

* A shortened version of this chapter is submitted to an international journal

Abstract:

A fast, versatile and reproducible method to make arbitrary nanoscale patterns of functional metal oxides by edge transfer printing of aqueous metal-loaded water-soluble polyacrylic acid (PAA) solutions on silicon is reported. Patterns of ZnO, CuO, NiO and Fe_2O_3 with lateral dimensions below 50 nm were realized. The process uses elastomeric PDMS stamps with microscale feature sizes to fabricate nanoscale patterns, so that stamp deformation problems are minimized despite the high resolution. The edge transfer mechanism is attributed to an interplay between the adhesion strengths of the SiO_2-PAA and PDMS-PAA interfaces, the cohesive strength of the PAA film, and the fact that the stress build-up at the corners of the stamp is higher than at the central areas under the stamp.

2.1. Introduction:

Patterning of functional materials such as nanoparticles, functional oxides, nanoparticle polymer composites, etc. are very important in materials science to understand the properties of materials at different length scales, and to realize micro and nano-scale devices by novel fabrication technologies. Functional patterns can be applied in the fabrication of electronic [1,2], optoelectronic [3], data storage [4] and sensing devices [5], to name a few. Large area, cost-effective fabrication of high quality functional oxide patterns with sub-micrometer resolution is a challenging issue in nanofabrication.

Several methods have demonstrated to generate functional material patterns, such as electron beam lithography [5,6], nanoimprint lithography [7,8], photolithography [9] and soft lithographic techniques such as microcontact printing [10], micromoulding in capillaries (MIMIC) [11], microtransfer moulding [12,13] and nanotransfer printing [14],. Among these technologies the soft lithographic methods that employ an elastomeric polydimethylsiloxane (PDMS) stamp or mold for pattern replication attracted wide research interest due to its technical simplicity, cost effectiveness and flexibility. However, patterning at the nanometer scale, especially below 100 nm length scale, remains a challenge. In the capillary molding processes such as MIMIC, the friction exerted by the capillary walls and the high viscosity of the sol-gel or polymeric precursors prevents their flow in nanometer-scale patterned PDMS molds.

On the other hand, molding processes require application of relatively high pressures on the PDMS stamps to avoid the formation of a thick residual layer [13]. This may cause stamp deformation or buckling of the PDMS stamp, resulting in the loss of fidelity of the patterns [15,16,17] and limiting the use of this technique in sub-micrometer length scales. Stiffer molds may be employed, but results in residual layers[16,17]. Electron beam and ion beam lithography can be used for resolution patterning down to sub-10 nm, but the costs of investment and exploitation, and the long processing times are still a serious limitation. To overcome these, innovative novel techniques utilizing the edge of patterned PDMS stamps or the edge of patterned photoresist structures, such as edge transfer lithography,[18] electrochemical edge decoration[19,20,21] and gas phase pattern deposition[21] have been developed to overcome this problem and pattern materials on nanometer scale. In edge contact

printing,[18] self-assembling organic molecules such as octadecanethiol (ODT) are selectively deposited on the side walls of a micropatterned PDMS stamp and transfer printed to a gold surface.[17] In electrochemical edge decoration,[19,20,21] patterned photoresist structures on metallic thin films were first used as etch resist and subsequently used as template for electrodeposition at the edges. A wide range of functional materials could be made. In the gas phase edge pattern process that we proposed recently, organosilane molecules are condensed preferentially in the corners between the protruding parts of the patterned PDMS mold, and the substrate with which it is in conformal contact.[22] This yields organosilane nanopatterns with lateral resolutions that are much smaller than the original dimensions of the PDMS mold used. The advantage of all these techniques is that they employ micrometer scale patterning techniques to achieve a final pattern with higher resolution than the features of the molds or the photoresists.

Here we report a novel, simple, inexpensive, fast and reproducible method to realize sub-50 nanometer scale to micrometer scale patterning of functional metal oxides, i.e. ZnO, CuO, Fe_2O_3 and NiO, by a number of modes of transfer printing of water soluble polymers. The process uses elastomeric PDMS stamps with large feature sizes to fabricate high-fidelity patterns of much smaller dimensions. The process is residual layer-free without application of high pressure on the PDMS stamp. A schematic diagram of the patterning process is shown in Figure 1. First, an aqueous solution of a water-soluble polymer was spincoated onto an oxygen plasma-treated PDMS stamp [23] to obtain a thin film of the polymer on the substrate. Then PDMS stamp was placed on a Si substrate to make conformal contact, and kept on a hot plate heated to 80°C for 10 min. Then the substrate-stamp assembly was cooled down to room temperature before peeling off the PDMS stamp from the substrate. Depending on the polymer used or the additive metal salt used, three different modes of pattern transfer were observed as explained schematically in Figure 1.

When a high molecular weight (M_w=27000 g/mol) polyvinyl alcohol (PVA) was used then cohesive failure of the PDMS stamp occurred and a pattern containing PVA film and protruding parts of the PDMS stamp transferred to the substrate. When a low molecular weight polyacrylic acic (PAA) or PAA mixed with metal salts of different concentration was used, film transfer only occurred at the edges of the protruding features of the PDMS stamp. When PVA loaded with metal salts was used, complete film transfer from the protruding features of the PDMS stamp was observed, without rupture of the protruding parts of the PDMS stamp.

The edge transfer mechanism of PAA thin films from the PDMS stamp was exploited to create sub-50 nm material patterns of functional oxides. The transfer mechanism of PVA-metal salt complex films was used to pattern micrometer-scale particle arrays of materials with similar stamps. Our method provides a simple and cost-effective way to fabricate nanometer- to micrometer-scale patterns using micrometer scale PDMS stamps, and it avoids the technological issue of buckling or mechanical failure of stamps in conventional soft lithographic processes. And as shown below, the method is applicable to most oxides.

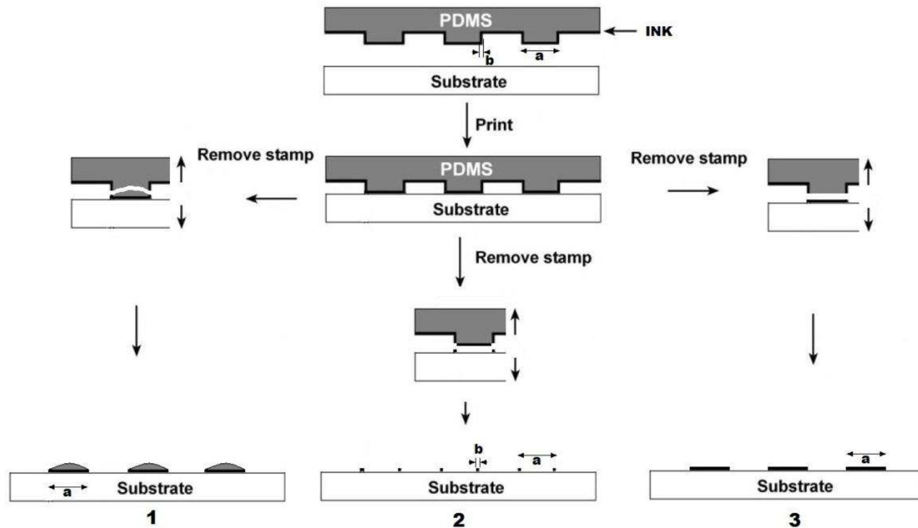

Figure 1: Schematic diagram of patterning process 1) PDMS cohesive failure when using PVA film. 2) Edge transfer printing when using PAA film. 3) Complete transfer printing when using PVA-metal salt complex film

2.2. Experimental

Preparation of PDMS stamps: PDMS and curing agent (Sylgard 184) were purchased from Dow Corning Corporation and mixed in a ratio 10:1 and poured over the micro/nano-patterned silicon master (created by photolithography or e-beam lithography). The PDMS was cured at a temperature of 70°C for 48 h. After curing, the PDMS stamps were removed from the master and cut into pieces of desired size prior to use. The PDMS stamps were treated with oxygen plasma at 24 watts (Harrick Plasma) for 30 s to 2 min to increase the surface energy of PDMS and promote its wetting by the water-soluble polymers during the spin coating process.

Preparation of substrates: p-Type silicon substrates were cleaned with piranha solution (a mixture of H_2O_2 and H_2SO_4 in 1:3 volume ratio). The substrates were washed several times with de-ionized water after piranha cleaning and stored in de-ionized water. Prior to use, the substrates were taken out from de-ionized water and blow-dried in a nitrogen stream.

Materials: Zinc nitrate hexahydrate ($Zn(NO_3)_2{\cdot}6H_2O$, 98% purity), gold(III) chloride trihydrate ($HAuCl_4$, 99.9% purity), copper (II) nitrate ($Cu(NO_3)_2$, 99.9% purity) and iron(III)nitrate nonahydrate ($Fe(NO_3)_3{\cdot}9H_2O$, 98% purity) and polyvinyl alcohol (M_w 27000 g/mol, 98% purity) were purchased from Sigma Aldrich. Anhydrous iron (III) chloride ($FeCl_3$, 97% purity) was obtained from Fluka. Poly acrylic acid (M_w 1800 g/mol) was obtained from Aldrich.

Pattern Fabrication

PVA and PAA solutions with different concentrations (0.5, 0.75, 1, 1.5 and 3 wt%) were made in de-ionized water. The solution was spincoated onto the PDMS stamps at 3000 to 5000 rpm. After spin coating the polymer films were allowed to dry for 5 minutes at room temperature. Multiple coatings were applied to make thicker polymer films, with intermediate drying at room temperature before each next coating. The PDMS stamps were then carefully placed over the substrates manually and pressed with slight tapping with tweezers. The substrates were dried at 80°C for 5 min on a hot plate and peeled off from the substrate to obtain a pattern of the water-soluble polymer.

Metal salts of various concentrations (0.1 to 3 wt %) were mixed with PVA and PAA solutions and transfer printed as described above. After patterning the polymer film, the substrates were heat-treated at 620 ^{o}C to remove the polymers and obtain the metal oxide patterns.

Solution phase growth ZnO nanowires: ZnO nanowires were grown on edge transfer printed ZnO-patterned substrates. $Zn(NO)_3{\cdot}6H_2O$ (0.15 g) and hexamethylenetetramine (0.07 g; HMTA, Fluka, purity 99.5%) were mixed in 100 ml water. The solution was heated to 70-85 °C. The substrates were

then placed floating upside down on the surface of the ZnO precursor solution. ZnO nanowires were grown for 2 to 15 h, depending on the desired length of the nanowires.

Characterization: Patterns of polymers and oxides were imaged using high resolution scanning electron microscopy (HR-SEM, Zeiss 1550). Atomic Force Microscopy (AFM; Veeco Dimension Icon) was used to determine the surface morphology. Tunneling current AFM (TUNA) was used to map the conductivity of patterned surfaces [37]. X-ray diffraction (XRD, Philips diffractometer PW 3020, Software X'Pert Data Collector 2.0e, Panalytical B.V., Almelo, The Netherlands) was used for phase determination of the patterns.

2.3. Results and discussion

Figure 2a illustrates the type of patterns on silicon that are obtained when a PVA solution of high molecular weight (M_w ~ 27 kg/mol; 3 wt% in water) was used as transferrable ink. Figure 2b shows a similar image, and the corresponding AFM height profile of patterns from a 3wt % PVA solution to which 3 wt% $FeCl_3$ had been added. Both solutions were spin coated at 4000 rpm for 2 min, and dried at 80^oC for 10 min on patterns PDMS stamps. This yielded 80 nm thick films on PDMS, which were then transferred to the Si substrate after drying and peeling off. The height profile in Figure 2a shows high aspect ratio features with a height of 350 nm, much more the thickness of the spincoated film. The structures are therefore torn-off protruding parts of the micropatterned PDMS stamp. Figures 2c and 2d show height profiles of PDMS stamps before and after the PVA printing process. Figure 2c shows a profile with a flat top surface, as expected for PVA- thin film coated PDMS stamp. The shape of the profile in Figure 2d confirms the cohesive failure in the protruding parts of the PDMS stamp after PVA transfer.

The AFM image and height profile of patterns of $FeCl_3$-loaded PVA on silicon in Figure 2b indicate much thinner structures than in Figure 2a. Apparently, cohesive failure of PDMS did not take place and only transfer of the metal salt incorporated PVA film from protruding features of the PDMS stamp in conformal contact with the substrate occurred.

Figure 3a and 3b show HR-SEM images of PAA patterns that were transfer-printed onto Si substrates in a similar way. But in this case, film transfer occurred only at the edges of the protruding features of the PDMS stamp. The thin lines in Figure 3a were patterned with a PDMS stamp with 600 nm wide line features with a spacing of 800 nm. The edge-transferred line features have a line width of 300 nm. Figure 3b shows edge-transferred PAA line features with a line width and spacing of 4 μm. The transfer printed features in both figures have a line width of 85 nm. The width of the features obtained corresponds to the thickness of the PAA thin film that was coated on the PDMS stamp. Metal salt-incorporated PAA films show the same patterning behavior as pure PAA films.

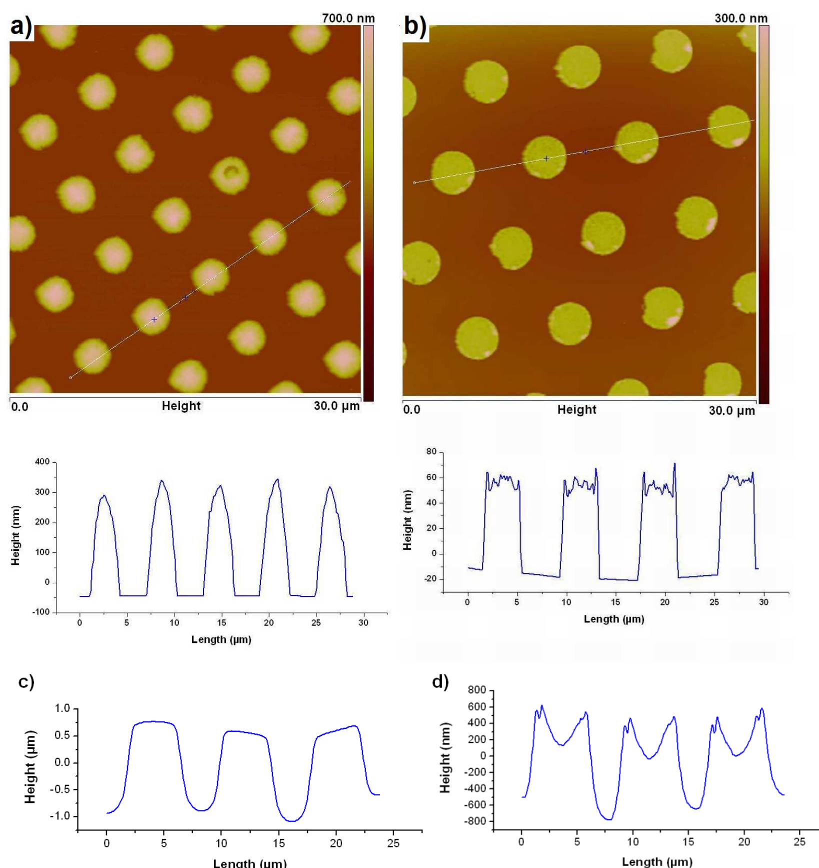

Figure 2: a) PVA dot patterns by transfer printing from 3 wt% PVA solution. b) PVA-metal salt dot pattern by transfer printing 3 wt% PVA – 3 wt% $FeCl_3$ solution. c) AFM height profile of PDMS stamp coated with PVA thin film. d) AFM height profile of PDMS stamp after the printing process. The shape of the profiles in the protruding parts of the stamp illustrates the ruptured PDMS parts that transferred to the substrate together with the PVA film.

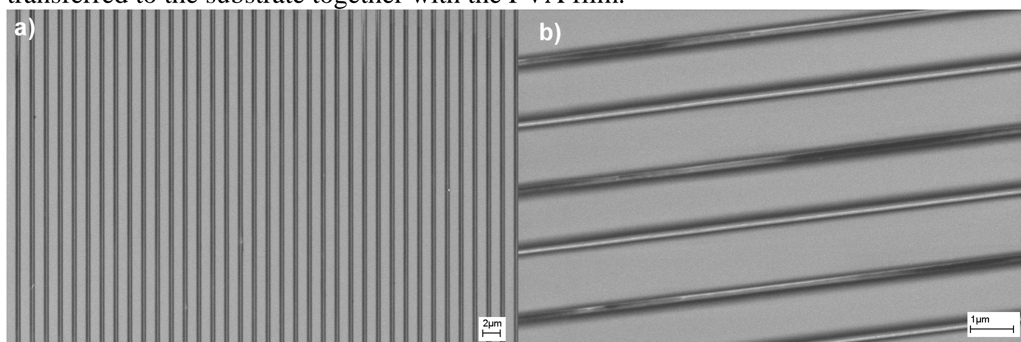

Figure 3: HR-SEM images of edge transfer printed PAA patterns a) patterns with 300 nm line width and spacing of 600 nm b) Line pattern with 100 nm line widths and spacing of 1 µm.

The difference in pattern transfer between PVA film, metal salt-incorporated PVA film, and PAA(-metal salt) solutions is attributed to differences in the cohesive strength of the different polymers or polymer-metal salt complex solutions, and to differences in adhesion strength between substrate surface and polymer/polymer-metal salt solutions. Since we used high molecular weight PVA with M_w ~27 kg/mol, and low molecular weight PAA with M_w ~1.8 kg/mol, the cohesive strength of the PVA (τ_{PVA}) thin film will be much higher than the cohesive strength of the PAA (τ_{PAA}) thin films.

We performed a lap shear test to obtain average values of the adhesion force between the dried water-soluble polymers (PVA and PAA), and the participating surfaces, i.e. SiO_2 and oxygen plasma treated PDMS. A schematic configuration of the test specimens used in the lap shear test is shown in Figure 4. We prepared glass-PVA/PAA-glass and PDMS-PVA/PAA-PDMS test specimens with similar dimensions and polymer film thicknesses. The lap shear strength (τ) of the adhesive joint is given by the formula

$$\tau = P/bL, \quad (1)$$

where P is the maximum failure load, b the joint width and L the joint length.

In the test, it was observed that the adhesion strength between PVA and both PDMS and glass was high enough to break the glass slides or PDMS blocks used in the experiments. Adhesive failure, i.e. separation of the glass or PDMS slides from the PVA film was never observed. This indicates that the PVA film acts as a strong glue between PDMS and substrate after the printing and drying processes, possibly due to strong hydrogen bonds between OH groups from PVA and surface -OH groups on SiO_2 and oxidized PDMS. The high cohesive strength of PVA (τ_{PVA}), which due to its high molecular weight, also contributed to this phenomenon. Since PDMS is the weakest material in the Si substrate-PVA-PDMS stamp configuration, cohesive failure of the protruding features of the PDMS stamp occurred when PVA was used as transferrable ink.

Adhesive failure was observed during the lap shear test when using PAA between glass slides or PDMS blocks. Interestingly, we observed that the adhesion force between PAA and the PDMS surface ($\tau_{PDMS\text{-}PAA}$) is three times higher than the adhesion force between PAA and glass surface ($\tau_{Si\text{-}PAA}$). This provides an explanation of the edge transfer mechanism of PAA thin films that we observed. Due to the low molecular weight of PAA, its cohesive strength (τ_{PAA}) is lower than the adhesion forces at the PAA - silicon ($\tau_{Si\text{-}PAA}$) and PAA-PDMS ($\tau_{PDMS\text{-}PAA}$) interfaces. And since $\tau_{Si\text{-}PAA}$ is three times smaller than $\tau_{Si\text{-}PDMS}$, adhesion was lost occurred at the Si-PAA interface. However, because the cohesive strength of PAA (τ_{PAA}) is very low compared to the adhesive strength at the Si-PAA interface ($\tau_{Si\text{-}PAA}$), cohesive failure of PAA thin film occurred at the weak parts of the PAA film, namely at the edges which were not connected directly to the PDMS stamp.

In contrast to the results with PAA, the combination of PVA with metal salts such as $FeCl_3$ and $HAuCl_4$ resulted in complete film transfer from the protruding features of the PDMS stamp without breaking the PDMS stamp. The most likely explanation for his is the association of metal cations to the hydroxyl groups of PVA. The number of available free hydroxyl groups for hydrogen bond formation with surface hydroxyl groups was strongly reduced. This reduced the cohesive strength of the PVA films, as well as the adhesion forces between the PVA - PDMS and PVA - Si substrate interfaces. To test this hypothesis several experiments were done with varying metal salt concentrations in an aqueus 3 wt% PVA solution. Film transfer occurred in a similar way as with pure PVA thin films at metal salt concentrations up to 0.6 wt%, i.e. the PVA films were transferred together with part of the protruding features of the PDMS stamp. The best results were obtained with a solution of 3 wt% PVA with 3 wt% metal salt.

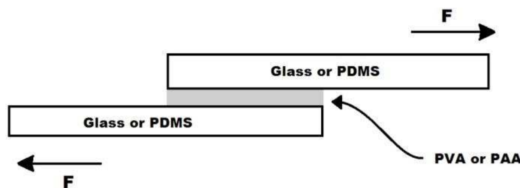

Figure 4: Schematic configuration of the test specimens used for the lap shear test to determine approximate values of adhesion forces between water soluble polymers and participating substrates.

Figure 5a shows ZnO line patterns fabricated by edge transfer printing of PAA-zinc nitrate complex (1.5 wt% PAA + 0.75 wt % $Zn(NO_3)_2$ in water) using a PDMS stamp with a feature width of

600 nm and spacing 800 nm. The patterned area of the stamp was 8x8 mm^2. The substrate was annealed at 620°C to convert the as-deposited patterns into ZnO. XRD analysis confirmed the polycrystalline ZnO wurtzite phase (Figure 5b). The final ZnO line patterns had a line width of 120 nm and a height of 38 nm with a spacing of 600 nm between the lines. Figure 5c shows the corresponding tapping mode AFM height profile. Figure 5d shows TUNA conductivity map of the ZnO lines measured at an applied sample bias voltage of 2 V versus the conducting AFM tip. [27] The results indicate uniform conductivity along the lines.

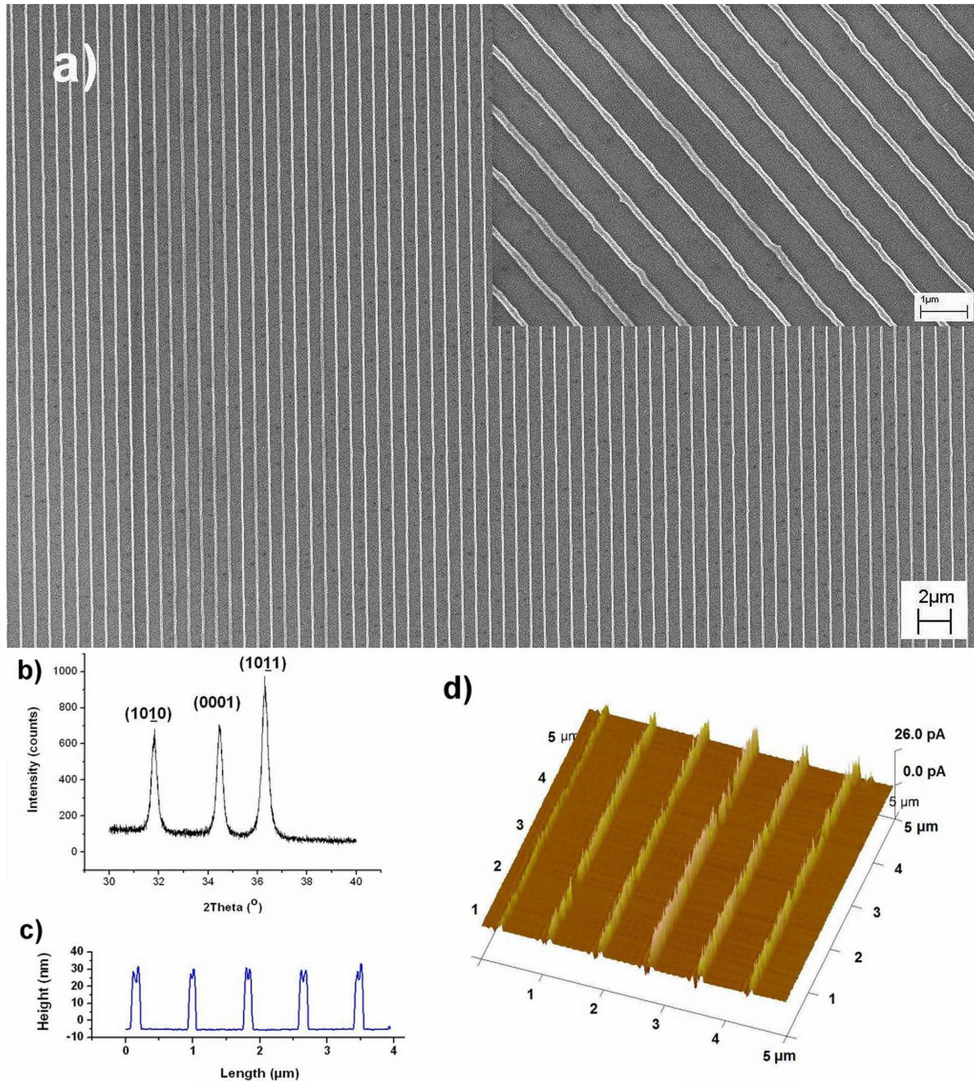

Figure 5: ZnO line patterns created using edge transfer printing of PAA-zinc nitrate thin film and subsequent annealing at 620°C. a) HR-SEM image of ZnO line pattern with a line width of 120 nm and a spacing of 600 nm; b) XRD diffractogram of polycrystalline wurtzite structure; c) Tapping mode AFM height profile; d) TUNA conductivity map of ZnO lines.

The height of the ZnO patterns can be controlled by varying the concentration of metal salt in the solution. Figure 6a shows the variation in thickness as a function of zinc nitrate concentration in 1.5 wt% PAA solution. The pattern width can be controlled by the thickness of the PAA-metal salt layer on the PDMS stamp. Figure 6b shows pattern width as a function of spin coating speed and PAA concentration. Best results were obtained when spincoating a solution of 1.5 wt% PAA with metal salts at an angular speed of 4000-5000 rpm. Formation of higher and wider patterns required

application of multiple layers of precursor solution on the PDMS stamp prior to transfer. In such cases the film was allowed to dry 10 minutes at room temperature after deposition of each layer.

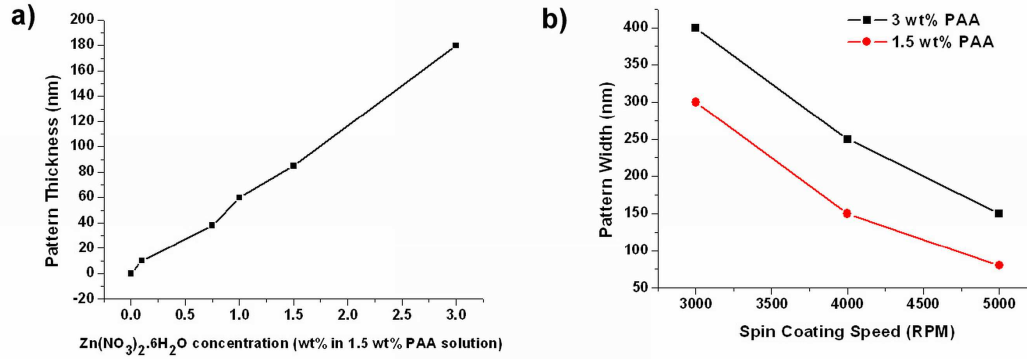

Figure 6: a) Variation in pattern thickness with metal salt concentrations; All samples where spincoated at 4000 rpm for 2 min; b) Variation in pattern thickness with spin coating speed.

In order to illustrate the versatility of the technique, stamps with different geometries and dimensions were tested. Figure 8a shows a ZnO nano-ring array fabricated using a nanometer-scale PDMS stamp with arrays of circular protruding pillars of 180 nm diameter, 200 nm spacing and 350 nm height. A solution of PAA-zinc nitrate solution with a concentration of 0.5 wt% of both PAA and zinc nitrate was used to generate the ring patterns with a width of 45 nm and a height of 15 nm. Figure 8b shows ring patterns fabricated using a micrometer scale-patterned PDMS stamp with circular pillar arrays with a diameter, spacing and height of 3 µm. A solution of 1.5 wt% PAA and 3 wt% zinc nitrate in water was used. The rings have a width of 300 nm and height of 150 nm measured using AFM. Figure 8c shows CuO ring patterns fabricated using a solution of 1.5 wt % PAA and 1.5 wt% $Cu(NO_3)_2$. The samples were annealed at 600°C for 30 min after transfer printing. The rings have a width of 100 nm. Figure 8d shows the XRD spectrum obtained from a Si-supported thin film that confirms the CuO phase. Examples of Fe_2O_3 and NiO nanopatterns are provided in the Appendix of this chapter.

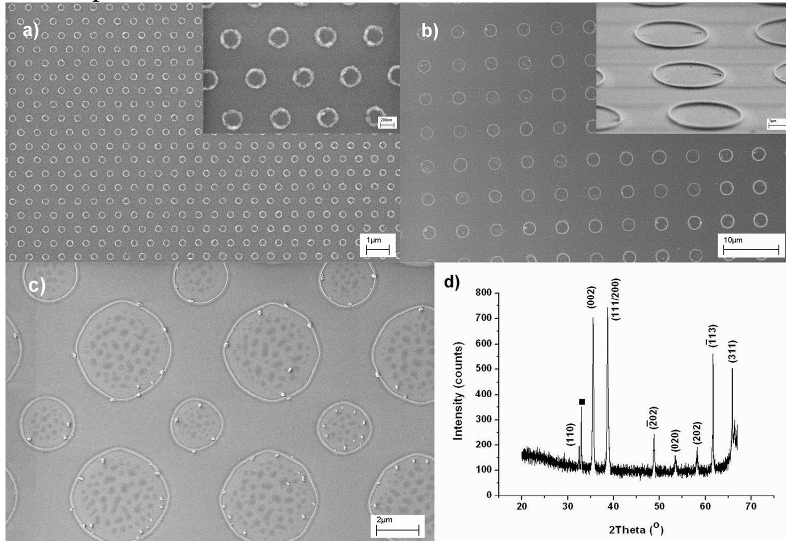

Figure 8: a) ZnO nano-ring array with a ring width of 45 nm. Inner diameter of the rings is 180 nm; b) ZnO ring array with a ring width of 300 nm. Inner diameter of the ring is 2.5 µm; c) Array of CuO rings with ring width of 100 nm; d) XRD diffractogram of CuO thin film.

We used the thin ZnO patterns as nucleation areas for site-selective solution phase growth of patterned ZnO nanoneedle arrays. Figure 9a show single-crystalline ZnO nanoneedles grown on the ring patterns of Figure 8b. Figure 9b shows nanoneedles grown on the line patterns of Figure 5a. Certain locations on the ZnO lines served as nucleation areas for growth of single-crystalline ZnO nanoneedles. The pictures clearly demonstrate the absence of a residual ZnO layer in the areas that were in contact with the PDMS stamp.

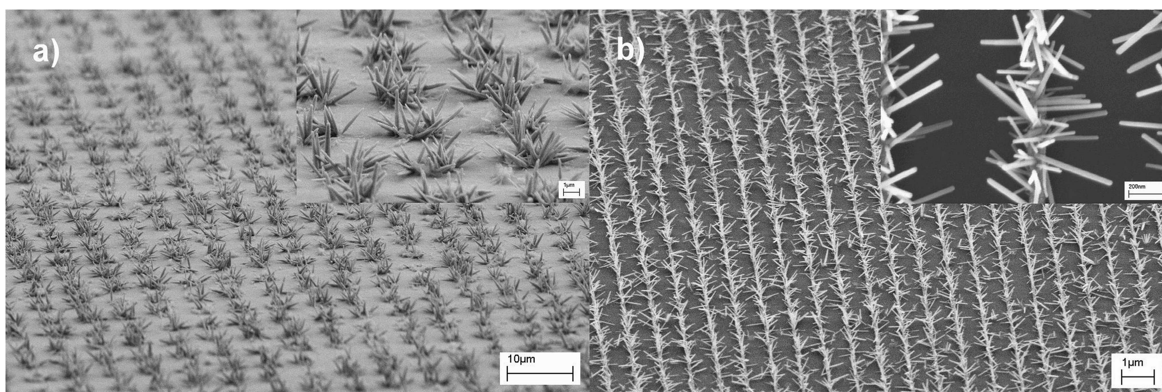

Figure 9: HR-SEM images of single crystalline ZnO nanowires grown selectively on a ZnO micropatterns. a) Nanoneedles grown on ZnO ring pattern of Figure 6b; b) Nanoneedles grown on ZnO line pattern of Figure 5a and 5b

Figure 10a shows a micropattern of a PVA-$FeCl_3$ complex that was transfer printed on Si from a PVA-iron chloride solution (3% PVA+3%iron chloride in water). Figure 10b shows a micropattern of a PVA-$HAuCl_4$ complex on Si substrate that was printed in a similar way.

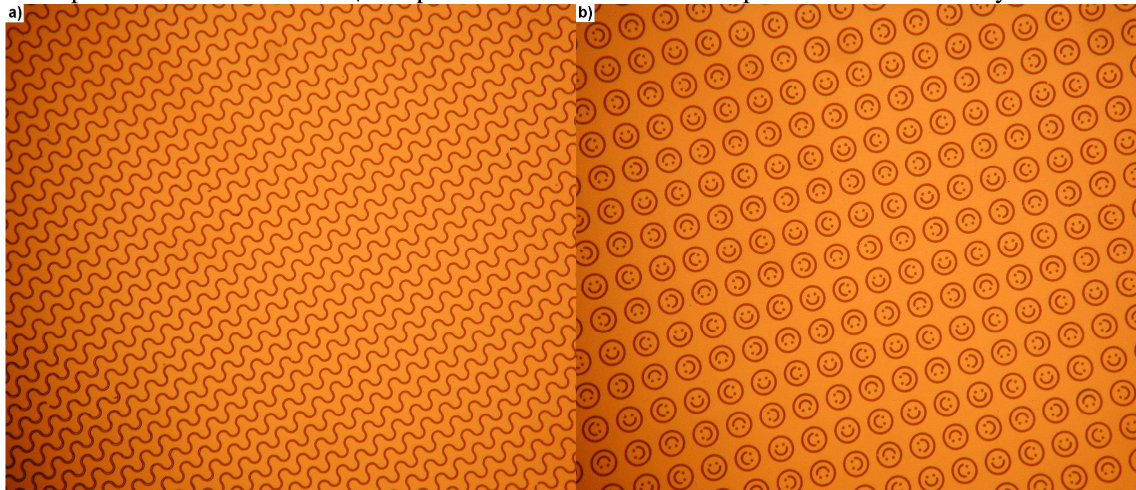

Figure 10: a-b) Optical microscope images of transfer printed micropatterns on Si from metal salt incorporated PVA solutions: a) Curved lines of PVA-$FeCl_3$ complex with a line width of 3 µm; b) smiley patterns of PVA-$HAuCl_4$ complex. The width of the circular feature is 3 µm.

Figure 11a-b shows isolated ZnO dot array formed by transfer printing PAA-Zn $(NO_3)_2$ complex (3 wt% PAA +3wt% Zn $(NO_3)_2$) using a PDMS mold with 500 nm holes separated by 800 nm with a height of 1 µm height. Only the sol filled inside the holes were transferred to the substrate. After annealing at 620°C the ZnO dots formed has an average diameter of 250 nm.

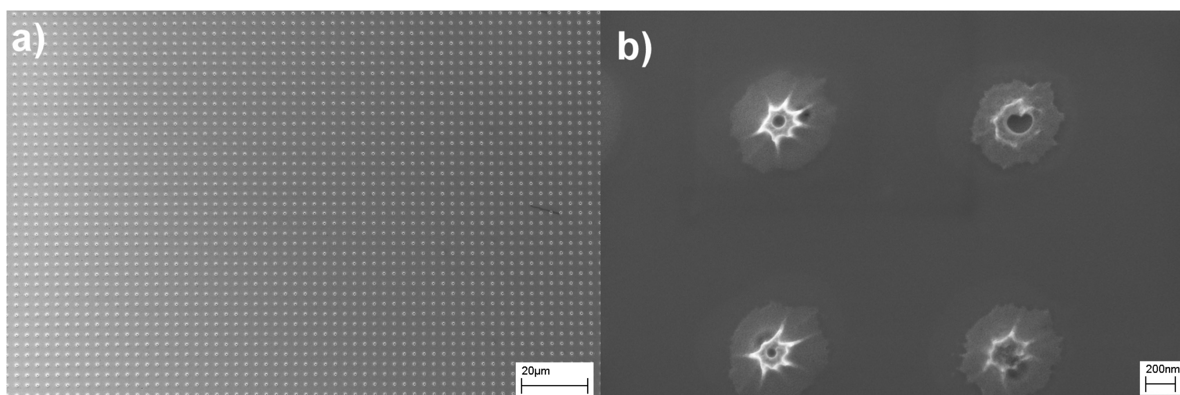

Figure 11: a-b) ZnO dot patterns of 250 nm diameter separated by 800 nm fabricated using a PDMS mold with pit array.

2.4. Conclusions

We have demonstrated a simple, fast and parallel approach for cost effective large area patterning of a wide range of oxide materials from sub-50 nm to micrometer scale dimensions using transfer printing of two water soluble polymers, PVA and PAA. PVA and PAA showed different pattern transfer mechanisms, depending on the molecular weight of the polymers, and the adhesion forces between the polymers and the participating interfaces**.** We demonstrated ZnO ring patterns with a ring width down to ~ 45 nm. The method is suitable to fabricate nanoscale and microscale patterns of a wide range of oxide materials or noble metal nanoparticles by mixing the metal salts with the water-soluble polymer solutions and subsequent annealing or oxygen plasma treatment.

2.5. References:

1. Jeon, N.L.; Hu, J.; Whitesides, G.; Erhardt, M. K.; Nuzzo, R. G., Fabrication of silicon MOSFETs using soft lithography. *Adv. Mater.* **1998**, *10*, 1466-1469.

2. Hu, J.; Beck, R. G.; Westervelt, R. M.; Whitesides, G. M., The use of soft lithography to fabricate arrays of Schottky diodes. *Adv. Mater.* **1998**, *10*, 574-577.

3. Pisignano, D.; Persano, L.; Visconti, P.; Cingolani, R.; Gigli, G.; Barbarella, G.; Favaretto, L., Oligomer-based organic distributed feedback lasers by room-temperature nanoimprint lithography. *Appl. Phys. Lett.* **2003**, *83*, 2545-2547.

4. Hu, Z.; Tian, M.; Nysten, B. Jonas, A. M., Regular arrays of highly ordered ferroelectric polymer nanostructures for non-volatile low-voltage memories. *Nat. Mater.* **2009**, *8*, 62-67.

5. Xue, M.; Zhang, Y.; Yang, Y.; Cao, T., Processing matters: In situ fabrication of conducting polymer microsensors enables ultralow-limit gas detection. *Adv. Mater.* **2008**, *20*, 2145-2150.

6. Saifullah, M. S. M.; Subramanian, K. R. V.; Kang, D. J.; Anderson, D.; Huck, W. T. S.; Jones, G. A. C.; Welland, M. E., Sub-10 nm high-aspect-ratio patterning of ZnO using an electron beam. *Adv. Mater.* **2005**, *17*, 1757-1761.

7. Yang, K.-Y.; Yoon, K.-M.; Choi, K.-W.; Lee, H., The direct nano-patterning of ZnO using nanoimprint lithography with ZnO-sol and thermal annealing. *Microelectron. Engin.* **2009**, *86*, 2228-2231.

8. Maury, P.; Péter, M.; Mahalingam, V.; Reinhoudt, D. N.; Huskens, J., Patterned self-assembled monolayers on silicon oxide prepared by nanoimprint lithography and their applications in nanofabrication. *Adv. Funct. Mater.* **2005**, *15*, 451-457.

9. Brevnov, D. A.; Barela, M.; Piyasena, M. E.; López, G. P.; Atanassov, P. B., Patterning of nanoporous anodic aluminum oxide arrays by using sol-gel processing, photolithography, and plasma etching. *Chem. Mater.* **2004**, *16*, 682-687.

10. Rogers, J. A.; Bao, Z.; Baldwin, K.; Dodabalapur, A.; Crone, B.; Raju, V. R.; Kuck, V.; Katz, H.; Amundson, K.; Ewing, J.; Drzaic P., Paper-like electronic displays: Large-area rubber-stamped plastic sheets of electronics and microencapsulated electrophoretic inks. *Proc. Natl. Acad. Sci. U. S. A.* **2001**, *98*, 4835-4840.

11. Kim, E.; Xia, Y.; Whitesides, G. M., Micromolding in capillaries: Applications in materials science. *J. Am. Chem. Soc.* **1996**, *118*, 5722-5731.

12. Göbel, O. F.; Nedelcu, M.; Steiner, U., Soft lithography of ceramic patterns. *Adv. Funct. Mater.* **2007**, *17*, 1131-1136.

13. Göbel, O. F.; Blank, D. H. A.; ten Elshof, J. E., Thin Films of Conductive ZnO Patterned by Micromolding Resulting in Nearly Isolated Features. *ACS Appl. Mater. Interfaces* **2010**, *2*, 536-543.

14. Niskala, J. R.; You, W., Metal-Molecule-Metal Junctions via PFPE Assisted Nanotransfer Printing (nTP) onto Self-Assembled Monolayers. *J. Am. Chem. Soc.* **2009**, *131*, 13202-13203.

15. Sharpe, R. B. A.; Burdinski, D.; Huskens, J.; Zandvliet, H. J. W.; Reinhoudt, D. N.; Poelsema, B., Chemically patterned flat stamps for microcontact printing. *J. Am. Chem. Soc.* **2005**, *127*, 10344-10349.

16. Odom, T. W.; Love, J. C.; Wolfe, D. B.; Paul, K. E.; Whitesides, G. M., Improved pattern transfer in soft lithography using composite stamps. *Langmuir* **2002**, *18*, 5314-5320.

17. Schmid, H.; Michel, B., Siloxane polymers for high-resolution, high-accuracy soft lithography. *Macromolecules* **2000**, *33*, 3042-3049.

[18] Sharpe, R. B. A.; Titulaer, B. J. F.; Peeters, E.; Burdinski, D.; Huskens, J.; Zandvliet, H. J. W.; Reinhoudt, D. N.; Poelsema, B., Edge transfer lithography using alkanethiol inks. *Nano Lett.* **2006**, *6*, 1235-1239.

19. Yang, Y.; Kung, S. C.; Taggart, D. K.; Xiang, C.; Yang, F.; Brown, M. A.; Guell, A. G.; Kruse, T. J.; Hemminger, J. C.; Penner, R. M., Synthesis of PbTe nanowire arrays using lithographically patterned nanowire electrodeposition. *Nano Lett.* **2008**, *8*, 2447-2451.

20. Xiang, C.; Kung, S.-C.; Taggart, D. K.; Yang, F.; Thompson, M. A.; Guell, A. G.; Yang, Y.; Penner, R. M., Lithographically patterned nanowire electrodeposition: A method for patterning electrically continuous metal nanowires on dielectrics. *ACS Nano* **2008**, *2*, 1939.

21. Yang, Y.; Taggart, D. K.; Brown, M. A.; Xiang, C.; Kung, S.-C.; Yang, F.; Hemminger, J. C.; Penner R. M., Wafer-Scale Patterning of Lead Telluride Nanowires: Structure, Characterization, and Electrical Properties. *ACS Nano* **2009**, *3*, 4144-4154.

22. George, A.; Blank, D. H. A.; ten Elshof, J. E., Nanopatterning from the gas phase: high resolution soft lithographic patterning of organosilane thin films. *Langmuir* **2009**, *25*, 13298-13301.

23. George, A.; Maijenburg, A.W.; Nguyen, M. D.; Maas, M. G.; Blank, D.H.A.; ten Elshof, J. E., Nanopatterning of functional materials by gas phase pattern deposition of self assembled molecular thin films in combination with electrodeposition. *Langmuir* **2011**, DOI 10.1021/la202210s.

24. Zhu, X.; Zhang, Y.; Zhang, J.; Xu, J.; Ma, Y.; Li, Z.; Yu, D. Ultrafine and Smooth Full Metal Nanostructures for Plasmonics. *Adv. Mater.* **2010**, *22*, 4345-4349.

25. Donzel, C.; Geissler, M.; Bernard, A.; Wolf, H.; Michel, B.; Hilborn, J.; Delamarche, E., Hydrophilic poly (dimethylsloxane) stamps for microcontact printing. *Adv. Mater.* **2001**, *13*, 1164-1167.

26. Gersappe, D.; Robbins, M. O., Where do polymer adhesives fail? *Europhys. Lett.* **1999**, *48*, 150-155.

27. Veeco AFM manual, Application Modules, Nanoscope V7-B (004-1020-000).

2.6. Appendix to chapter 2

Examples of Fe_2O_3, ZnO and NiO nanopatterns

Figure S2 shows a HR-SEM image of a Fe_2O_3 ring pattern, and an XRD pattern of a thin film fabricated using the same precursor solution (1.5 wt% PAA + 1 wt% $Fe(NO_3)_3 \cdot 9H_2O$). The sample was annealed at 620 ^oC to convert the precursor pattern into Fe_2O_3.

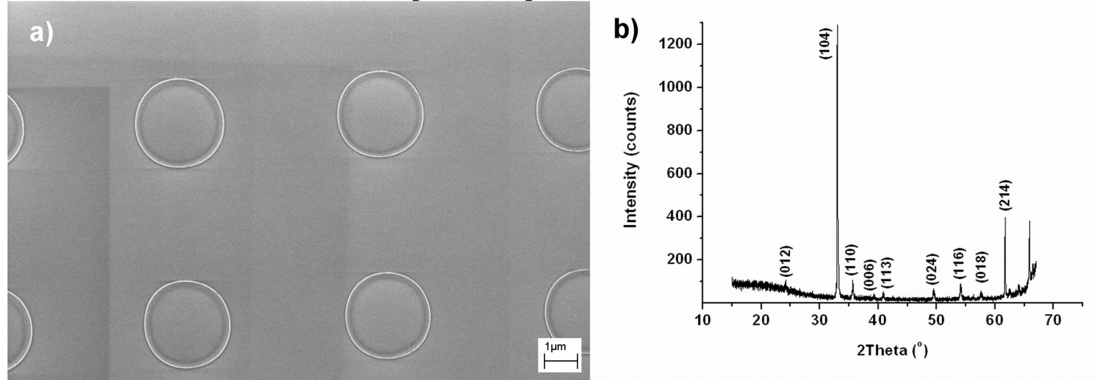

Figure S2: a) Fe_2O_3 ring pattern with a ring width of 250 nm; b) XRD pattern of Fe_2O_3 thin film.

Figure S3 shows a tapping mode AFM image and a height profile of ZnO line patterns fabricated using a PDMS stamp with line width and spacing of ~4 µm. Figure S3c and S3d show a ZnO ring pattern with a ring width of 80 nm, and a NiO pattern with a line width of 300 nm.

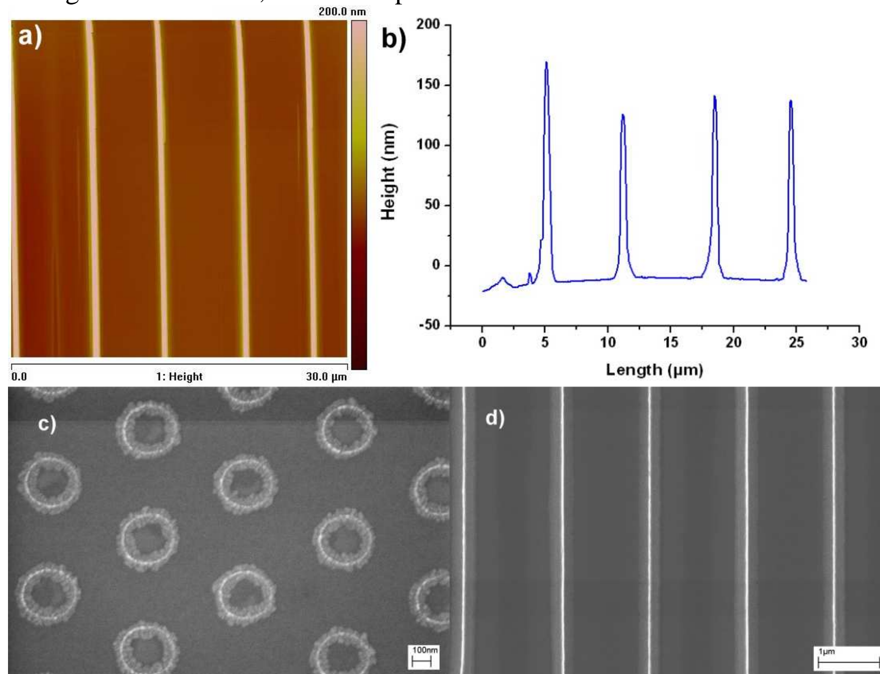

Figure S3: a) Tapping mode AFM image and (b) tapping mode height profile of ZnO line pattern with a line width of 600 nm and a spacing of ~ 4 µm; c) 80 nm ZnO ring patterns; d) 300 nm NiO line pattern.

Chapter 3

Nanopatterning from the gas phase: high resolution soft lithographic patterning of organosilane thin films

* This chapter was published in Langmuir [**2009**, *25* (23), pp 13298–13301]

Abstract

A general methodology for nanopatterning organosilane thin films directly from vapor phase precursors is presented. Aminosilane line patterns with a width of ~ 200 nm in an area of 1 cm^2 were fabricated on silicon substrates by diffusion of aminosilane vapor through the open channels of PDMS stamps bonded to a substrate. The patterned thin films were characterized by atomic force microscopy (AFM) and x-ray photoelectron spectroscopy (XPS). Patterns were initially formed at the three-phase boundary lines between substrate, PDMS mold and vapor, by exploiting the fact that vapors condense preferentially in geometrically restricted areas with a concave shape compared to flat surfaces. The lateral resolution of the formed patterns is about one order of magnitude smaller than the feature sizes of the PDMS stamp. Prolonged exposure to the precursor vapor resulted in micron-sized patterns with similar features and dimensions as the stamp. This methodology provides an easy and low cost parallel fabrication route of functional organosilane nanoscale patterns of arbitrary shape and composition from micron-size patterned stamps.

3.1. Introduction

Patterned self-assembled monolayers (SAMs) or thin films of organosilane molecules can be used to modify the surface chemical properties at specific locations [1]. For example, patterned SAMs and multilayer films can provide hydrophilicity, hydrophobicity or a desired chemical functionality on specific locations on the substrate during device fabrication [1]. They have also been employed in nanofabrication technology as etch resist [2], and as templates for electroless deposition [3] and site selective immobilization of different materials like nanoparticles [4], polymers [4] and biomolecules [5]. Patterned organosilane SAMs or thin films can therefore be used for nanofabrication of electronics, data storage devices, MEMS and biological sensors. The very small size and the chemical stability of the organosilane molecules enable them as a very powerful material for high resolution nanopatterning [1].

Electron beam lithography [2,6,7], focused ion beam lithography [7], photolithography [8], scanning probe lithographic methods [9,10], microcontact printing [11] and nanoimprint lithography [4] are the most widely used serial and parallel patterning methods for organosilane thin films and SAMs. Serial techniques based on electron and ion beams can be used for high resolution nanopatterning either by using a polymer resist or directly modifying/destroying the SAM or thin film upon irradiation. The processing times are relatively long and the cost of fabrication and maintenance are considerable [12]. Photolithography gives good results in standard clean room fabrication processes, and yields resolutions up to the diffraction limit of the wavelength of light used for patterning the photoresists [12]. Scanning probe lithography can also be used for patterning up to sub-10 nm resolution. The processing time for scanning probe pattern generation is high comparing to parallel methods. Microcontact printing (μCP) using a soft polydimethylsiloxane (PDMS) stamp is a versatile approach due to its parallel nature, speed and low cost to generate massively patterned substrates. However, the resolution of μCP is limited due to the noticeable effect of diffusion of ink on the substrate at higher resolutions [11]. Nanoimprint lithography (NIL) is a successful tool for

patterning nanoscale patterning of SAMs. NIL is a fast parallel patterning method. It does require elevated pressures and temperatures during the processing and a residual layer is present after the imprint has been made [4].

Here we propose a new single step method to pattern organosilane molecules on silicon substrates directly from the vapor phase using a PDMS stamp as template. The approach belongs to the family of soft-lithography techniques since it makes use of a polymeric mould in conformal contact with a substrate for replicating the features of a master structure [13]. Our technique enables the effective fabrication of organosilane patterns on large surface areas. The patterns have a high resolution, down to 200 nm, and a high packing density. A special feature of our methodology is that the resolution of the formed patterns is about one order of magnitude higher than the features of the PDMS stamp with which the pattern is generated. The reason is that precursor deposition takes place primarily in areas that are very near to the triple phase contact lines between substrate, PDMS mold and organosilane vapor, i.e., in those areas that have a sharp concave shape. The schematic diagram of the patterning process is shown in Figure 1. A patterned PDMS stamp is pressed against a pretreated silicon substrate. A connected channel structure is formed between stamp and substrate, with openings to the ambient on the vertical sides of the stamp. The open channel pattern is then exposed to an organosilane saturated environment in an evacuated desiccator. The silane molecules diffuse into the channels via the openings and react with the exposed regions of the substrate. The regions in conformal contact with the PDMS stamp are protected from the organosilane molecules. Depending on the time of exposure to vapor, two different modes of pattern generation are possible with this technique. When the substrate is exposed to vapor for a limited period of time, patterns are formed only in the regions where the edges of the protruding regions of the PDMS stamp are in contact. When the substrate is exposed for a longer period of time the flat areas of the substrate are also covered by reactive organosilane molecules.

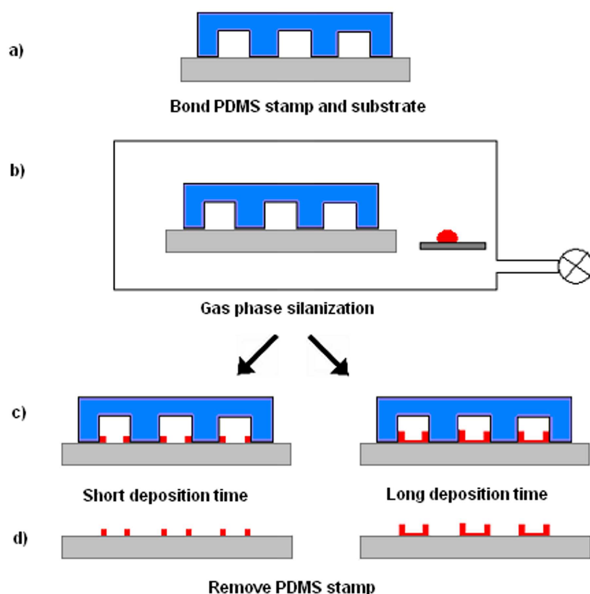

Figure 1: Procedure of direct gas phase patterning of organosilane thin films using a PDMS stamp template. a) Reversible bonding of PDMS stamp to substrate. b) Deposition of organosilane in desiccator. c) Removal of substrate and stamp from desiccator after exposure. d) Removal of stamp from substrate.

3.2. Experimental section

Preparation of PDMS stamps: PDMS and curing agent (Sylgard 184) were purchased from Dow Corning Corporation and mixed in a ratio 8:1 and poured over the micro/nano-patterned silicon master

(created by photolithography or e-beam lithography). The PDMS was cured at a temperature of 70°C for 48 hours. After curing, the PDMS stamps were removed from the master and cut into pieces of desired size and stored in absolute ethanol for 15 days before use. Every five days the PDMS stamps were taken out of the ethanol, washed with ethanol, and stored again in fresh ethanol. This treatment reduced the amount of unreacted PDMS oligomers in the stamp which might otherwise contaminate the substrate during the patterning process. After this treatment, the PDMS stamps were dried at 90°C for 3 hours to remove any trace of ethanol prior to use.

Preparation of silicon substrates: P-Type silicon substrates cleaned with piranha solution (a mixture of H_2O_2 and H_2SO_4 in 1:3 volume ratio) were used in the experiments. The substrates were then washed several times with de-ionized water and stored in de-ionized water. Prior to use the substrates were blow-dried in a nitrogen stream.

Fabrication of organosilane patterns: (3-Aminopropyl)triethoxysilane (APTES, 98% pure) was purchased from Sigma Aldrich and used in the experiments as received. The dried PDMS stamps with micro/nano-patterned features were gently pressed against silicon substrates facing the patterned side of the stamp against the polished side of the silicon substrate. The PDMS stamp made conformal contact with the substrate via attractive Van der Waals forces. Substrates with a bonded PDMS stamp were transferred to a desiccator. A drop of aminosilane precursor was placed in the desiccator. After evacuation of the atmosphere by a mechanical pump to 100 mbar, the desiccator was closed and an organosilane vapor-saturated environment formed inside it. The substrates were exposed to the organosilane environment for a time period of 3 to 12 hours. The substrates were taken out from the desiccator and washed with absolute ethanol followed by deionized water and stored for further analysis.

Characterization: The patterned organosilane thin films were characterized using atomic force microscopy (AFM, Dimension D3100 Nanoscope IVa controller, Veeco Instruments) for surface morphology and X-ray photoelectron spectroscopy (XPS, Quanta SXM scanning electron microprobe, Physical Electronics) for surface chemical information.

3.3. Results and discussion

Figure 2 and Figure 3 show tapping mode AFM height and phase images of patterned aminosilanes on silicon wafers after deposition for 3 and 12 hours, respectively. The PDMS stamp used for patterning the organosilane lines in Figure 2 has a line width of 1 μm and a spacing of 1.3 μm in an area of 1 cm^2. The width of organosilane line patterns is approximately 200 nm and the height is ~7 nm. The phase image indicates that the areas in between the aminosilane lines did not contain noticeable amounts of aminosilane. The organosilane molecules entered the PDMS channels through the openings located on the side walls of the stamp. The effective diameter d of APTES is smaller than 0.8 nm, and the vapor pressure at 293 K is 2 Pa [14]. With a background pressure p~10 kPa inside the desiccator, the mean free path $\lambda = k_B T/(\sqrt{2}\pi d^2 p)$ (k_B is the Boltzmann constant, and T the temperature) of APTES in the gas phase is of the order of 200 nm. This is almost an order of magnitude smaller than the dimensions of the channels. Therefore, the predominant mechanism of gas transport inside the channels is bulk diffusion. The molecules then deposited on the substrates, forming covalent bonds with the OH terminated silicon surface. Upon exposure to ambient air, the alkoxy-functional organosilane molecules react with water vapor by sol-gel hydrolysis and condensation into a polymerized network. Interestingly, the AFM data clearly show that patterns are generated that have much smaller dimensions than the original PDMS stamp template.

Figure 3 shows micropatterns of condensed γ-aminopropyl silane after deposition for 12 hours. The PDMS stamps shown had a line width and spacing of approximately 4 μm in an area of 1 cm^2. The thick lines at the edges of the line confirm that the molecules deposited first at the PDMS–silicon-air triple phase boundary lines and then deposited in the region between the edges. The AFM height-distance plot shows that the thickness of the aminosilane thin film is approximately 3 nm in the central regions, with well-defined thicker edges of approximately 10 nm height and 200 nm width. The method bears some resemblance to the gas transfer lithography process proposed by De la Rica et al. [15], because it uses PDMS molds and gaseous aminosilanes as precursors, but there are some essential differences with our technology. It also bears resemblance to the solvent-assisted soft

lithography method introduced recently by Shi et al. [16], but our method uses gaseous precursors instead of liquid sols.

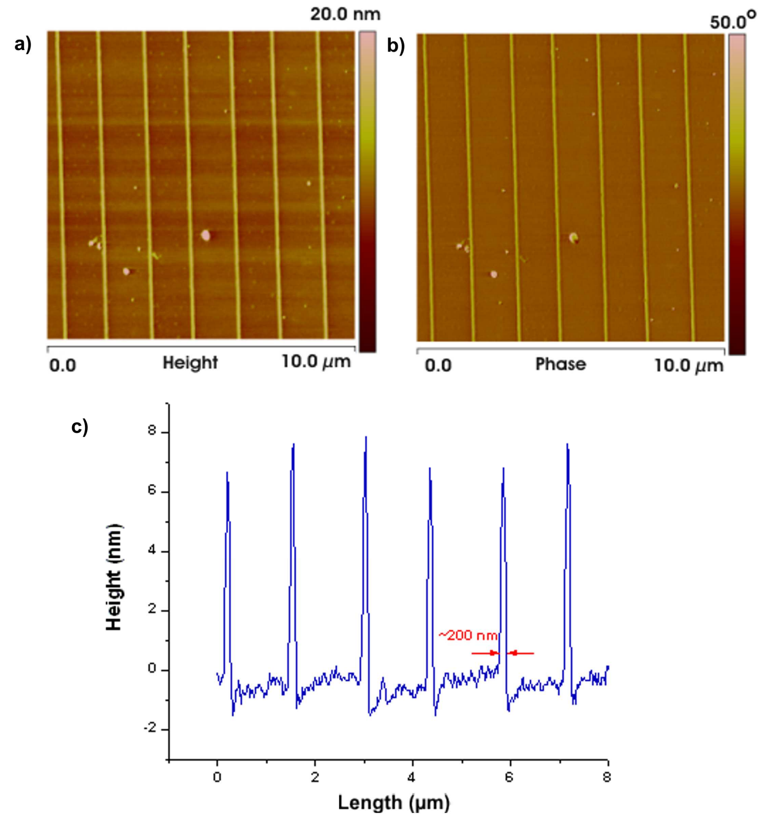

Figure 2: γ-Aminopropylsilane based thin line patterns formed after a deposition time of 3 hours. (a) AFM height image; (b) AFM phase image; (c) Distance – height line scan in a direction perpendicular to the line pattern.

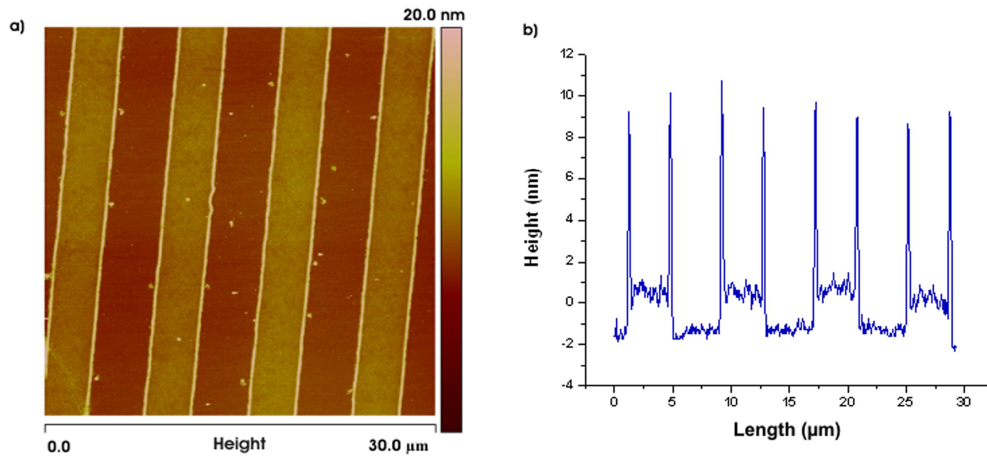

Figure 3: γ-Aminopropylsilane based line patterns formed after a deposition time of 12 hours. (a) AFM height image; (b) Distance – height line scan in a direction perpendicular to the line pattern.

XPS experiments were done to validate the chemical identity of the patterns and confirm the presence of an aminosilane line structure. Figure 5 shows the XPS N 1*s* spectrum obtained on the thin

line patterns of Figure 2. The data indicate a notable presence of nitrogen from the end functional groups of the condensed aminosilane molecules on the substrate. This confirms the deposition of an aminosilane network on the substrate, and rules out the possibility that the lines are composed of PDMS oligomers that somehow segregated from the stamp. The asymmetry of the N 1*s* peak suggests that more than one type of nitrogen was present. The peak could be deconvoluted into two Gaussians, with peak positions at 399.7 and 401.5 eV. Most likely these correspond to the amine end group (-NH_2) and the protonated amine end group (NH_3^+) of the patterned aminosilane thin film, respectively.

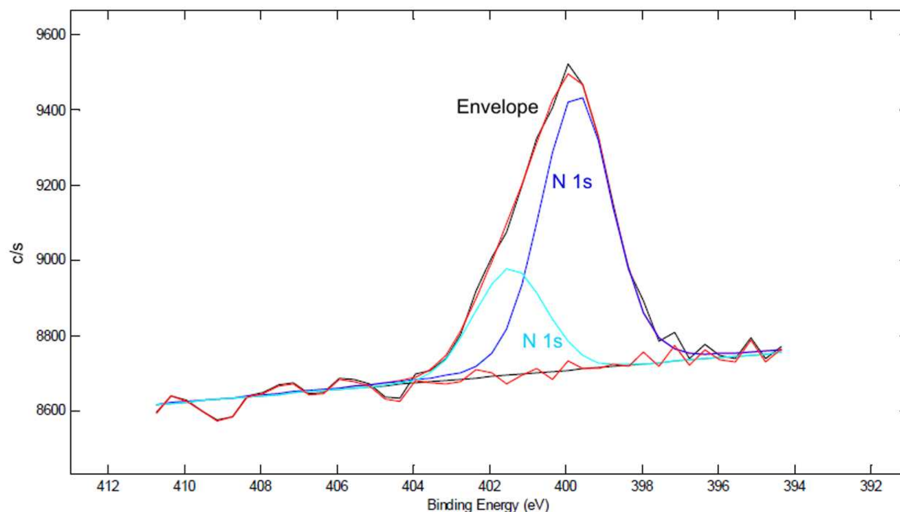

Figure 4: XPS N 1*s* spectrum of patterned γ-aminopropylsilane based lines from Figure 2. The peaks at 399.7 eV and 401.5 eV represent $–NH_2$ and $–NH_3^+$ groups, respectively.

The AFM images in Figure 2 and Figure 3 confirmed two modes of pattern generation, depending on the time of exposure of the substrate to the organosilane vapor. Short exposure led to pattern formation along lines where the silicon substrate was in contact with the edges of the protruding regions of the stamp. Upon increasing the exposure time, the molecules also condensed and assembled in the regions between the edges and filled all unmasked areas of the substrate surface. This means that the aminosilane molecules condense first along edges rather than homogeneously over the entire OH terminated silicon substrate. Although the process is not understood in microscopic detail, this type of preferential wetting is generally interpreted in terms of increased Van der Waals interaction of vapors due to size confinement [17]. The edges of the protruding PDMS features in contact with the silicon substrate form very sharp concave corners. This geometry promotes the initial condensation of organosilanes compared to deposition on flat areas. Upon prolonged exposure, the organosilanes eventually also condense on flat surfaces, resulting in micron-sized organosilane patterns with a thickness of 10 nm.

3.4. Conclusions

In conclusion, we have presented a novel gas phase patterning technique using PDMS templates as a reliable method for nanopatterning organosilane thin films. Some aspects of this gas phase patterning procedure may make it more suitable for organosilane nanopatterning than soft lithographic techniques based on printing liquid precursors. The methodology does not depend on the application of a controlled pressure on the mold, so that stamp deformation is limited, and contact times are less critical. Secondly, gas-phase deposition of organosilanes prevents aggregation of reactants prior to deposition and results in regular patterns of controlled thickness. The process had a high fidelity and high quality patterns were obtained over large surface areas. Further experiments to make materials using other organic and inorganic precursors are under way.

3.5. References:

1. Onclin, S.; Ravoo, B.J.; Reinhoudt, D.N. *Angew. Chem. Int. Ed.* **2005**, 44, 6282-6304.

2. Carr, D.W.; Lercel, M.J.; Whelan, C.S.; Craighead, H.G.; Seshadri, K.; Allara, D.L. *J. Vacuum Sci. Technol. A* **1997**, 15, 1446-1450.

3. Hsu, C.-H.; Yeh, M.-C.; Lo, K.-L.; Chen, L.-J. *Langmuir* **2007**, 23, 12111-12118.

4. Maury, P.; Peter, M.; Mahalingam, V.; Reinhoudt, D.N.; Huskens, J. *Adv. Funct. Mater.* **2005**, 15, 451-457.

5. Hoff, J.D.; Cheng, L.-J.; Meyhofer, E.; Guo, L.J.; Hunt, A.J. *Nano Lett.* **2004**, 4, 853-857.

6. Lercel, M.J.; Tiberio, R.C.; Chapman, P.F.; Craighead, H.G.; Sheen, C.W.; Parikh, A.N.; Allara, D.L. *J. Vac. Sci. Technol. B* **1993**, 11, 2823-2828.

7. Gillen, G.; Wight, S.; Bennett, J.; Tarlov, M.J. *Appl. Phys. Lett.* **1994**, 65, 534-536.

8. Dulcey, C.S.; Georger, J.H., Jr.; Krauthamer, V.; Stenger, D.A.; Fare, T.L.; Calvert, J.M. *Science* **1991**, 252, 551-554.

9. Ginger, D.S.; Zhang, H.; Mirkin, C.A. *Angew. Chem. Int. Ed.* **2004**, 43, 30-45.

10. Maoz, R.; Frydman, E.; Cohen, S.R.; Sagiv, J. *Adv. Mater.* **2000**, 12, 424-429.

11. Jeon, N.L.; Finnie, K.; Branshaw, K.; Nuzzo, R.G. *Langmuir* **1997**, 13, 3382-3391.

12. Mijatovic, D.; Eijkel, J.C.T.; van den Berg, A. *Lab on a Chip* **2005**, 5, 492-500.

13. Xia, Y.; Whitesides, G.M. *Ann. Rev. Mater. Sci.* **1998**, 28, 153-184.

14. Ditsent, V.E.; Skorokhodov, I.I.; Terent'eva, N.A.; Zolotareva, M.N.; Belyakova, Z.V.; Belikova, Z.V. *Zh. Fiz. Khim.* **1976**, 50, 1905-1906.

15. de la Rica, R.; Baldi, A.; Mendoza, E.; San Paulo, A.; Llobera, A.; Fernandez-Sanchez, C. *Small* **2008**, 4, 1076-1079.

16. Shi, G.; Lu, N.; Gao, L.; Xu, H.; Yang, B.; Li, Y.; Wu, Y.; Chi, L. *Langmuir* **2009**, 25, 9639–9643.

17. Rascon, C.; Parry, A.O. *Nature* **2000**, 407, 986-989.

Chapter 4

Nanopatterning of functional materials by gas phase pattern deposition of self assembled molecular thin films in combination with electrodeposition

* This chapter was published in Langmuir, (2011, 27 (20), pp 12760–12768)

Abstract.

We present a general methodology to pattern functional materials on the nanometer-scale using self assembled molecular templates on conducting substrates. A soft lithographic gas phase edge patterning process using PDMS molds was employed to form electrically isolating organosilane patterns of a few nanometer thickness and a line width that could be tuned by varying the time of deposition. Electrodeposition was employed to deposit patterns of Ni and ZnO on these prepatterned substrates. Deposition occurred only on patches of the substrate where no organosilane monolayer was present. The process is simple, inexpensive and scalable to large areas. We achieved formation of metallic and oxide material patterns with a lateral resolution of 80 nm.

4.1. Introduction

Microcontact printing of alkanethiols [1,2,3] is the most studied method to pattern self-assembled monolayers (SAMs) on gold films. It has attracted wide research interest due to the ability of the patterned SAMs to act as etch resist [1], or as template for electrodeposition [2] or electroless deposition [3]. This makes patterned SAMs very important in future micro and nanofabrication technologies. In microcontact printing a soft poly-dimethyl siloxane (PDMS) stamp inked with alkane thiol inks is pressed against a gold substrate to release the ink molecules in a controlled way to the substrate. The method is a scalable parallel process which is already implemented in industry to fabricate micrometer scale features. However, the miniaturization is still a challenge in microcontact printing due to the limitations of the elastomeric property of the PDMS stamp used and the limitation of ink diffusion [4, 5, 6, 7] which may cause loss of fidelity and larger defect concentration of the patterns fabricated.

In order to minimize the defect concentration and overcome the problem of ink diffusion, it is necessary to develop new methodologies for patterning self-assembling molecules. Patterning a prefabricated film by area selective destruction or chemical modification by an electron beam [8,9] or AFM tip [10,11,12] are very efficient in terms of pattern fidelity and resolution. Preformed molecular films can have high film quality since the molecules are reacted from the liquid or gas phase for longer times when compared to short time microcontact printed films. Due to the serial nature and high capital investment costs of electron beam lithography and AFM lithography, these techniques can only be used in research. It is also possible to pattern high quality molecular thin films in a parallel manner using a preformed mask such as photoresist on a substrate, fabricated by photolithography [13] or nanoimprint lithography [14], and followed by a gas phase or liquid phase deposition process of the self assembling molecules and finally a resist removal step. However, these techniques require multiple process steps of resist patterning, etching and/or residual layer removal [13,14]. Recently, we demonstrated a single step process for patterning organosilane SAMs from the gas phase using PDMS molds on silicon substrates [15]. The method can be employed to generate nanometer scale organosilane patterns using micrometer-sized PDMS molds due to the fact that organosilane molecules prefer to condense in geometrically restricted areas rather than condensing onto planar

areas of the substrate. Patterns are therefore formed first at the three-phase boundary lines between substrate, PDMS mold and vapor, before condensing on geometrically planar patches. The lateral resolution of the formed patterns was about one order of magnitude smaller than the feature sizes of the PDMS mold [15].

In the present paper we used the same patterning methodology to form mercaptosilane (MPTS) monolayers and thin films to act as patterned resists for subsequent fabrication of functional materials by electrodeposition. The process is a fast, inexpensive and large area approach for pattern generation and can be employed in future device fabrication technologies. The schematic diagram of the process is described in Figure 1. A micro or nanopatterned PDMS mold is pressed against a silicon substrate with a sputter deposited gold film of thickness ~75 nm. A connected channel structure is formed between the mold and the substrate with openings to the ambient on the vertical side of the mold. The substrate-mold assembly is then exposed to a low pressure environment containing a source of self-assembling molecules for a certain period of time at a temperature of 60°C. The natural vapor pressure of the mercaptosilane molecules at the given temperature leads eventually to the formation of a molecular thin film on the unshielded areas of the substrate. Depending on the time of exposure to vapor, two different modes of pattern generation are possible [15]. When the substrate is exposed to vapor for a limited period of time, patterns are formed only in the regions where the edges of the protruding regions of the PDMS mold are in contact. When the substrate is exposed for a longer period of time, the flat areas of the substrate are also covered by reactive mercaptosilane molecules. And as will be shown below, the difference between these two modes vanishes when the pattern resolution goes into the nanometer-scale domain. The three modes of patterning are shown schematically in Figure 1. After organosilane deposition, the substrates were used as electrodes in an electrodeposition process to generate functional micropatterns of Ni and ZnO. We generated patterns with lateral resolutions ranging from ~ 80 nm to a few micrometers.

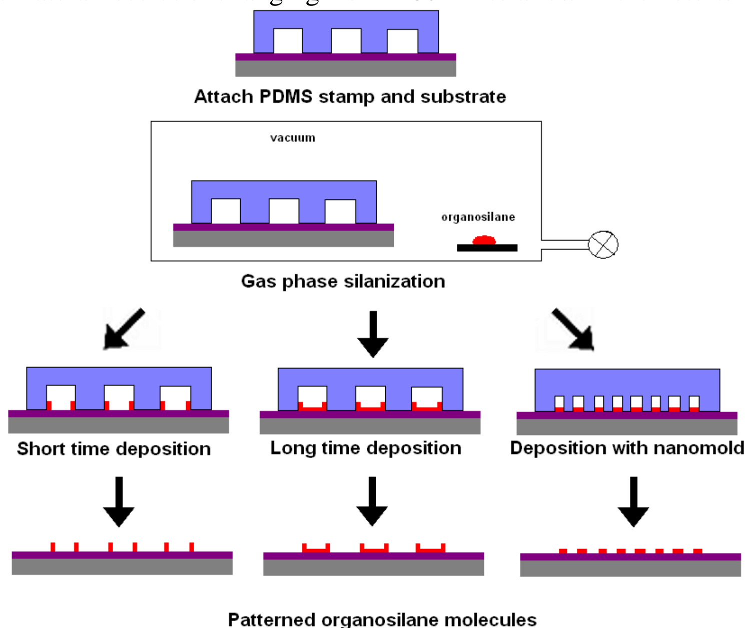

Figure 1: Schematic diagram of the patterning process.

4.2. Experimental

Fabrication of PDMS molds: PDMS and curing agent (Sylgard 184) were purchased from Dow Corning Corporation, mixed in a ratio 10:1 and poured over the micro/nanopatterned silicon master (created by photolithography or e-beam lithography). The PDMS was cured at a temperature of 70°C for 48 h. After curing, the PDMS molds were removed from the master and cut into pieces of 1 x 1 cm^{2} size.

Preparation of gold coated silicon substrates: p-Type silicon substrates cleaned with piranha solution (a mixture of H_2O_2 and H_2SO_4 in 1:3 volume ratio) were used in the experiments. The substrates were washed several times with deionized water and blow-dried in a nitrogen stream. Gold thin films of 75 nm thickness on silicon substrates were prepared using a Perkin-Elmer sputtering machine operating at 50 W at a deposition pressure of $2x10^{-5}$ mbar using Argon as sputtering gas. A titanium film of thickness 10 nm was sputtered at 150 W as an adhesion promotion layer prior to gold sputtering.

Patterning organosilanes: (3-Mercaptopropyl) methyldimethoxysilane (95% purity) (MPTS) was obtained from Sigma-Aldrich. The PDMS molds with micro/nano-patterned features were gently pressed against the gold coated silicon substrate. The patterned side of the mold faced the gold coated side of the silicon substrate. The PDMS mold made conformal contact with the substrate via Van der Waals adhesion to the substrate. The PDMS can be peeled off the substrate easily by gentle force. The substrates with bonded PDMS mold were transferred to a desiccator. A drop of MPTS was placed in the desiccator and evacuated by a mechanical pump. The desiccator was heated to a temperature of 60°C. A MPTS vapor saturated environment formed inside the desiccator. The organosilane molecules diffused from the gas phase into the PDMS channels and deposited on the substrates, forming covalent bonds with the Au surface. The substrates were exposed to the environment for a period of 1 to 12 h to study the effect of deposition time on pattern formation. After deposition, the substrates were taken from the desiccator and washed with absolute ethanol and deionized water, and stored for further analysis.

Electrodeposition of ZnO and Ni: MPTS patterned Au thin film substrates were used as substrate for electrodeposition. Electrodeposition was carried out using a three-electrode potentiostat (Autolab PGSTAT 128N, Metrohm Autolab B.V., The Netherlands). The SAM-patterned substrates were used as working electrodes. A small Pt mesh was used as counter electrode. The reference electrode was Ag/AgCl in 3M KCl (Metrohm Autolab). Nickel patterns were formed from an electrolyte containing 0.23 M nickel sulphate hexahydrate ($NiSO_4.6H_2O$, Sigma-Aldrch, purity 99%,) and 0.15 M boric acid (H_3BO_3, Aldrich, purity 99.99%). Deposition occurred at -1.00 V versus reference. Zinc oxide patterns were formed at 60 °C at -1.00 V in an electrolyte containing 0.10 M zinc nitrate hexahydrate ($Zn(NO_3)_2.6H_2O$, Sigma-Aldrich, purity 98%,). Further details can be found elsewhere [16].

Characterization: MPTS patterns were characterized using tapping mode Atomic Force Microscopy (AFM; Veeco Dimension Icon) to determine the surface morphology. Tunnelling current AFM (TUNA) was used to study the conductivity of the grown patterns, as well as to map the conductivity of patterned surfaces [17]. Grown metal and oxide patterns were imaged using high resolution scanning electron microscopy (HR-SEM, Zeiss 1550) and tapping mode AFM. X-ray diffraction (XRD, Philips defractometer PW 3020, Software XPert Data Collector 2.0e, Panalytical B.V., Almelo, The Netherlands) was used for phase determination of the patterns. The in-plane magnetic anisotropy of the polycrystalline Ni line arrays was characterized by a vibrating sample magnetometer (VSM, Model 10 VSM, Digital Measurement System 'DMS', ADE Technologies) at room temperature. Hysteresis loops were taken at different *in-plane* field directions with intervals of 10° field angle.

4.3. Results and discussion

1. Deposition of organosilane patterns

Figure 2a shows tapping mode AFM height image and AFM height profile of patterned mercaptosilane film on Au coated silicon substrate. The patterns were grown at a temperature of 60 ^{o}C for a period of 5 h. In principle, it should be possible to increase the rate of deposition further by working at higher vapor pressures, e.g. by employing higher temperatures for deposition. The dimensions of the patterns in the PDMS molds are 110 nm line width, 140 nm spacing and 100 nm channel height. A negative replica of the PDMS mold formed over the substrate with an approximate height of ~2-3 nm. Figure 2b shows AFM image and AFM height profile of patterned mercaptosilane film on Au coated silicon substrate. The patterns were grown at a temperature of 60°C for a period of 5 h. The dimensions of the patterns in the PDMS molds are 350 nm line width, 450 nm spacing, and 200 nm channel height. A negative replica of the MPTS mold formed over the substrate with an

approximate height of ~2-3 nm. The patterns were very homogeneous and of high quality. No difference could be observed between patterned areas near the outer edges of the PDMS mold, and areas near the center of the mold.

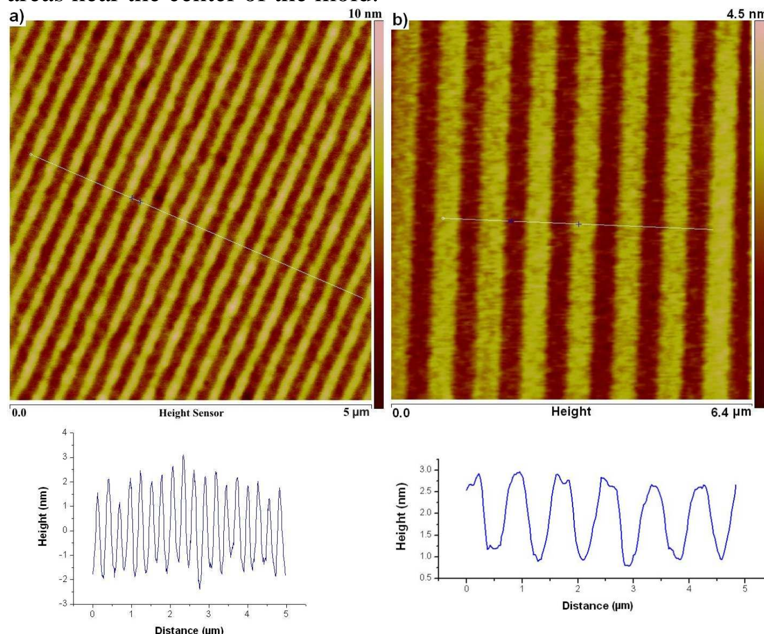

Figure 2: AFM image and AFM height profile of MPTS pattern. a) pattern with line width 110 nm, spacing 140 nm; b) pattern with line width 350 nm, spacing 450 nm. Both patterns have a height of ~2-3 nm and were grown at 60°C for 5 h.

We also used PDMS molds with micrometer and nanometer scale features for patterning MPTS thin films to exploit the possibility of preferable edge condensation of the organosilane molecules as we reported previously [15]. We grew MPTS patterns for different periods of time and studied the pattern formation process with a series of tapping mode AFM scans. Figure 3a-b show tapping mode AFM images and height profiles of MPTS patterns grown for 180 and 240 min using a PDMS mold with a line pattern with lines of ~4 µm width and ~ 2 µm heights grown at 60 ^{o}C. The thick lines formed at the corners between the PDMS mold and the substrate indicate that MPTS molecules prefer to condense and polymerize initially in the corners rather than on the planar Au surface. The height of these edge patterns increased from ~1 nm after 60 min, to about 7-8 nm after 180-240 min. Further growth did not lead to a further increase of the height of the edge pattern. However, the AFM images also show an ongoing increase of the width of the edge patterns with time, as shown in Figure 3c. On the other hand, the unshielded planar areas of the Au substrate showed no signs of significant condensation of MPTS molecules during the first 180 min of deposition. Figure 3b shows an AFM image pattern after ~240 min of growth. Here the uncovered planar areas between the corners clearly increased height by <1 nm. AFM scans of samples grown for 12 and 48 h (not shown here) showed that these areas did not increase thickness upon prolonged exposure to MPTS vapor. This indicates that after the formation of about one monolayer, no further growth of the thickness of the SAM occurred. It is also possible to grow patterned MPTS films (up to 5-7 nm) by increasing the deposition temperature to 70-80 ^{o}C for 3 h or more. An external load was applied to the PDMS mold to keep the mold on the substrate during the deposition process, since the PDMS molds were not stable and lifted off from the Au thin film (or lost conformal contact) above 65 ^{o}C, probably due to expansion of the molds above this temperature.

Similar experiments with a nanometer scale patterned PDMS mold with a line width of 450 nm, an interline spacing of 350 nm, and a height of 200 nm also showed preferential condensation in the corners where PDMS and substrate meet during the first 2 h of deposition. After 1 h of deposition, the edge-condensed lines had a width of 80-90 nm as shown in the HR-SEM image of Figure 3d. However, due to the narrow size of the channels, a homogeneous MPTS film of 2-3 nm thickness

formed across the width of the channels upon longer exposure. When we used a PDMS mold with a line width of 140 nm, a spacing of 110 nm, and a height of 100 nm (as shown in Figure 2a), we did not observe preferential corner condensation but only film formation across the entire surface of the channel.

By comparing the AFM images of MPTS patterns grown using microscale and nanoscale patterned PDMS molds it can be concluded that the predominant mechanism of MPTS deposition in PDMS-substrate formed channels is geometry dominated adsorption/condensation of molecules in narrow corners by an effect similar to capillary condensation as described by Rascon and Perry [18]. Only in later stages of growth does complete coverage of the Au surface occur. When the channel dimensions go down to ~100 nm or less, deposition by condensation occurs predominantly on the inside substrate surface.

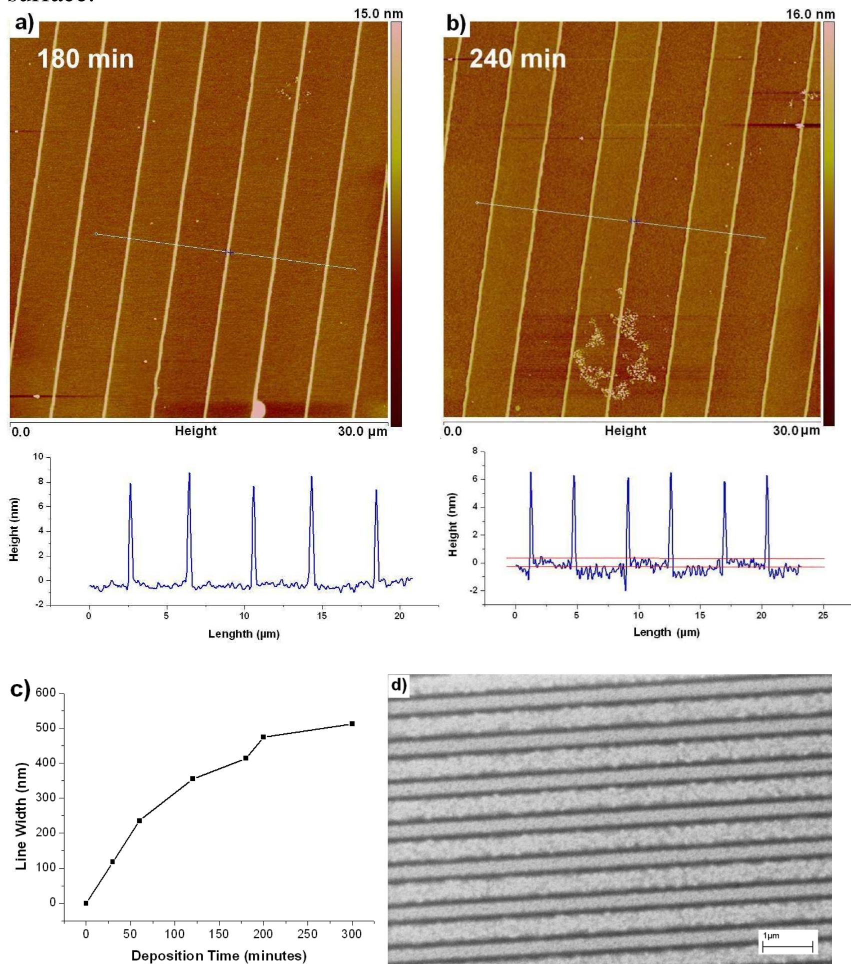

Figure 3: Tapping mode AFM height images and AFM height profiles of MPTS lines formed; a) after 180 min of deposition. b) after 240 min of deposition. The red lines in the height profile in Figure 3b illustrate the height increase of >1 nm of the planar area of the gold substrate. c) Increase of width of edge-condensed lines with time. d) HR-SEM image of condensed MPTS lines of 80 nm width on Au substrate, deposited using a PDMS mold of line width 350 nm, spacing 450 nm and height 200 nm for 1 h at 60°C.

2. Electrodeposition experiments

The patterned MPTS thin films were used as templates to grow Ni and ZnO micro and nanopatterns by electrodeposition. Ni was deposited on the uncovered parts of the MPTS patterned Au substrates using a bath containing nickel sulphate and boric acid at a potential of -1 V. Figure 4a-c show HR-SEM images of Ni line and dot patterns. The Ni line width is ~350 nm and has a spacing of 450 nm.

The square dot patterns have a width of 350 nm, with a spacing of 450 nm between two dots. The patterns were deposited on an area of approximately 1x1 cm^2. We deposited Ni patterns for different periods of time, ranging from 5 s to 120 min. The Ni patterns could be grown up to ~200 nm thickness without significant lateral growth. The rate of deposition was approximately 2 nm/s, and was independent of deposition time. The grown Ni patterns were continuous and smooth irrespective of the deposition time. Longer deposition times (> 2 min) caused lateral growth and resulted in widening of the lines. Figure 4d shows the Ni film thickness as function of deposition time.

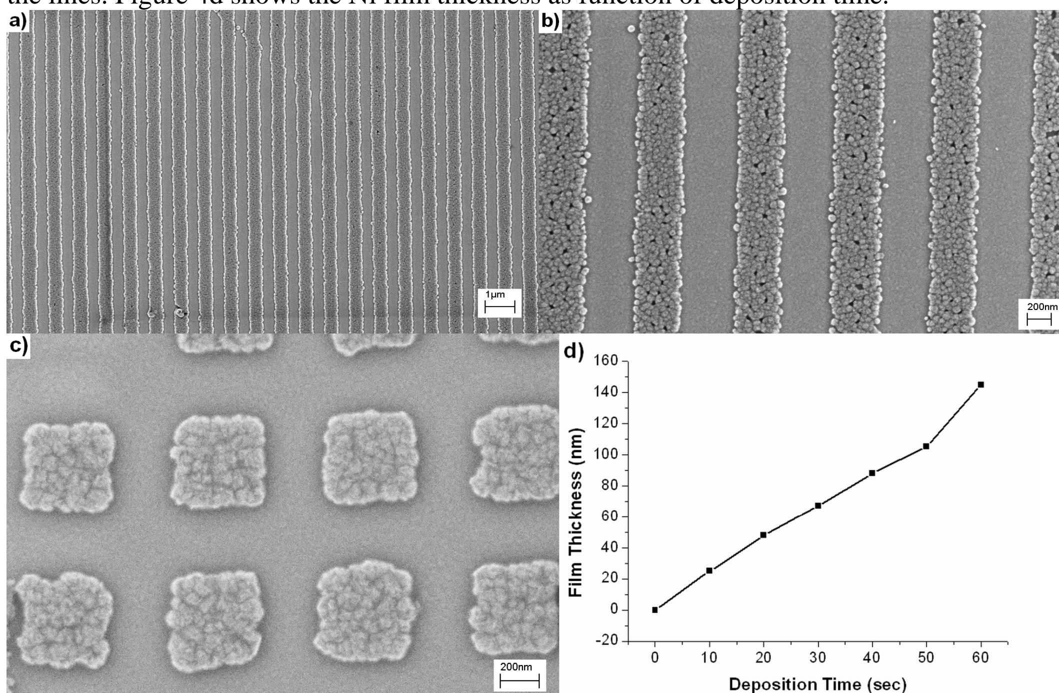

Figure 4: a-b) Ni line patterns with width of ~350 nm at two different magnifications; c) Ni square patterns with a width of ~350 nm; Patterns were grown for 30 s to ~60 nm height; d) Film thickness of Ni pattern by electrodeposition versus deposition time.

Figure 5 a-d show Ni patterns grown on MPTS patterned Au substrates with edge-condensed ~80 nm wide MPTS lines. Figure 5a shows 10 nm thick Ni nanopatterns by electrodeposition for 5 s on a substrate that was made using a nanometer scale-patterned PDMS mold with a line width of 350 nm and a spacing of 450 nm. After the first deposition step the mold was rotated by 90 degrees, followed by a second deposition step under the same conditions to obtain a pattern of crossing lines. The spacing between all rectangular Ni dots was ~ 80 nm, in agreement with the width of the patterned MPTS lines. Figure 5b and 5c show Ni patterns grown for 1 min to obtain a thickness of ~ 120 nm on Au substrates with ring-shaped MPTS patterns. The MPTS patterns had been grown for 3 h to a line width of ~350 nm.

Figure 5d shows a Ni pattern electrodeposited on an MPTS line patterned substrate that had grown for 12 h. In this case the MPTS film covered both corners and planar areas of the substrate. It is noted that the Ni film grew over the MPTS film. The SEM image shows that the density of the Ni film grown on the MPTS monolayer film was lower than the density of the film that had formed on bare patches of the electrode. It shows that the thin MPTS film is not completely isolating the substrate from electron transfer, which could be due to the low chain length of the molecules (>1 nm), and/or small structural defects in the MPTS film. A film of MPTS with a height above ~1.5 nm is completely isolating the substrate from electron transfer, as will be demonstrated below using TUNA conductivity mappings.

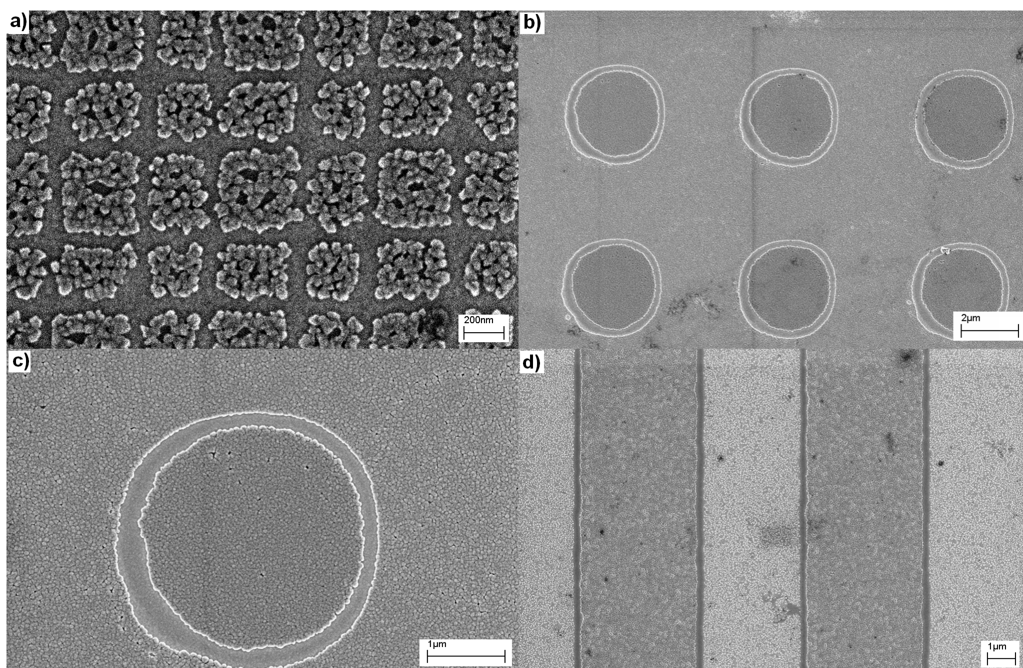

Figure 5: Nickel patterns on MPTS patterned Au substrates. a) Square pattern (thickness 10 nm), MPTS line width ~80 nm; b,c) Inverse ring structure (thickness 120 nm), MPTS line width 350 nm; d) Line patterns (thickness 120 nm) of ~4 µm width, MPTS line pattern had grown for ~ 12 h.

The conductivity of the Ni patterns was characterised via tunnelling AFM (TUNA). Figure 6 shows the contact mode AFM image, TUNA conductivity map, and contact mode height profile of Ni line patterns with a nominal thickness of 20 nm (10 s of deposition time). The contact mode image and conductivity map were recorded simultaneously with an applied sample bias of 1.221 mV versus the AFM tip. The data illustrate the uniform high conductivity of the Ni patterns.

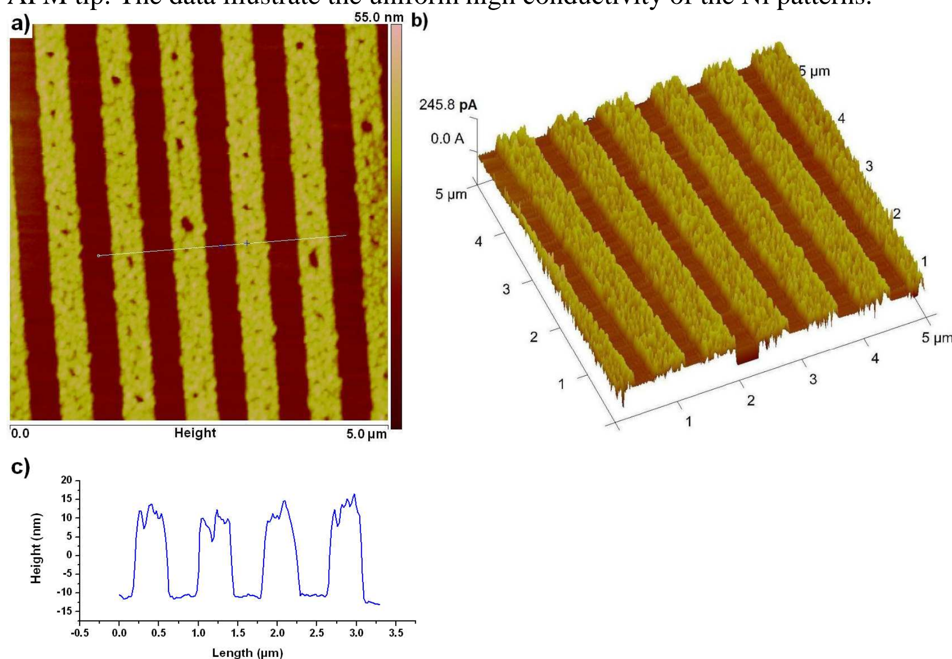

Figure 6: a) AFM contact mode image of Ni pattern on MPTS-prepatterned Au substrate; b) TUNA AFM conductivity map of Ni line pattern recorded at 1.121 mV applied sample bias versus AFM tip; c) contact mode height profile of the same pattern.

Figure 7a shows the *M-H* loops at room temperature at directions 0°, 30°, 60° and 90° with respect to the edge of the substrate. As can be seen in Fig. 7b, both M_r and M_s oscillate with a periodicity of 180°, with the highest value at 0° and the lowest value at 90°. The highest values of M_r and M_s, are 115 and 158 emu/cm^3, respectively.

The saturation magnetization is smaller than that of bulk Ni (484 emu/cm^3) [19]. However, the values did not change much with the change of field angle. This indicates that the films have a weak in-plane magnetic anisotropy. Regarding the origin of magnetic anisotropy in the films, we consider two main sources of the magnetic anisotropy: magnetic dipolar interaction (shape anisotropy) and spin–orbit interactions (magnetocrystalline anisotropy and magneto-elastic anisotropy), as outlined in detail in ref. [20]. As can be seen in the *M-H* loops, the M_r value was much smaller than the M_s value at any filed angle, and the easy axis could not be determined easily. So the magnetocrystalline anisotropy is not dominant and this points to the polycrystalline nature of the electrodeposited Ni patterns. The M_r and M_s values were probably affected by shape anisotropy normally observed in polycrystalline materials.

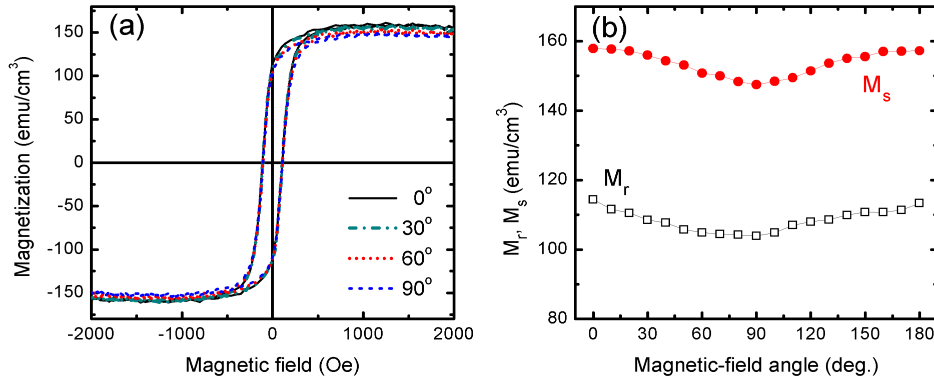

Figure 7: (a) Magnetic hysteresis (*M-H*) loops and (b) Remnant magnetization (M_r) and saturation magnetization (M_s) as a function of field angle of 80 nm thick Ni line arrays with a period of 800 nm and a line width of 450 nm on Au coated Si (100) substrate. The magnetic field was applied in-plane along a number of angles with respect to the direction of the lines.

ZnO patterns were grown from an aqueous zinc nitrate electrolyte solution at a voltage of -1 V versus reference. Figure 8a shows ZnO patterns that were deposited on a MPTS line-patterned substrate with ~400 nm line width. The ZnO patterns have a line width of 450 nm and a spacing of 350 nm. Figure 8b shows ~600 nm wide patterned ZnO lines with a gap of ~150 nm between them. The gap was formed using edge condensation of MPTS for ~ 90 min using a PDMS mold with a line width of 600 nm and a spacing of 800 nm. Figure 8c-d shows a ZnO line pattern grown on a MPTS prepatterned gold substrate. The MPTS lines had been deposited for 60 min, and condensation had occurred preferentially in the corners. The lines had a width of ~160 nm. After ZnO electrodeposition a spacing of ~140 nm was present between the ~ 4 µm wide ZnO lines.

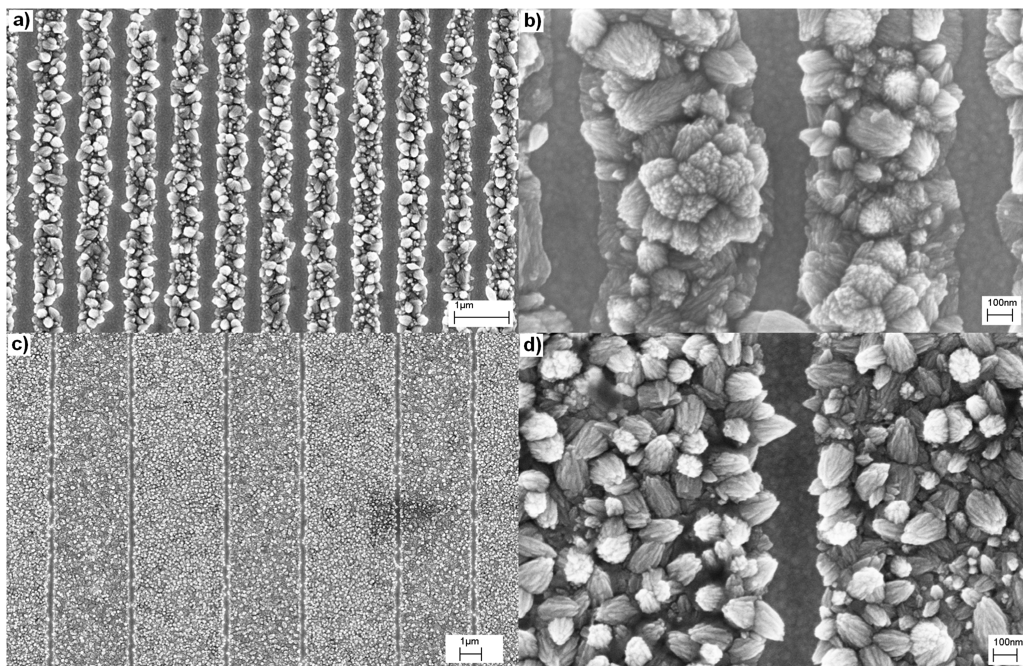

Figure 8: HR-SEM images of ZnO patterns on MPTS pre-patterned Au thin film. a) Line width ~450 nm, spacing ~350 nm; b) line width 550 nm, spacing ~150 nm; c, d) ZnO lines grown on Au substrates with ~150 nm wide MPTS line patterns.

The conductivity of ZnO patterns was also characterized via tunnelling AFM (TUNA). Figure 9a shows a tapping mode AFM image of a MPTS film formed using a PDMS mold with a line width and spacing of ~4µm. The MPTS thin film was grown for 2 h at 70°C to a thickness of ~1.5 nm. A small load was placed on the PDMS mold to keep it in conformal contact with the substrate at this temperature. Figure 9b-e show the contact mode AFM image, TUNA conductivity map recorded at a sample bias of 1 V versus AFM tip, TUNA conductivity map recorded at a sample bias of 3 V versus AFM tip, and an AFM height profile of the ZnO line patterns grown by electrodeposition on MPTS patterned Au substrate as shown in Figure 9a. Figures 9b, 9c and 9e were recorded simultaneously with an applied sample bias of 1 V versus the AFM tip. The data show uniform conductivity of the ZnO patterns. The relatively low tunnelling currents at both applied voltages shows semiconducting nature of ZnO line pattern. In this case the MPTS-covered patches of the substrates showed no conductivity at applied voltages between up to at least 5 V, which illustrates the high electrical resistance of MPTS thin films of ~1.5 to 2 nm thickness. This is very important when they are to be used as resists in electrodeposition processes. Figure 9f shows TUNA *IV* characteristics of electrodeposited ZnO measured at a particular position in a patterned line. The shape of the *IV* curve is characteristic of semiconducting materials, and illustrates the semiconducting behaviour of the ZnO patterns. In order to obtain consistent data, the *IV* characteristics were recorded at several points of the patterned lines.

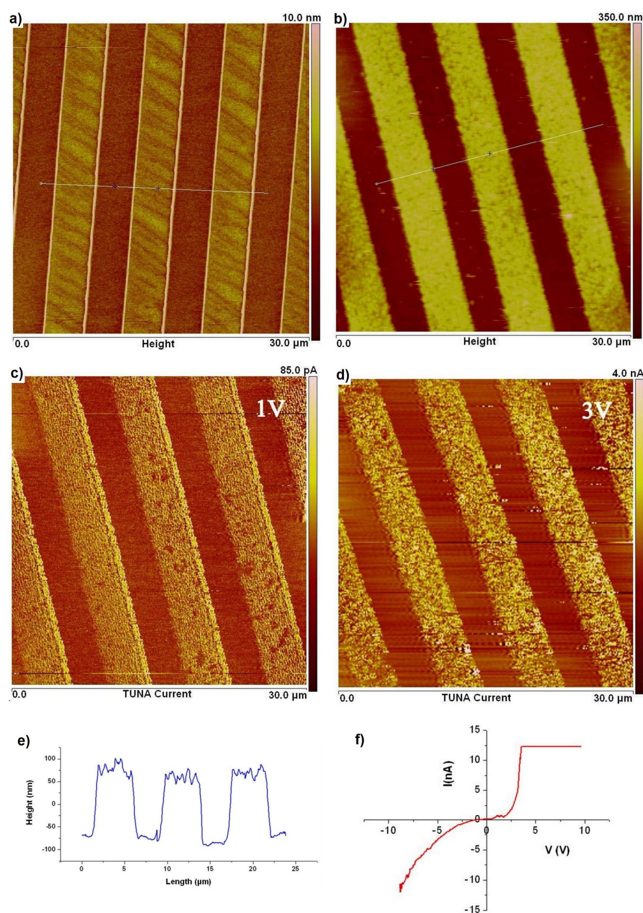

Figure 9: a) Tapping mode AFM image of patterned MPTS thin film grown at 70°C for 2 h; b) Contact mode AFM image of ZnO line pattern electrodeposited on MPTS thin film as shown in (a); c) TUNA conductivity of ZnO line patterns at applied sample bias of 1 V with respect to AFM tip; d) TUNA conductivity of ZnO line patterns at applied sample bias of 3V with respect to AFM tip; e) Contact mode AFM height profile of ZnO pattern. f) TUNA *IV* characteristics of electrodeposited ZnO.

4.4. Conclusions

We presented an easy and cost effective methodology to pattern mercaptosilane thin films on the nanoscale using micro and nanometer-scale PDMS molds. We observed preferable condensation of mercaptosilane molecules in the corners where the vertical wall of the PDMS channel came in contact with the gold substrate during the initial stages of the deposition process, so that very thin lines of MPTS with a width of 80 nm could be established when the deposition time of MPTS was kept limited. After prolonged periods of MPTS deposition, we also observed a thin mercaptosilane layer on all unshielded areas of the substrate, but no film thickness increase was observed when the time of exposure was increased further. When nanometer-scale molds were used the MPTS molecules condensed directly across the width of the channels, due to its small dimensions. The method can be used to pattern mercaptosilane lines down to a lateral dimension of 80 nm on gold substrates. We used mercaptosilane patterns as templates for electrodeposition of Ni and ZnO. The method can be employed to deposit a wide range of functional material patterns that can have potential applications in the fabrication of functional devices. The process is easily upscalable provided that the mold is carefully designed to minimize the diffusion length of condesable vapor inside the channels of the substrate-mold assembly.

4.5. References

1. Kumar, A.; Whitesides, G. M., *Appl. Phys. Lett.* **1993**, *63*, 2002-2004.

2. Pesika, N. S.; Radisic, A.; Stebe, K. J.; Searson, P. C., *Nano Lett*. **2006**, *6*, 1023-1026.

3. Hsu, C.-H.; Yeh, M.-C.; Lo, K.-L.; Chen, L.-J. *Langmuir* **2007**, *23*, 12111-12118.

4. Jeon, N.L.; Finnie, K.; Branshaw, K.; Nuzzo, R.G. *Langmuir* **1997**, *13*, 3382-3391.

5. Biebuyck, H. A.; Larsen, N. B.; Delamarche, E.; Michel, B., *IBM J. Res. Dev.* **1997**, *41*, 159-170.

6. Delamarche, E.; Schmid, H.; Bietsch, A.; Larsen, N. B.; Rothuizen, H.; Michel, B.; Biebuyck, H., *J. Phys. Chem. B* **1998**, *102*, 3324-3334.

7. Dameron, A. A.; Hampton, J. R.; Smith, R. K.; Mullen, T. J.; Gillmor, S. D.; Weiss, P. S., *Nano Lett*. **2005**, *5*, 1834-1837.

8. Zhang, G.-J.; Tanii, T.; Zako, T.; Hosaka, T.; Miyake, T.; Kanari, Y.; Funatsu, T.; Ohdomari, I., *Small* **2005**, *1*, 833-837.

9. Pallandre, A.; Glinel, K.; Jonas, A. M.; Nysten, B., *Nano Lett*. **2004**, *4*, 365-371.

10. Maoz, R.; Frydman, E.; Cohen, S. R.; Sagiv, J., *Adv. Mater.* **2000**, *12*, 725.

11. Rosa, L. G.; Jiang, J. Y.; Lima, O. V.; Xiao, J.; Utreras, E.; Dowben, P. A.; Tan, L., *Mater. Lett.* **2009**, *63*, 961-964.

12. Seo, K.; Borguet, E., *Langmuir* **2006**, *22*, 1388-1391.

13. Anderson, M. E.; Srinivasan, C.; Hohman, J. N.; Carter, E. M.; Horn, M. W.; Weiss, P. S., *Adv. Mater.* **2006**, *18*, 3258-3260.

14. Maury, P.; Péter, M.; Mahalingam, V.; Reinhoudt, D. N.; Huskens, J., *Adv. Funct. Mater.* **2005**, *15*, 451-457.

15. George, A.; Blank, D. H. A.; ten Elshof, J. E., *Langmuir* **2009**, *25*, 13298-13301.

16. Maas, M.G.; Rodijk, E.J.B.; Maijenburg, A.W.; Blank, D.H.A.; Ten Elshof, J.E., *J. Mater. Res.* **2011**, DOI: 10.1557/jmr.2011.93.

17. Veeco AFM Manual, Application Modules, Nanoscope V7-B (004-1020-000).

18. Rascon, C.; Parry, A. O., *Nature* **2000**, *407*, 986-989.

19. Chow, G. M.; Zhang, J.; Li, Y. Y.; Ding, J.; Goh, W. C., *Mater. Sci. Eng. A* **2001**, *304-306*, 194-199.

20. Johnson, M. T.; Bloemen, P. J. H.; denBroeder, F. J. A.; deVries, J. J., *Rep. Prog. Phys.* **1996**, *59*, 1409-1458.

Chapter 5

Patterning of Organosilane Molecular Thin Films from Gas Phase and its Applications: Fabrication of Multifunctional Surfaces and Large Area Molecular Templates for Site Selective Material Deposition

*This chapter is submitted to an international journal

Abstract:

A simple methodology to fabricate micro and nanometer-scale patterned surfaces with multiple chemical functionalities is presented. Patterns with lateral dimensions down to 110 nm were made. The fabrication process involves multi-step gas phase patterning of amine, thiol, alkyl and fluorinated alkyl-functional organosilane molecules using PDMS molds as shadow masks. Also a combination process of channel diffused plasma etching of organosilane molecular thin films in combination with masked gas phase deposition to fabricate multi-length scale, multi-functional surfaces is demonstrated.

5.1. Introduction

Patterning of organosilane self-assembled monolayers (SAMs) and thin films on silicon substrates [1] has attracted a wide interest due to the ability of patterned SAMs to act as etch resists [2] or as templates for area selective atomic layer deposition [3,4], solution phase deposition [5], or electroless deposition [6]. Patterned organosilanes have also been used for site selective immobilization of nanoparticles [7], biomaterials [8,11] and polymers [7]. Deposition of organosilanes with different chemical functionalities can be used to create multifunctional surfaces in micrometer and nanometer scale [9,10]. This makes patterned SAMs very promising for future micro- and nanofabrication technologies for nanoelectronics, data storage and sensing devices.

Several serial and parallel technologies to pattern organosilane SAMs on various substrates have been demonstrated, including electron beam lithography (EBL) [9,11], ion beam lithography (FIB) [12], photolithography [13,14], scanning probe lithography [15,16], nanoimprint lithography [7], colloidal lithography [10] and microcontact printing [4]. Serial processes including EBL, FIB and scanning probe techniques are excellent tools to generate high resolution material patterns down to a resolution in the order of sub-10 nm [9,11,12]. However, due to the serial nature of these processes and their high capital investment and maintenance costs, these methods can only be used as research tools. Scaling-up for industrial applications is difficult. Photolithography requires standard clean room conditions but can be employed for large area patterning of organosilane molecules [13,14] and yields high quality patterns with resolutions up to the diffraction limit of the light used for patterning process [17]. Nano imprint lithography (NIL) has also been demonstrated as a tool for the patterning organosilane SAMs/thin films. NIL provides capability to pattern SAMs in sub-100 nm resolutions. The process is a multi-step process that includes the patterning of a resist at high temperature and pressure, followed by plasma etching of the residual resist layer before organosilane deposition [7]. Microcontact printing provides an alternative method, by using an elastomeric polydimethylsiloxane (PDMS) stamp that is employed for large area, fast patterning of organosilane molecules by controlled release of organosilane inks to the receiving substrate [4]. Here the challenges are to overcome the limitations of ink diffusion [18], which may cause large defect concentrations in the fabricated patterns, and to increase the resolution to sub-micrometer dimensions without compromising the

quality of the replication process. The reason is that the elastomeric property of the PDMS stamp can lead to mechanical deformation at high resolutions, thereby limiting the fidelity of the process.

Recently, we demonstrated a single step process to pattern organosilane SAMs or thin films from the gas phase using PDMS mold templates on silicon substrates [19,20]. A schematic diagram of the patterning process is shown in Figure 1. PDMS molds with micrometer scale features were used to pattern nanometer scale organosilane patterns by selectively condensing organosilane vapor at the corners formed between the protruding features of the PDMS mold and the Si substrate in a short time period (up to 5 h). This resulted in features with lateral sizes of less than 100 nm. Upon increasing the deposition time the entire unshielded substrate area also became covered with deposited organosilane molecules, resulting in micrometer-scale features.

In the present contribution we demonstrate that the same approach can also be used to generate multiple patterned surfaces. Surfaces with multiple patterned chemical functionalities are interesting both for fundamental research and device fabrication technologies. Patterning of organosilane molecules with multiple chemical functionalities can be an ideal strategy to create surfaces with multifunctional surfaces as described previously by different techniques such as electron beam lithography [9], colloidal lithography [10], photolithography [21] and photochemical modification [22,23]. As will be shown, gas phase patterning of organosilanes is a simple, fast and cost effective methodology to create multifunctional surfaces with control over dimensions and geometry. We also demonstrate the applicability of patterned organosilane molecular thin films by using them as templates for site-selective immobilization of nanoparticles and area selective atomic layer deposition (ALD).

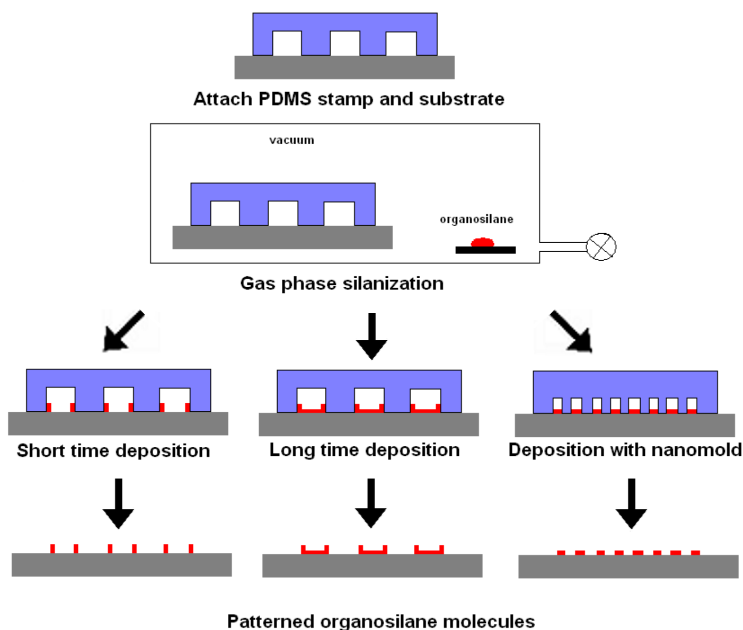

Figure 1: Schematic diagram of the patterning process, showing the influence of variation of feature size and deposition time on pattern formation.

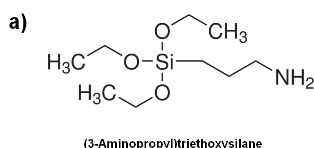

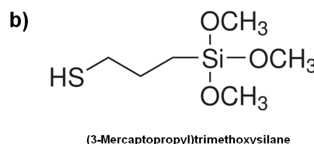

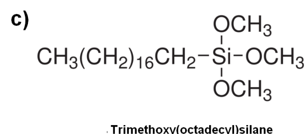

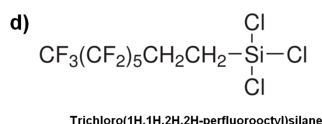

Figure 2: Schematic diagram of the organosilane molecules used for experiments as illustrated in suppliers website (Sigma Aldrich)

5.2. Experimental section

Preparation of PDMS Molds: PDMS and curing agent (Sylgard 184) were purchased from Dow Corning Corporation and mixed in a ratio 8:1 and poured over the micro/nanopatterned silicon master (created by photolithography or e-beam lithography). The PDMS was cured at a temperature of 70 ^{o}C for 48 h. After curing, the PDMS molds were removed from the master and cut into pieces of desired size and stored in absolute ethanol for 15 days before use. Every 5 days, the PDMS molds were taken out of the ethanol, washed with ethanol, and stored again in fresh ethanol. This treatment reduced the amount of unreacted PDMS oligomers in the mold which might otherwise contaminate the substrate during the patterning process. After this treatment, the PDMS molds were dried at 90 ^{o}C for 3 h to remove any trace of ethanol prior to use.

Preparation of Silicon Substrates: P-Type silicon substrates cleaned with piranha solution (a mixture of H_2O_2 and H_2SO_4 in 1:3 volume ratio) were used in the experiments. Caution! Due to potential risk of explosion this treatment has to be carried out with proper safety precautions. The substrates were then washed several times with deionized water and stored in deionized water. Prior to use, the substrates were blow-dried in a nitrogen stream.

Fabrication of Organosilane Patterns: (3-Aminopropyl)-triethoxysilane (APTES, 98% pure), (3-Mercaptopropyl)methyltrimethoxysilane (95% purity), octadecyltrimethoxysilane (OTS, 97% pure) and 1H,1H,2H,2H-perfluorooctyl-trichlorosilane (97% purity) were purchased from Sigma Aldrich and used as received. A schematic diagram of the chemical structure of the organosilanes used in the experiments is shown in Figure 2. The dried PDMS molds with micro/nanopatterned features were gently pressed against silicon substrates facing the patterned side of the mold against the polished side of the silicon substrate. The PDMS mold made conformal contact with the substrate via attractive Van der Waals forces. The desiccators were pre-heated in an oven at 120°C before organosilane deposition in order to remove adsorbed water and obtain a low humidity deposition environment inside the desiccator. Substrates with a bonded PDMS mold were transferred to a desiccator. A drop of organosilane was placed in the desiccator. The desiccator was closed, and after evacuation of the atmosphere by a mechanical pump to 100 mbar, an organosilane vapor-saturated environment formed inside. The substrates were exposed to the organosilane vapor for 0.5 - 48 h. The substrates were taken out from the desiccator and washed with absolute ethanol followed by deionized water and then stored for further analysis.

Fabrication of multifunctional surfaces: Two different types of organosilane were deposited in two successive gas phase deposition processes. After depositing the first organosilane pattern, the PDMS mold was rotated by 90° and the second type of organosilane was deposited. Several fabrication schemes are shown in the Supporting Information.

Combination of channel diffused plasma surface modification and gas phase patterning: An OTS monolayer on silicon wafer (without using any PDMS mold) was made by gas phase deposition at 90^oC for 12 h inside an evacuated desiccator. The PDMS stamps with micro/nano-patterned features were gently pressed against the SAM-coated substrates. The patterned side of the stamp faced the SAM-coated side of the substrate. The PDMS stamp made conformal contact with the substrate via attractive Van der Waals forces. The substrate-stamp assembly was transferred to an oxygen plasma cleaner (Harrick Plasma) operating at 25 W at a pressure < 1 mbar. The substrates were exposed to oxygen plasma for 20 min. After plasma surface modification the PDMS stamp was peeled off the substrate. Then a second organosilane pattern was formed by gas phase deposition using a PDMS mold as template, as explained in the previous section.

Atomic Layer Deposition: ALD deposition was carried out using a commercial ALD reactor (Savannah 100, Cambridge Nanotech Inc) operating with Ar as carrier gas. 20 cycles of ZnO deposition, corresponding to a pattern thickness of 5 nm, was carried out at 120^oC with diethyl zinc ($Zn(C_2H_5)_2$, DEZ) and water as precursors. Pulsing and purging times of 0.5 and 10 s were applied for DEZ, and of 1.3 and 10 s for water.

Preparation of Au nanoparticles and site selective adsorption: Gold(III) chloride trihydrate ($HAuCl_4{\cdot}3H_2O$), purity 99.9%) and sodium citrate dihydrate ($HOC(COONa)(CH_2COONa)_2{\cdot}2H_2O$, purity 99%) was obtained from Sigma-Aldrich. A colloidal solution of gold nanoparticles was prepared, as described in ref. [24]. The substrates were immersed in the gold nanoparticle solution for 12 h to immobilize the nanoparticles on the mercaptosilane line patterns on Si substrate.

Characterization: The patterned organosilane thin films were characterized using atomic force microscopy (AFM, Veeco Dimension Icon by Bruker Nano) for surface morphology and X-ray photoelectron spectroscopy (XPS, Quanta SXM scanning electron microprobe, Physical Electronics) for surface elemental information. Helium ion microscopy (HIM, UHV Orion+ Carl Zeiss NTS) [25] was used to image substrates with multiple organosilane patterns. HIM utilizes a beam of He ions to scan the specimen surface with a sub-nanometer spot size. Secondary electrons generated by the ions during interaction with the sample are used for image formation. Good lateral resolution (<0.5 nm), a high surface sensitivity and the possibility to image charging samples distinguishes this technique from conventional scanning electron microscopy. High resolution scanning electron microscope (HR-SEM, Zeiss 1550) was used to image patterns of ALD deposited ZnO and Au nanoparticles patterns.

5.3. Results and discussion

5.3.1. Formation of multiple functional surfaces by sequential gas phase deposition of organosilane patterns

An example of a patterned 3-aminopropyl-silane (APTES) SAMs on Si wafer after deposition for 4 h is given in Figure 3a, where a tapping mode AFM height image and profile are shown. The height of the features is 8-9 nm. The PDMS mold used for this pattern has a line width of ~1 µm and a spacing of ~1.5 µm over a total area of 1 cm^2. The AFM image and height profile show no indications of the presence of aminosilane molecules on the planar patches in between the condensed lines of aminosilane molecules in the corners. To study the influence of deposition time on pattern formation, edge-patterned APTES molecules were deposited at room temperature for periods ranging from 30 min to 48 h, followed by tapping mode AFM scans. PDMS with patterned channels of approximately ~ 4 µm width and ~2 µm height were used. The height of the edge features remained almost constant with increasing deposition time. The width of the condensed lines can be controlled by varying the deposition time, as shown in Figure 4. After 5-6 h of deposition isolated clusters of organosilane molecules could be observed on the planar areas in between the corner-condensed organosilane lines. A continuous thin film formed when the samples were exposed to the organosilane vapour for longer periods of time, and after 8 h of deposition all unshielded regions were completely covered with 3-aminopropyl-silane molecules as shown in Figure 3b. However, the relationship line width-deposition

time varies with the geometry and edge features of the PDMS stamps. Smaller features were obtained when using PDMS stamps with sharp edges at the protruding features [20]. We observed similar behavior when other organosilane molecules, such as mercaptopropylsilane, octadecylsilane, perfluorooctylsilane, etc., were used [19,20].

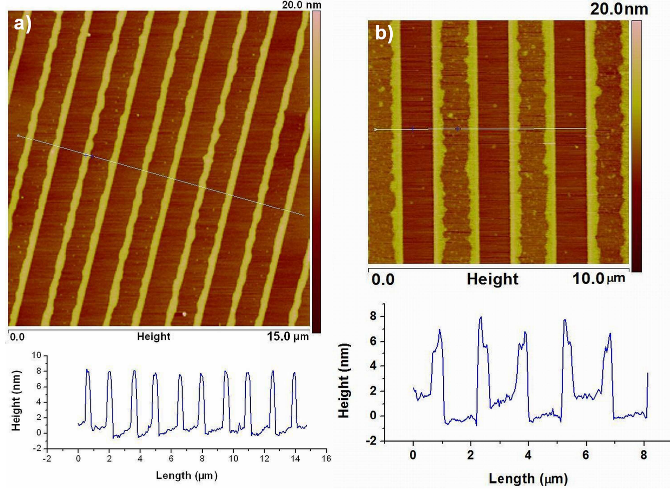

Figure 3: a) APTES line patterns (line width 300 nm and spacing 1.1 µm) formed over Si substrate after 4 h of deposition by edge condensation. b) APTES line pattern (line width 1.3 µm and spacing 1 µm) after 8 h of deposition, showing the presence of an APTES thin film in between the thick corner-condensed lines.

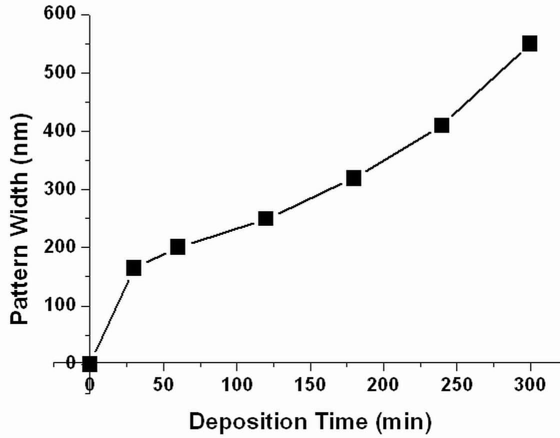

Figure 4: Increase of line width of corner-condensed lines with time. The experiments were performed with a PDMS mold with channel width and spacing of 4 µm, and a channel height of 2 µm.

The effective diameter d of most organosilanes is ~0.8 nm. The saturation vapour pressure of APTES and octadecyltrimethoxysilane at 293 K are 2 Pa and 1.3 Pa [26], respectively. The background pressure inside the desiccator, p, is ~ 10 kPa. So the mean free path $\lambda = k_B T/(\sqrt{2}\pi d^2 p)$ (k_B is the Boltzmann constant, and T the temperature) in the gas phase is of the order of 200 nm. This is an order of magnitude smaller than channel dimensions. The predominant mechanism of gas transport inside the mold is therefore bulk diffusion. The organosilanes condense first at the PDMS-silicon-air triple phase boundary lines due to the increased Van der Waals interaction in the corners formed between the PDMS mold and the substrate as described by Rascon and Perry [27]. We also tested the deposition of organosilanes on other substrates, including Au and 1H,1H,2H,2H-perfluorooctylsilane SAM coated silicon substrates. Interestingly, we observed preferential condensation of APTES in the corners even with hydrophobic substrates such as the perfluorooctylsilane SAM coated silicon wafer.

No difference in condensation behaviour was observed when hydrophilic substrates were used instead of hydrophobic ones. Figure 5 shows a secondary electron HIM image of a substrate patterned with perfluorooctylsilane and mercaptosilane, produced by multiple silanization steps. First an antidot pattern of perfluorooctylsilane was deposited from the gas phase using a PDMS mold with circular pillars with a feature of 2 µm, and a spacing of 2 µm during 12 h at 60°C. The pattern has essentially SiO_2 patches of ~2 µm diameter, embedded in a patterned matrix of a perfluorooctylsilane SAM. The fluorinated areas are indicated as Area 1 in Figure 5. Then a second silanization step from the gas phase was performed using (3-mercaptopropyl)methyltrimethoxysilane and a PDMS mold with line features of 1 µm width and 1.3 µm spacing, for 12 h at 60 °C,. The condensed mercaptopropylmethylsilanes formed a continuous film on the SiO_2 patches to which it was exposed, and only edge-patterned lines on the fluorinated silane regions. The mercaptosilane SAM patches on SiO_2 are indicated as Area 2. Although mercaptosilanes cannot react easily with a perfluorosilane SAM, they showed preferential condensation on perfluorosilane regions in the corner areas due the increased interaction as a result of size confinement. The HIM images clearly proved this hypothesis.

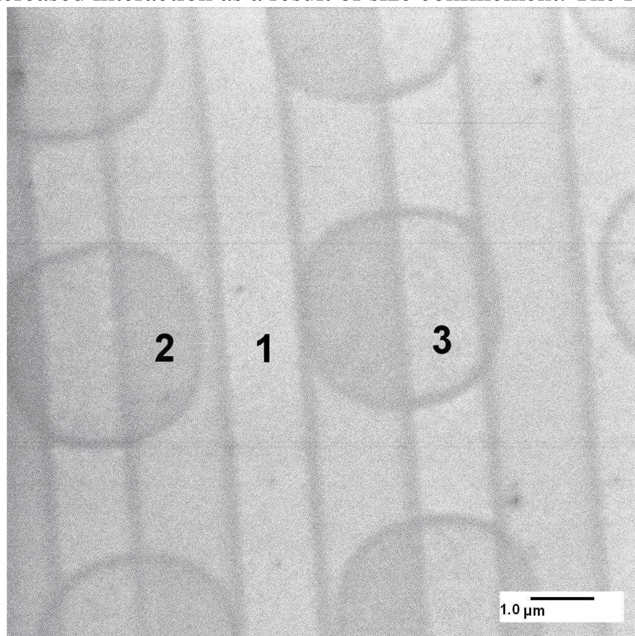

Figure 5: Helium Ion Microscopic (HIM) image of a silicon oxide substrate, patterned with two different organosilanes deposited in two successive gas phase silanization steps using different PDMS molds. The different surface terminations yield different contrast depending on their work function. Area 1: perfluorooctylsilane layer. Area 2: mercaptosilane layer. Area 3: Native SiO_2 surface.

We also used PDMS molds with sub 200-nanometer-scale features for patterning organosilanes from the gas phase. Figure 6 shows tapping mode height profiles of OTS patterns on a Si substrate, deposited at room temperature. The PDMS mold used has a line width of 140 nm, a spacing of 110 nm and a height of 110 nm. When the dimensions diminished no preferential corner condensation was observed. In this experiment the channel dimensions were smaller than the mean free path of the organosilane molecules. This led to a situation in which no preferential corner condensation occurred and the OTS molecules condensed directly as a flat thin film of ~ 4 nm thickness, as shown in Figure 6.

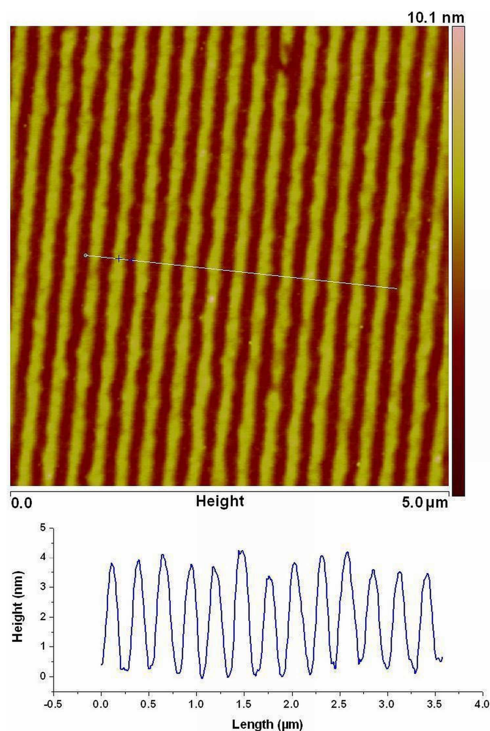

Figure 6: OTS pattern formed on Si substrate with a line width of 110 nm and a spacing of 140 nm.

Figure 7a shows a tri-functional surface fabricated by a two-step gas phase deposition process using a PDMS mold with meandering line patterns. First a perfluorooctylsilane pattern (Area 2) was formed by gas phase patterning at 60 ^{o}C for 10 h using a PDMS mold with meandered line patterns as patterning mask. Then a second masked gas phase deposition step was employed by first rotating the mold by 90° angle, followed by depositing a mercaptopropylsilane (Area 3) pattern at 60 ^{o}C for 6 h. The difference in morphology, i.e., planar condensation in Area 2 and corner condensation in Area 3, is caused by the difference in deposition times. The final surface contains three different chemical functionalities: perfluorooctylsilane, mercaptopropylsilane, and SiO_2 (Area 1). The meandering lines have a width of 5.5 µm separated by 23.5 µm between the lines. Figure 7b shows a similar trifunctional surface fabricated using a PDMS mold with line width and spacing of 4 µm. The surface has three different areas; SiO_2 (area 1), perfluorooctylsilane (area 2) and mercaptopropylsilane (area 3). All deposition steps were monitored with tapping mode AFM scans and XPS. The XPS data confirming the presence of the elements sulphur and fluorine from mercaptosilane and perfluorosilane, respectively, are provided in the supporting information.

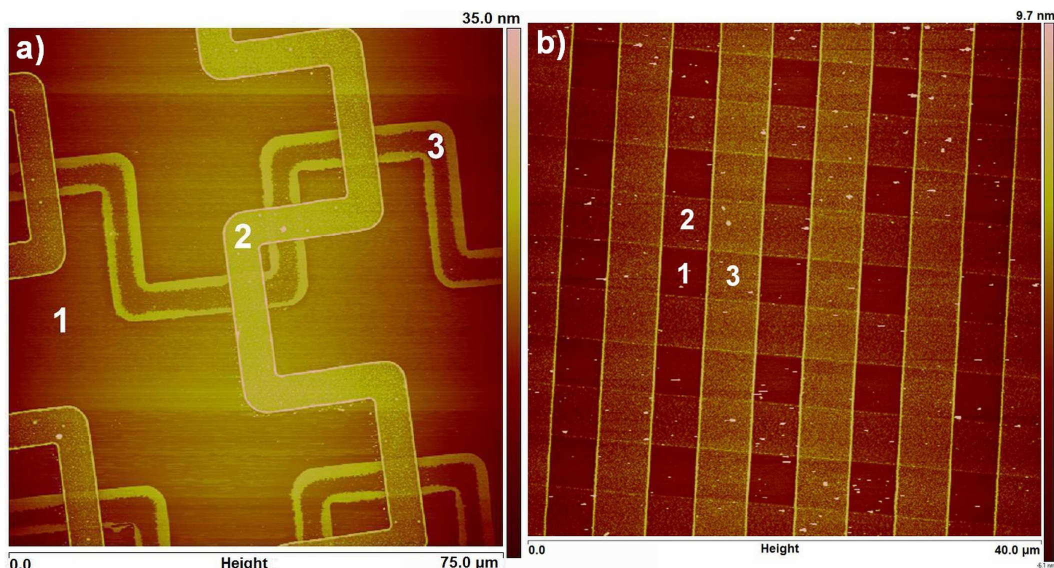

Figure 7: Multifunctional surfaces fabricated by two step gas phase patterning process. a) Tri-functional surface fabricated using PDMS mold with meandering line patterns. The surface has three types of regions: SiO_2 (area 1). perfluorooctylsilane (area 2) and mercaptopropylsilane (area 3). b) Tri-functional surface fabricated using PDMS mold with line features of ~4 µm width and spacing. The surface has three types of regions: SiO_2 (area 1), perfluorooctylsilane (area 2), and mercaptopropylsilane (area 3).

We employed also another soft lithographic method, termed channel diffused plasma surface modification [28,29], in combination with masked gas phase patterning to fabricate more complex multifunctional surface patterns on multiple length scales. In the example shown in Figure 8a, an OTS SAM that covered the entire substrate was made first. Then the SAM was patterned by channel diffused oxygen plasma surface modification. Area 1 in the figure indicates the masked areas of the OTS SAM, and area 2 indicates the OTS-oxidized regions. Oxygen plasma exposure of the C_{18} hydrocarbon chains of OTS creates OH, CO-, and COOH- terminated regions [28]. After this plasma patterning step another PDMS mold with similar features but rotated by 90° with respect to the underlying pattern was placed onto the substrate, and an edge patterning step using 3-mercaptopropylsilane was carries out. The result was a trifunctional surface with (1) hydrophobic $C_{18}H_{37}$- terminated OTS patches, (2) hydrophilic plasma-treated OTS lines with OH, CO-, and COOH- surface terminations, and (3) thiol-terminated silane lines, as shown in Figure 8b and 8c.

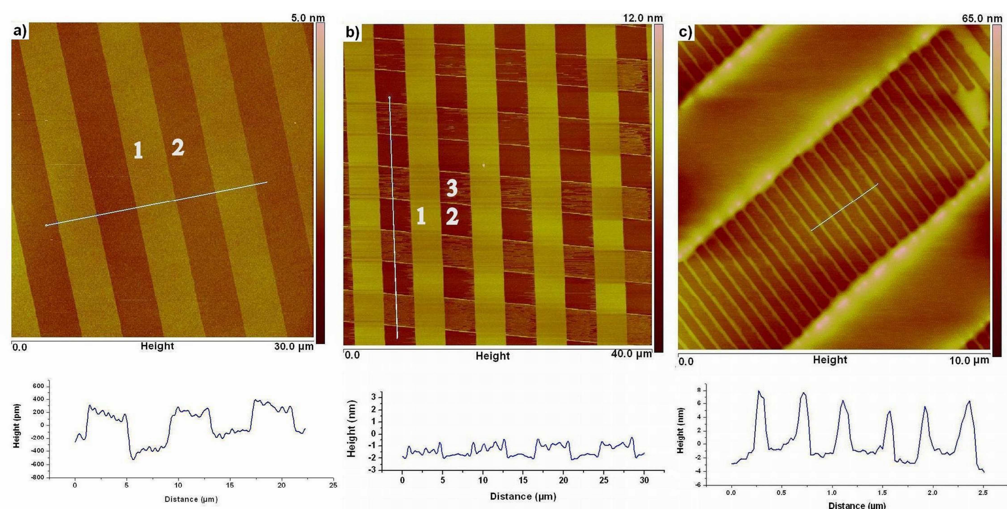

Figure 8: Multifunctional surfaces fabricated by a combination of channel diffused plasma surface modification of SAMs and gas phase patterning process. a) AFM height image and height profile of surface created by a channel diffused plasma modified pattern of an OTS SAM film (line width 4 µm, spacing 4 µm). Area 1 is the original OTS SAM; area 2 is the oxygen plasma modified area of the OTS SAM; b) Tri-functional surface created from the previous pattern by rotating the PDMS mold by 90° angle, followed by gas phase patterning of mercaptopropylsilane monolayer. Area 1 is the original OTS SAM, area 2 the plasma-functionalized OTS SAM, and area 3 is the mercaptopropylsilane-functional region. c) A multi-length scale multifunctional patterned surface similar to Figure 6b. The MPTS lines have a dimension of 450 nm and the –COOH functionalized area has a dimension of 350 nm.

Figure 9a and 9b show nanoscale tri-functional surfaces produced by the combination technique of channel diffused plasma patterning and gas phase pattern deposition. First an OTS monolayer was patterned by channel diffused plasma patterning to obtain 600 nm oxidized lines of OTS, each separated by 800 nm. Then another PDMS stamp with line features was placed on the oxidized line patterns under a 90° angle to the oxidized lines. Mercaptosilane lines with a line width of 450 nm and a spacing of 350 nm between lines were formed in this step. The final surface contains three different chemical functionalities: OTS (area 1), mercaptopropylsilane (area 2), and oxidized OTS (area 3).

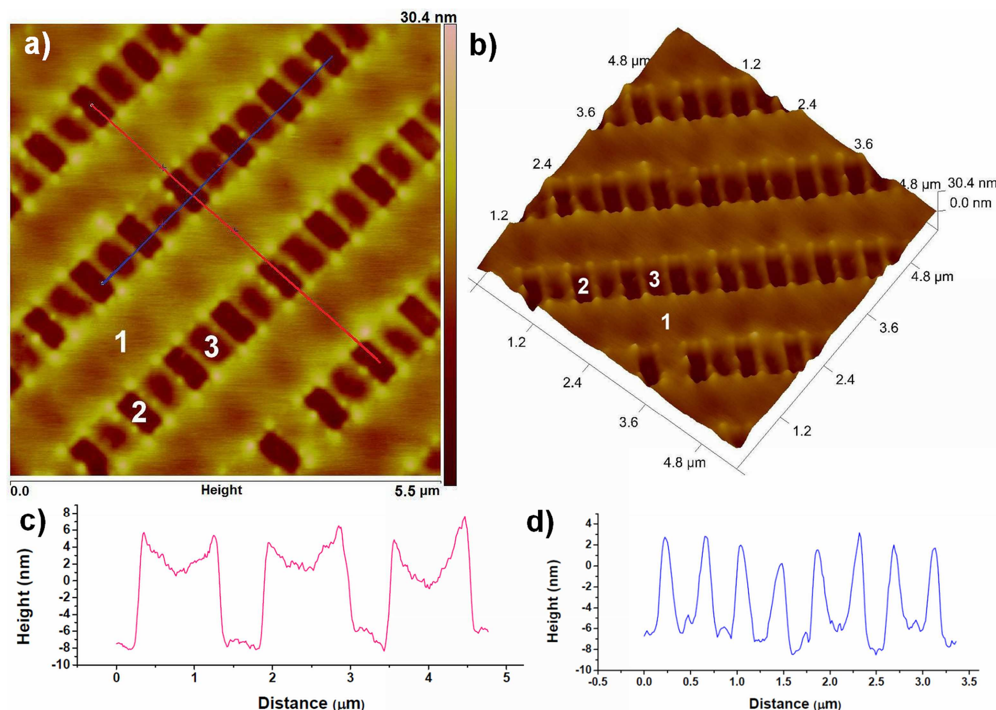

Figure 9: Nanoscale multifunctional surfaces fabricated by a combination of channel diffused plasma surface modification of SAMs and gas phase patterning process. a) Tapping mode AFM height image; b) tapping mode surface morphology; c) AFM height profile of OTS lines corresponding to the red line in Figure 9a; d) AFM height profile of mercaptosilane lines corresponding to the blue line in Figure 9b. Area 1 represents the original OTS SAM; Area 2 represents the oxygen plasma modified area of the OTS SAM; Area 3 represents mercaptosilane patches. The unmodified OTS lines have a width of 800 nm with a spacing of 600 nm between each line. The mercaptosilane patches have a width of 450 nm and a spacing of 350 nm between each patch.

5.3.2. Area selective ALD of ZnO

Atomic layer deposition (ALD) is a versatile technique to fabricate ultrathin conformal layers of materials such as ZnO [30,31], TiO_2 [31,32] and Al_2O_3 [31,32], using a surface reaction of organometallic precursors from the gas phase under controlled physical and chemical conditions [31,32,33]. Here we used nanopatterned perfluorooctylsilane monolayers as templates for ALD of ZnO line patterns. After perfluorosilane SAM deposition the substrate was treated with a freshly prepared piranha solution for 1 min to maximize the concentration of hydroxyl groups on the non-perfluorinated regions of the substrate. The hydroxyl groups on the surface of the SiO_2 substrate promote the initiation of the ALD reaction by chemisorbing the organometallic precursor, in this case DEZ, and providing reactive sites for water to form ZnO in the subsequent half-reaction.. The perfluorinated areas are hydrophobic, and no ALD reaction occurs there, since neither DEZ nor water can chemisorb. Figure 9a and 9b show HR-SEM images of ZnO patterns (~90 nm line width and 140 nm spacing) formed selectively on the hydrophilic regions of a perfluorooctylsilane patterned substrate. Figure 9c shows AFM height profile and Figure 9d shows the AFM-3D topography of the ZnO lines. The formation of ZnO by ALD was confirmed by XPS.

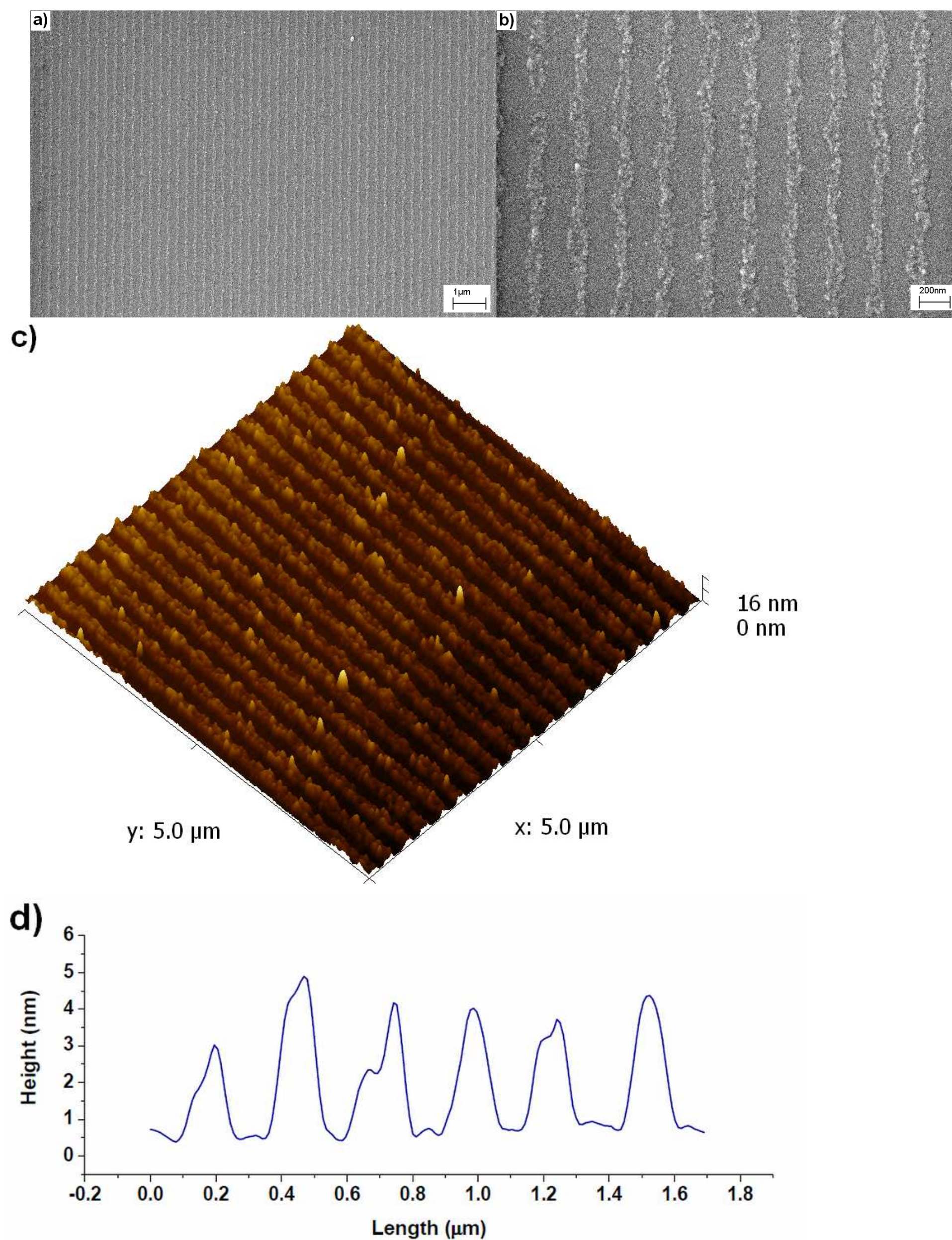

Figure 9: a-b) Nanoscale ZnO line patterns fabricated on perfluorooctylsilane patterned Si substrate by 20 cycles of ALD. The lines have a width of 90 nm and a spacing of 140 nm. The height of the ZnO lines is ~4 nm. c) AFM 3D surface topography. d) AFM height profile of the ZnO pattern.

5.3.3. Site selective immobilization of Au nanoparticles

Figure 8 shows a HR-SEM image of Au nanoparticles that were selectively immobilized on mercaptopropylsilane lines on a Si substrate. The thiol-functional groups of the silane nanopattern reacted with the surface of the Au nanoparticles in solution to form covalent S-Au bonds to attach the particles to the surface. The mercaptosilane patterns have a line width of 350 nm and the spacing between the lines is 450 nm. The homogeneous distribution of Au nanoparticles on the prepatterned lines illustrates the quality of the prepatterning process.

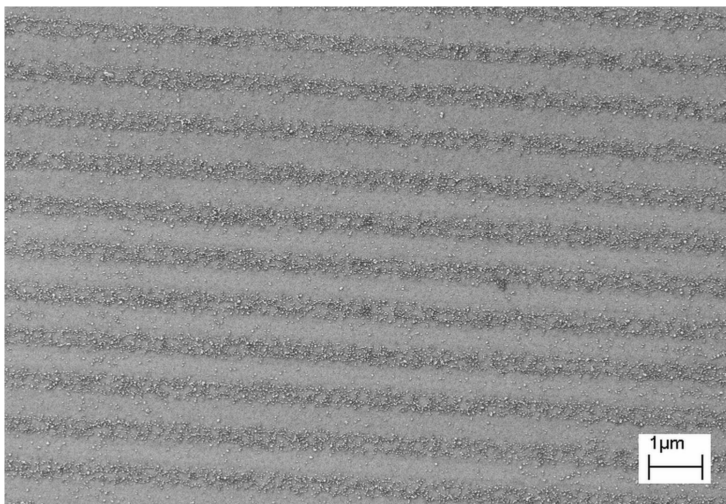

Figure 10: Au nanoparticles selectively immobilized on mercaptosilane lines patterned by gas phase pattern deposition

5.4 Conclusions

Sequential gas phase deposition of organosilane molecules and a combination process of channel diffused plasma surface modification along with gas phase pattern deposition were successfully demonstrated as a tool to create multifunctional surfaces. We successfully created di-, and tri-functional surfaces using different organosilane molecules. The applicability of nanopatterned organosilanes for site-selective adsorption of nanoparticles and site-selective atomic layer deposition was demonstrated.

5.5 References

1. Onclin, S.; Ravoo, B. J.; Reinhoudt, D. N. *Angew. Chem. Int. Ed.* **2005**, *44*, 6282-6304.

2. Jiang, P.; Li, S.-Y.; Sugimura, H.; Takai, O. *Appl. Surf. Sci.* **2006,** *252*, 4230-4235.
3. Chen, R.; Kim, H.; McIntyre, P. C.; Bent, S. F. *Appl. Phys. Lett.* **2004**, *84*, 4017-4019.

4. Yan, M.; Koide, Y.; Babcock, J. R.; Markworth, P. R.; Belot, J. A.; Marks, T. J.; Chang, R. P. H. *Appl. Phys. Lett.* **2001**, *79*, 1709-1711.

5. Koumoto, K.; Seo, S.; Sugiyama, T.; Seo, W. S.; Dressick, W. J., *Chem. Mater.* **1999**, *11*, 2305-2309.

6. Saito, N.; Haneda, H.; Sekiguchi, T.; Ohashi, N.; Sakaguchi, I.; Koumoto, K. *Adv. Mater.* **2002**, *14*, 418-421.

7. Maury, P.; Péter, M.; Mahalingam, V.; Reinhoudt, D. N.; Huskens, J. *Adv. Funct. Mater.* **2005**, *15*, 451-457.

8. Blawas, A. S.; Reichert, W. M. *Biomaterials* **1998**, *19*, 595-609.

9. Pallandre, A.; Glinel, K.; Jonas, A. M.; Nysten, B. *Nano Lett.* **2004**, *4*, 365-371.

10. Ogaki, R.; Cole, M. A.; Sutherland, D. S.; Kingshott, P. *Adv. Mater.* **2011,** *23*, 1876-1881.

11. Zhang, G.-J.; Tanii, T.; Zako, T.; Hosaka, T.; Miyake, T.; Kanari, Y.; Funatsu, T.; Ohdomari, I. *Small* **2005**, *1*, 833-837.

12. Ada, E. T.; Hanley, L.; Etchin, S.; Melngailis, J.; Dressick, W. J.; Chen, M.-S.; Calvert, J. M. *J. Vac. Sci. Technol. B* **1995**, *13*, 2189-2196.

13. Dulcey, C. S.; Georger, J. H., Jr.; Krauthamer, V.; Stenger, D. A.; Fare, T. L.; Calvert, J. M., *Science* **1991**, *252*, 551-554.

14. Herzer, N.; Hoeppener, S.; Schubert, U. S. *Chem. Commun.* **2010**, *46*, 5634-5652.

15. Maoz, R.; Frydman, E.; Cohen, S. R.; Sagiv, J., *Adv. Mater.* **2000**, *12*, 725-731

16. Rosa, L. G.; Jiang, J. Y.; Lima, O. V.; Xiao, J.; Utreras, E.; Dowben, P. A.; Tan, L. *Mater. Lett.* **2009**, *63*, 961-964.

17. Mijatovic, D.; Eijkel, J. C. T.; van den Berg, A. *Lab on a Chip* **2005**, *5*, 492-500.

18. Jeon, N. L.; Finnie, K.; Branshaw, K.; Nuzzo, R. G. *Langmuir* **1997**, *13*, 3382-3391.

19. George, A.; Blank, D. H. A.; ten Elshof, J. E., *Langmuir* **2009**, *25*, 13298-13301.

20. George, A.; Maijenburg, A. W.; Nguyen, M. D.; Maas, M. G.; Blank, D. H. A.; ten Elshof, J. E. *Langmuir* **2011**, *27*, 12760-12768.

21. Anderson, M. E.; Srinivasan, C.; Hohman, J. N.; Carter, E. M.; Horn, M. W.; Weiss, P. S. *Adv. Mater.* **2006,** *18*, 3258-3260.

22. Höfler, T.; Track, A. M.; Pacher, P.; Shen, Q.; Flesch, H.-G.; Hlawacek, G.; Koller, G.; Ramsey, M. G.; Schennach, R.; Resel, R.; Teichert, C.; Kern, W.; Trimmel, G.; Griesser, T. *Mater. Chem. Phys.* **2010,** *119*, 287-293.

23. Hlawacek, G.; Shen, Q.; Teichert, C.; Lex, A.; Trimmel, G.; Kern, W. *J. Chem. Phys.* **2009,** *130*, 044703.

24. Frens, G. *Nature-Physical Science* **1973,** *241*, 20-22.

25. Hill, R.; Faridur Rahman, F. H. M., *Nucl. Instrum. Meth. A* **2011***, 645*, 96-101.

26. Ditsent, V. E., Skorokhodov, I. I., Terent'eva, N. A., Zolotareva, M. N., Belyakova, Z. V. and Belikova, Z. V. *Zh. Fiz. Khim.* **1976**, *50*, 1905– 1906

27. Rascon, C.; Parry, A. O. *Nature* **2000**, *407*, 986-989.

28. Lin, M.-H.; Chen, C.-F.; Shiu, H.-W.; Chen, C.-H.; Gwo, S. *J. Am. Chem. Soc.* **2009,** *131*, 10984-10991.

29. George, A.; Maijenburg, A. W.; Maas, M. G.; Blank, D. H. A.; ten Elshof, J. E. *Langmuir* **2011**, *27*, 12235-12242.

30. Lee, S.-M.; Grass, G.; Kim, G.-M.; Dresbach, C.; Zhang, L.; Gosele, U.; Knez, M. *Phys. Chem. Chem. Phys.* **2009**, *11*, 3608-3614.

31. Lee, S. M.; Pippel, E.; Gosele, U.; Dresbach, C.; Qin, Y.; Chandran, C. V.; Brauniger, T.; Hause, G.; Knez, M. *Science* **2009**, *324*, 488-492.

32. Szeghalmi, A.; Helgert, M.; Brunner, R.; Heyroth, F.; Gosele, U.; Knez, M. *Appl. Optics* **2009**, *48*, 1727-1732.

Chapter 6

Patterning functional materials using channel diffused plasma-etched self-assembled monolayer templates

* This chapter was published in *Langmuir,* (2011, *27* (19), pp 12235–12242)

Abstract.

A simple and cost-effective methodology for large area micrometer-scale patterning of a wide range of metallic and oxidic functional materials is presented. Self-assembled monolayers (SAM) of alkyl thiols on Au were micropatterned by channel diffused oxygen plasma etching, a method in which selected areas of SAM were protected from plasma oxidation via a soft lithographic stamp. The patterned SAMs were used as templates for site-selective electrodeposition, electroless deposition and solution phase deposition of functional materials such as ZnO, Ni, Ag thin films and ZnO nanowires. The patterned SAMs and functional materials were characterized by scanning electron microscopy (SEM), x-ray diffraction (XRD), atomic force microscopy (AFM) and tunneling AFM (TUNA).

6.1. Introduction

Realization of patterns of functional materials is often crucial in all kinds of device fabrication technologies. Over the last two decades various technologies have been developed for achieving high fidelity micro and nanoscale patterns. Technologies that employ patterned self-assembled monolayers (SAMs) of organic molecules such as organosilanes and alkanethiols are very powerful tools in device fabrication due to their ability to act as templates or resists for etching [1], electrodeposition [2], and electroless deposition [3]. Patterned SAMs can also be used to add a site-selective local chemical functionality on the surface in order to attach nanomaterials [4], biomolecules [5] or polymers [4].

Several techniques including photolithography [6], ion beam lithography [7], electron beam lithography [1,8], microcontact printing [9], scanning probe lithographic techniques [10,11], gas phase soft lithography [12], gas phase pattern deposition [13], and nanoimprint lithography [4] have been demonstrated for patterning SAMs. The advantage of patterning technologies in which a pre-formed SAM on a substrate undergoes local destruction or chemical modification by photo-oxidation, focused ion beam (FIB) or e-beam lithography (EBL), is the high quality of the final SAM pattern, because the formation of SAMs from the liquid or gas phase is known to yield densely packed SAMs with a low defect density. Scanning probe techniques such as nanoshaving [14] can also be used to pattern SAMs by displacing the self-assembled molecules from selected regions. However, the serial nature of processes like EBL, FIB and scanning probe techniques limits their application window enormously, even though these methods can produce extremely high resolution patterns. In comparison, the more commonly used micro-contact printing technique can fabricate patterned SAMs directly in a potentially up-scalable patterning process, but the controlled release of ink molecules to the substrate from the elastomeric poly-dimethyl siloxane (PDMS) stamps leads to SAM patterns with a relatively higher defect concentration. Problems such as loss of fidelity due to ink diffusion in lateral direction may occur, which sets a limit to the contact pressure, contact duration and ink concentration in micro-contact printing processes [15, 16, 17].

Koumoto and co-workers used a photo-oxidation technique to micropattern preformed SAMs by modifying the chemical functionality of the SAM end groups via exposure to UV light through photomasks [18,19,20,21,22,23]. They used patterned SAMs as templates for site-selective solution phase or gas phase deposition of functional materials such as ZnO, SnO2, and TiO_2 by selectively adsorbing or precipitating materials [19,20,21], or by electroless deposition by binding Pd catalyst on

the oxidized regions of the substrate [22,23]. The technique was studied thoroughly and has proven its ability to pattern a wide range of functional materials on the micrometer scale. However, the technique can only be used for local chemical modification of the SAM, but is not suitable for complete uniform destruction of the SAM in order to expose the underlying substrate.

Recently, Lin et al. introduced another novel “ink-free” approach to pattern SAMs via channel diffused plasma surface modification [24]. In this technique the channels formed between a PDMS stamp and a SAM-coated substrate are used to guide oxidizing plasma to selected areas where the SAM has to be etched or modified. The plasma is spatially controlled inside the channels and only the patches of SAM that are directly exposed to the plasma are modified. The method provides easy nanometer-to-millimetre scale nanopatterning of SAMs over large surface areas. The method is faster than photo-oxidation, EBL, FIB and scanning probe techniques, and does not have the limitations of microcontact printing with respect to pattern resolution.

In the present paper we demonstrate the micropatterning of a wide range of functional metallic and oxide materials such as Ni, Ag, ZnO, and vertically aligned ZnO nanowires via the channel-diffused plasma surface modification technique. A schematic diagram of the patterning process is shown in Figure 1. First conformal contact is made between the PDMS stamp and the SAM-coated substrate. The substrate is a gold-covered silicon substrate with an octadecanethiol (ODT) SAM. The substrate-stamp assembly is then exposed to oxygen plasma. The oxidizing plasma diffuses into the PDMS channels and oxidizes the part of the SAM that is exposed to the plasma. The regions on the substrate that are in conformal contact with the protruding parts of the PDMS stamp are protected from etching. After plasma exposure the PDMS stamp is peeled off the substrate and functional materials are selectively patterned via electrodeposition, electroless deposition and solution phase deposition.

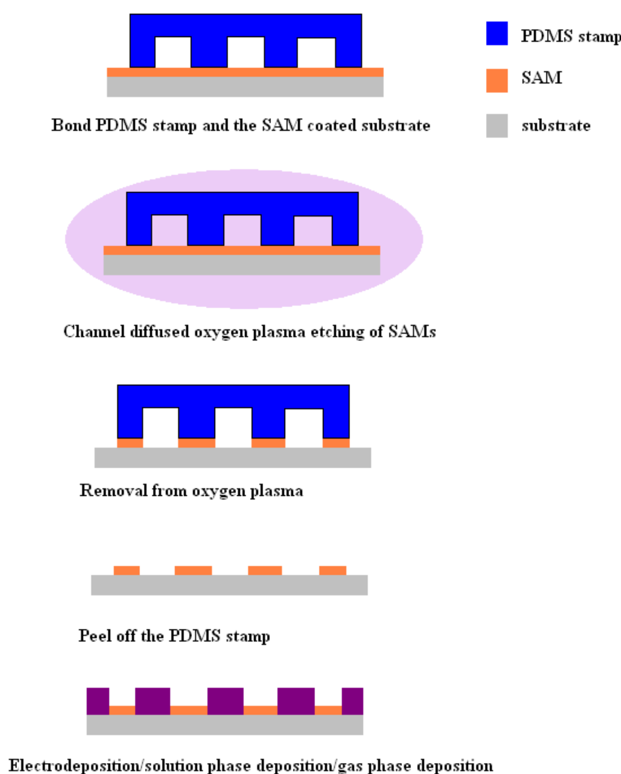

Figure 1: Schematic diagram of the channel diffused plasma patterning process.

6.2. Experimental

2.1. Preparation of PDMS stamps: PDMS and curing agent (Sylgard 184) were purchased from Dow Corning Corporation and mixed in a mass ratio 10:1 and poured over the micro/nano-patterned

silicon master (created by photolithography or e-beam lithography). The PDMS was cured for 48 h at 70°C. After curing, the PDMS stamps were removed from the master and cut into pieces of approximately 8 x 8 mm size.

2.2. Preparation of Au-coated silicon substrates: p-Type silicon substrates cleaned with piranha solution (a mixture of H_2O_2 and H_2SO_4 in 1:3 volume ratio) were used in the experiments. The substrates were washed several times with deionized water and stored in deionized water. Prior to use, the substrates were blow-dried in a nitrogen stream. Au films with a thickness of 10 to 75 nm were prepared on silicon substrates using a Perkin-Elmer sputtering machine operating at 50 W at a deposition pressure of 2×10^{-5} mbar using Ar as sputtering gas.

2.3. Preparation of ODT-SAM on Au, thin films: 1-Octadecanethiol (ODT, purity 97%) was purchased from Sigma-Aldrich and used for self-assembly. ODT SAMs on Au were prepared by soaking the substrate in a 0.5 M solution of ODT in ethanol for 12-48 h. After SAM deposition the substrates were taken out of the solution and washed in absolute ethanol and dried in a stream of nitrogen and stored for further use.

2.4. Channel diffused plasma etching of SAMs: The PDMS stamps with micro/nano-patterned features were gently pressed against the SAM-coated substrates. The patterned side of the stamp faced the SAM-coated side of the substrate. The PDMS stamp made conformal contact with the substrate via attractive Van der Waals forces. The substrate-stamp assembly was transferred to an oxygen plasma cleaner (Harrick Plasma) operating at 25 W at a pressure < 1 mbar. The substrates were exposed to oxygen plasma for 20 minutes. After plasma etching the PDMS stamp was peeled off the substrate and the substrate was stored until further use.

2.5. Electrodeposition of ZnO and Ni: ODT-SAM patterned Au thin films with an Au layer thickness of ~75 nm were used as substrate for electrodeposition. Electrodeposition was carried out using a three-electrode potentiostat (Autolab PGSTAT 128N, Metrohm Autolab, Netherlands). The SAM-patterned substrates were used as working electrodes. A small Pt mesh was used as counter electrode. The reference electrode was Ag/AgCl in 3M KCl (Metrohm Autolab). Nickel patterns were formed from an electrolyte containing 0.23 M nickel sulphate hexahydrate ($NiSO_4.6H_2O$, Sigma-Aldrch, purity 99%,) and 0.15 M boric acid (H_3BO_3, Aldrich, purity 99.99%). Deposition occurred at -1.00 V versus reference. Zinc oxide patterns were formed at 70 °C at -1.00 V in an electrolyte containing 0.10 M zinc nitrate hexahydrate ($Zn(NO_3)_2.6H_2O$, Sigma-Aldrich, purity 98%,). Further details can be found elsewhere [36].

2.6. Electroless deposition of ZnO: Electroless deposition of ZnO was carried out as described in ref. [25]. An ODT-SAM-patterned thin Au film of ~10 nm thickness was used as substrate. 1.5 g of Zinc nitrate hexahydrate and 0.058 g of dimethylamine borane (DMAB, Aldrich, purity 97%) were dissolved in 100 ml water. The solution was heated to 55 or 65 °C and the substrates were immersed in the solution for 15 minutes up to a few hours for ZnO thin film growth.

2.7. Deposition of silver: Ag deposition solutions (Silver enhancer A and Silver enhancer B) were obtained from Aldrich and mixed in equal proportions. The solution was diluted with water to 25%. The ODT-patterned Au substrates were placed in the solution for few minutes for Ag film growth.

2.8. Solution phase growth of vertically aligned ZnO nanowires: An ODT-SAM patterned thin Au film of ~10 nm thickness was used as substrate. Hexagonal ZnO seeds were grown at 65 °C for 15 min on the Au patches of the substrate by exposing the substrates to the solution used for thin film growth as described in section 2.6. After seeding, ZnO nanowires were grown on the substrate as described in more detail in ref. [26]. $Zn(NO)_3.6H_2O$ (0.15 g) and 0.07 g of hexamethylenetetramine (HMTA, Fluka, purity 99.5%) were mixed in 100 ml water. The solution was heated to 70-85 °C. The substrates were then placed floating upside down on the surface of the ZnO growth solution. ZnO nanowires were grown for 2 to 15 h, depending on the desired length of the nanowires.

2.9. Characterization: SAM patterns were characterized using tapping mode Atomic Force Microscopy (AFM; Veeco Dimension Icon) to determine the surface morphology. Tunnelling current AFM (TUNA) was used to study the conducting properties of the grown patterns, as well as to map the conductivity of patterned surfaces [37]. Grown metal and oxide patterns were imaged using high resolution scanning electron microscopy (HR-SEM, Zeiss 1550) and tapping mode AFM. X-ray

diffraction (XRD, Philips diffractometer PW 3020, Software XPert Data Collector 2.0e, Panalytical B.V., Almelo, The Netherlands) was used for phase determination of the patterns.

6.3. Results and discussion

3.1. Channel diffused plasma patterning of SAMs

Oxygen plasma treatment is a common technique to clean substrates [27, 28, 29] or chemically modify plastic surfaces to induce hydrophilicity [27]. In soft lithographic techniques like micromolding in capillaries (MIMIC) and microtransfer molding (µTM), oxygen plasma is used to increase the surface energy of the PDMS surface to improve the wetting and promote the flow of sol-gel precursor solutions in PDMS channels [28,29]. In the present paper we exploited the fact that the hydrocarbon chains of the alkanethiols and organosilane SAMs are oxidized by the plasma.

Figure 2a shows tapping mode AFM images of a patterned ODT-SAM on an Au substrate. The squares indicate the areas where the PDMS stamp was in conformal contact with the substrate. The SAM in that region was protected from exposure to oxygen plasma. The square patterns have a size of 5.2 µm and the spacing between the squares is 2.8 µm. The AFM height – distance plot shown in Figure 2b indicate that the plasma-modified regions are elevated by ~3 nm with respect to the non-modified SAM covered regions. We think that exposure of the Au surface to plasma affected the atomic packing in the close-packed structure of the Au film locally, so that the film density decreased and the Au film was lifted up slightly. To confirm this hypothesis, we plasma-patterned an OTS monolayer on a native oxide-coated silicon substrate and determined the local heights on the substrate. No height increase of regions that had been exposed to the plasma was observed in this case. This is attributed to the chemical resistance of the native oxide layer.

The plasma diffusion process inside the channels is time and geometry-dependent [24]. We found that the etching time for the complete removal of SAMs in an area of about 6x6 mm is ~15 minutes. However, a substantial degree of chemical modification can already be accomplished by partial oxidation over an area of 1x1 cm^2 within 10 minutes of exposure time. Large area patterning is possible using multiple stamps. We found that the stamps can be used for many patterning cycles without any loss of quality of the replicated patterns. We examined various PDMS stamp pattern geometries including straight lines and interconnected network-type channel structures such as square grids, circular grids and honeycomb-type channel arrays. Optical microscopy examination confirmed that relatively long exposure times were required for complete oxidation of SAMs in non-connected channel structures (straight lines, zigzag lines, bended lines, etc.) when compared to pattern geometries derived from interconnected channel structures. We also examined PDMS stamps with different height-to-width aspect ratios to determine the dependence of the plasma diffusion rate on aspect ratio. PDMS channels with a larger aspect ratio allowed faster diffusion of plasma, so that substantial diffusion distances could be accomplished in less time.

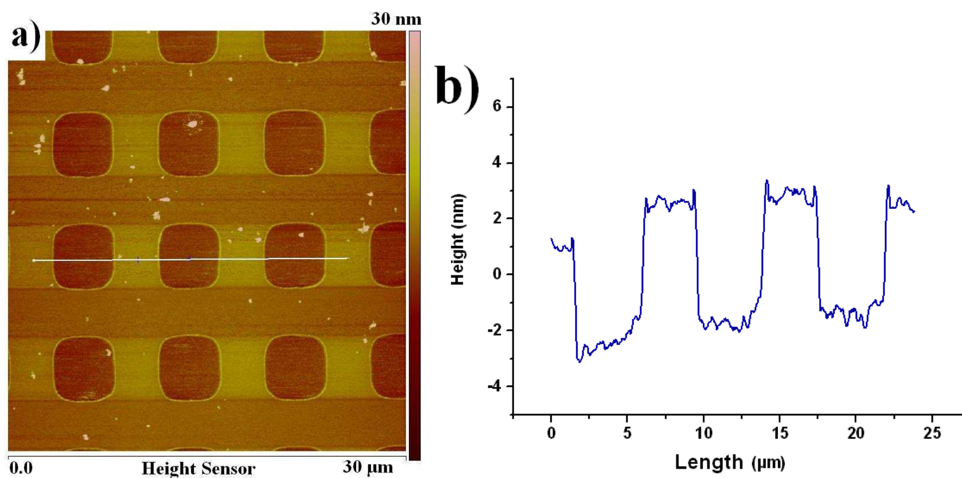

Figure 2: (a) AFM height image and height profile of ODT-SAM on Au substrate. The square pattern containing the SAM has a size of 5.2 µm and the spacing between the squares is 2.8 µm. (b) the height-distance plot shows that the etched regions are elevated with respect to the SAM-covered regions. The white line in (a) indicates the exact trajectory that is plotted in (b).

3.2. Deposition Experiments

3.2.1. Electroless deposition of ZnO thin films

ZnO thin films were deposited on SAM-etched regions following the recipe of Izaki and Omi as explained in section 2.3 [25]. The film growth mechanism is explained in detail in ref. [25]. Figure 3 shows various ZnO patterns grown on the etched regions of the substrate. The plasma-roughened Au patches were more hydrophilic than the hydrocarbon end groups of the SAMs. The hydrophilicity and roughness promoted the nucleation of ZnO on these areas, and their subsequent growth into thin films. To show the versatility of the technique we used different pattern geometries, including lines, dots, grids and honeycomb patterns. The SEM images in Figure 3 show that nucleation took place only within the etched regions of the substrate. No deposition of ZnO was observed on the SAM-covered regions even after 3 h of reaction.

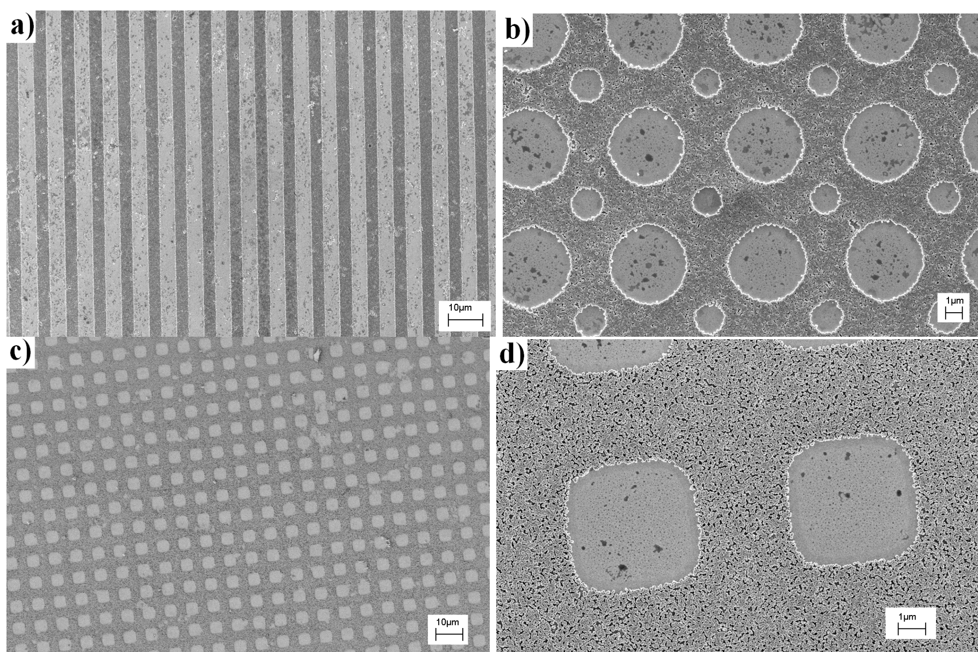

Figure 3: SEM images of ZnO patterns formed by area-selective electroless deposition on Au-covered regions of the substrate. All patterns were grown for 1 h and have a thickness of ~200 nm. **a)** Line pattern (width 3.5 µm; spacing 4.3 µm). **b)** Pit-patterned ZnO film (diameter large circles 4.5 µm; diameter small circles 2.5 µm; minimum spacing between circles ~2 µm). **c)** Square-patterned film (width 5.2 µm; spacing 2.8µm); **d)** Magnified image of the square-patterned film of Figure 3c.

It was also possible to fabricate isolated ZnO patterns when a slightly modified procedure was adopted. A PDMS mask with an interconnected square channel structure was used. After the plasma etching step, a Au etching step was introduced to remove the Au film from all plasma-etched areas. This yielded a pattern of isolated square Au patches on the substrate. The SAM was removed by a second exposure to plasma of the entire substrate. ZnO was grown by electroless deposition on the Au patches. The resulting ZnO square dot array on silicon is shown in Figure 4a. The polarity of the native silicon oxide layer is higher than of the ODT SAM. The hydrophobic-hydrophilic contrast of Au-patterned SiO_x substrates is therefore lower than on ODT-patterned Au substrates, which is why some isolated ZnO nuclei are found on the bare SiO_x areas of the substrate, as illustrated in Figure 4b.

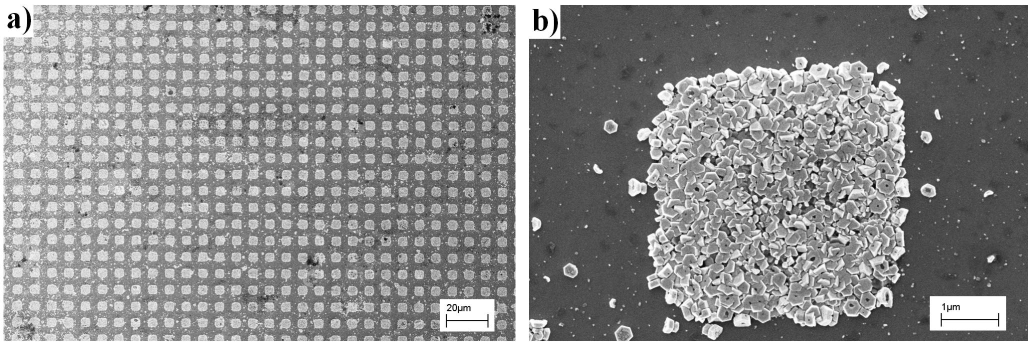

Figure 4: (a) Square array of ZnO square dots on-Au patterned silicon oxide substrate**; (b)** Magnified view showing a high concentration of ZnO nuclei on Au patches, and a low concentration of ZnO nuclei on the surrounding SiO_x substrate.

Figure 5 shows the AFM height profile corresponding with the ZnO patterned substrate of Figure 4. The deposition time was 1 h. A ZnO film of ~200 nm thickness formed on the patterned Au patches. Figure 6 shows the ZnO film thickness as function of deposition time. The rate of deposition was approximately 3–4 nm/min, independent of deposition time. However, the SEM images showed that during the initial 15-30 min of film growth the film density was not uniform. Longer deposition times yielded more uniformly covered films. Figure 7a and 7b shows the surface morphology of films grown at 55 and 65 °C, respectively. The films grown at 55 °C were continuous and dense. At 65 °C, individual hexagonal ZnO crystallites with a preferential orientation perpendicular to the substrate grew on the Au film. Their crystal structure was analysed by XRD. Figure 8 shows the XRD pattern of ZnO thin films grown at 65 °C. The peak at 2θ 34.5° corresponds to the (0002) orientation of the wurtzite crystal structure. This indicates preferentially (0001) oriented growth of the ZnO films, in agreement with the columnar structure that is visible in Figure 7b.

The conductivity of these patterns was characterised via tunnelling AFM (TUNAFM). Figure 9a-b show a contact mode AFM image, TUNA conductivity map and TUNA *IV* characteristics of isolated ZnO patterns obtained via electroless deposition. The contact mode image and conductivity map were recorded simultaneously with an applied sample bias of 3 V versus the AFM tip. The data shows uniform conductivity of the ZnO patterns. The shape of the *IV* curve is characteristic of semiconducting materials, and illustrates the semiconducting character of the ZnO patterns. In order to obtain consistent data, the *IV* characteristics were recorded at several locations. Furthermore, to exclude the possibility that the conductivity of the silicon substrate is measured instead of the sample, *IV* characteristics were also measured on the silicon substrate and no conductivity was observed during the measurements.

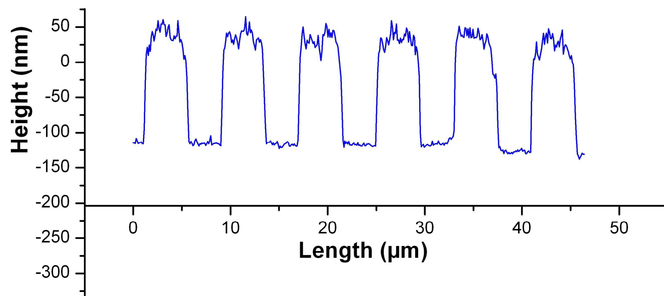

Figure 5: AFM height profile of ZnO square grid patterns after 1 hour of deposition time. The film has a thickness of ~200 nm, with a surface roughness of 40 nm.

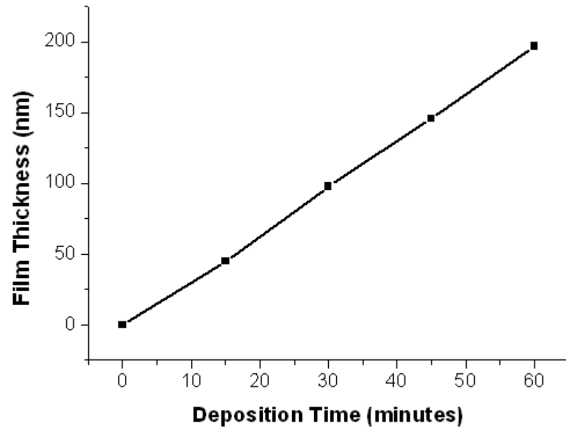

Figure 6: Film thickness of ZnO thin films by electroless deposition versus deposition time. The rate of deposition is 3-4 nm/min.

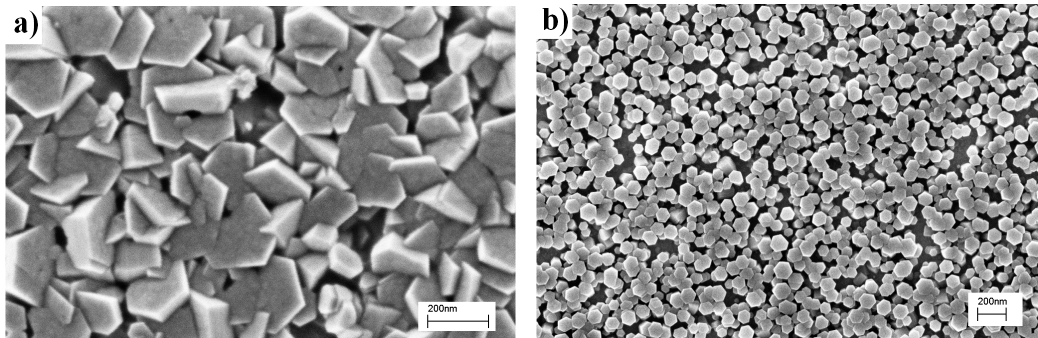

Figure 7: Morphology of ZnO thin films grown by electroless deposition; a) 55 °C; b) 65 °C.

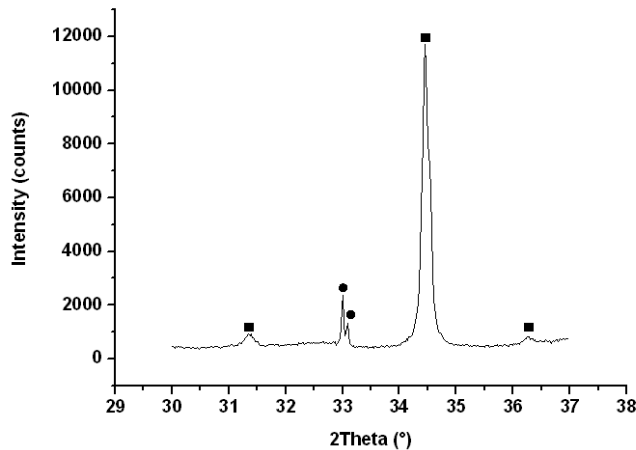

Figure 8: XRD pattern of ZnO thin films grown at 65 °C. The peak at 2θ 34.4° corresponds to the (0002) reflection of the ZnO wurtzite structure. The squares represent ZnO pattern peaks and the circles represent substrate peaks. The double peak at 2θ 33° is from the silicon substrate. The splitting of the silicon peak is due to presence of K_α and K_β radiation.

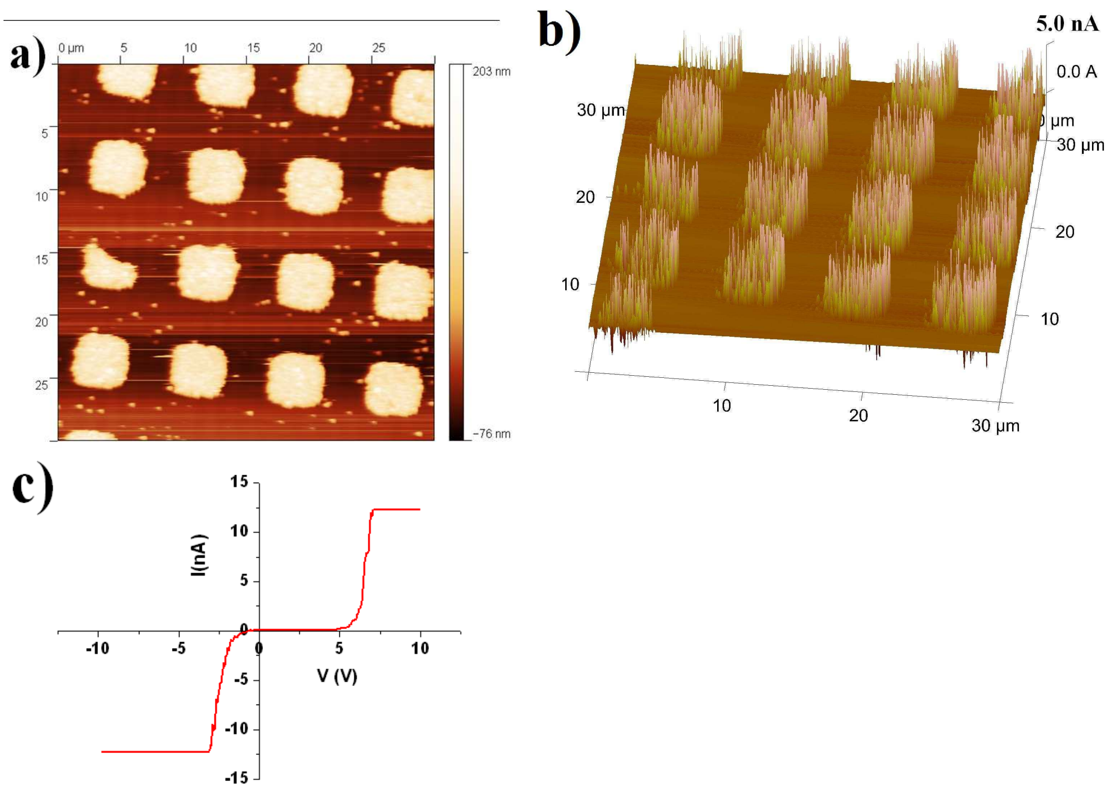

Figure 9: AFM contact mode image, contact mode height profile, TUNA AFM conductivity map and TUNA –*IV* characteristics of isolated electroless ZnO pattern.

3.2.2 Patterning ZnO nanowires

ZnO nanowires are important nanostructures with many potential applications in the fabrication of devices such as nanogenerators [30], nanophotonic devices [31], gas sensors [32], solar sells [33], field emission devices [34] and biosensors [35]. The fabrication of vertically aligned ZnO nanowires is very important for many device component applications. Figure 10 shows SEM images of vertically aligned ZnO nanowires deposited on plasma-etched Au patches. The ZnO nanowires were deposited following the recipe of Greene et al. [26]. First, a ZnO seed growth step was performed to generate hexagonal wurtzite seeds of ZnO. This step was essential because ZnO nanowires did not nucleate heterogeneously on the plasma-etched areas of the Au substrate in the nutrient solution, and only homogeneous nucleation in the solution occurred. The substrates were kept floating on the surface of the nutrient solution, with the ZnO seeded side facing downward into the solution. This was essential to avoid any homogeneously grown ZnO nanowires from depositing on the substrate. The ZnO nanowires were grown vertically downwards, following the crystal orientation of the ZnO seeds. The XRD data confirmed the preferential [0001] growth direction of wurtzite ZnO. The growth rate of the nanowires was ~100 nm/h. We grew nanowires for periods of 1 to 24 h. It was necessary to replace the nutrient solution after 10 h to maintain a constant growth rate, in view of the considerable reduction of Zn^{2+} ion concentration in the solution due to consumption by growth.

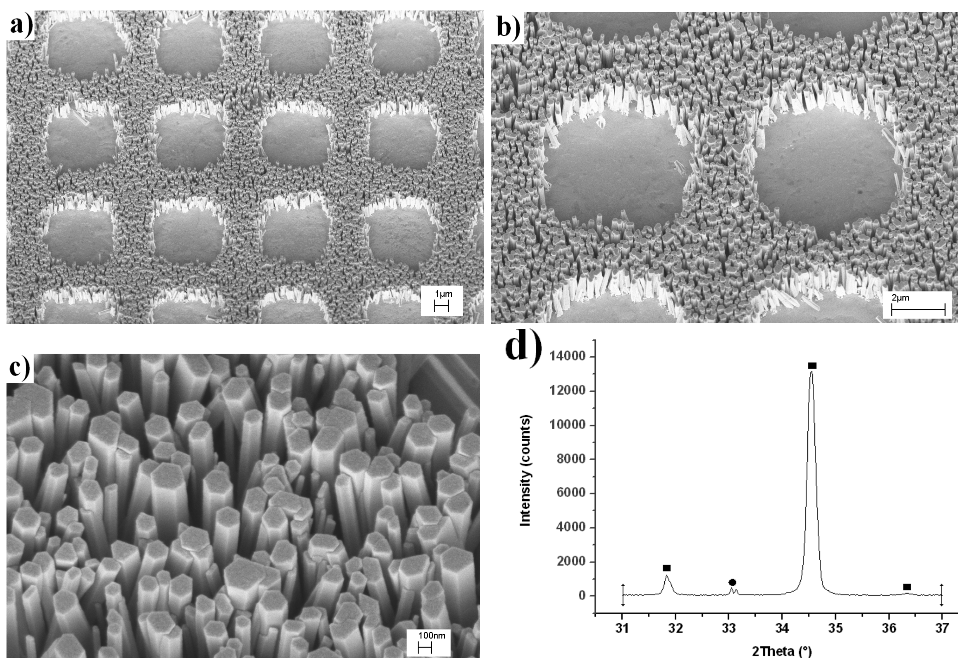

Figure 10: (a)-(c) show SEM images of ZnO nanowires grown on plasma-etched regions of the Au film at different magnifications. Growth time was 15 h. The nanowires were approximately 1.5 µm long. **d)** XRD pattern of ZnO nanowire patterns grown at 75 °C. The peak at 2θ 34.4° corresponds to the (0002) reflection of the ZnO wurtzite structure. The black squares designate ZnO pattern peaks and the black circles indicate substrate peaks. The double peak at 2θ 33° is from the silicon substrate. The splitting of the silicon peak is due to the presence of K_α and K_β radiation.

3.2.3. Electroless deposition of Ag

Figures 11a and 11b show Ag micropatterns formed over ODT patterned thin Au catalyst film. The deposition time was ~10 min for a thickness of 100 nm. The growth rate can be controlled by the dilution of the Ag enhancer solution. Film thickness can be controlled by the deposition time.

3.2.4. Electrodeposition of ZnO and Ni

Figures 11c and 11d show SEM images of electrodeposited Ni patterns on etch-patterned Au films. Figures 11e and 11f show AFM and SEM images of ZnO patterns deposited on etch-patterned Au thin films. The electrodeposition process was in both cases carried out at constant voltage for short intervals of time, i.e. 10 to 60 s. The deposition rate of ZnO was ~ 4 nm/min. The ZnO patterns shown in Figure 13 were grown for 30 s, and the thickness of the deposited film was ~120 nm.

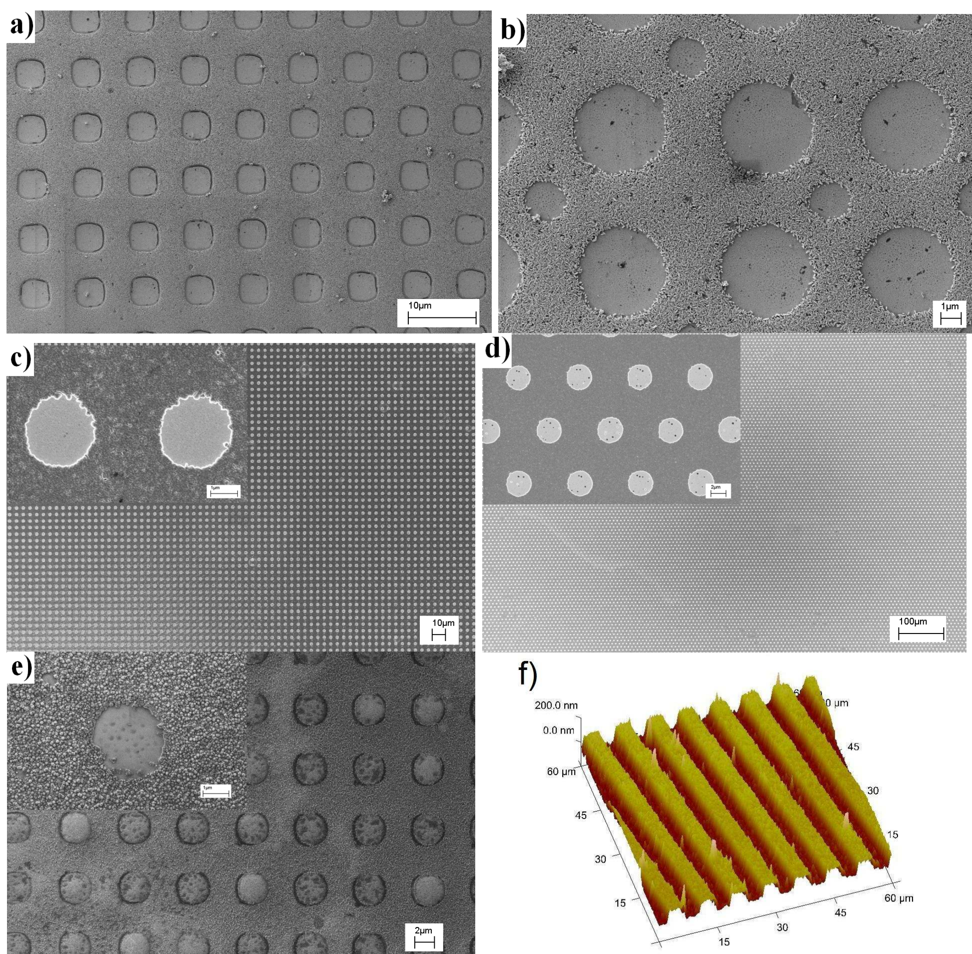

Figure 11: SEM images of patterned materials. **a)** Electroless Ag micropatterns formed on plasma-etched Au film with square array of square holes (width 5.3 µm; spacing 2.8 µm); **b)** electroless Ag film with a square array of circular pits (diameter large circles 4.5 µm; diameter small circles 2.5 µm; minimum spacing between circles ~2 µm); **c)** Electrodeposited Ni square array of circular pits (diameter 2.5 µm, spacing 2.5 µm); **d)** electrodeposited Ni hexagonal array of circular pits (diameter 3.3 µm, spacing 4.8 µm); **e)** Electrodeposited ZnO circular pit pattern (diameter and spacing 3 µm); **f)** 3D taping mode AFM image of electrodeposited ZnO line patterns with line width and spacing ~ 4 µm.

6.4. Conclusions

Channel diffused plasma etching is a simple, cost effective and efficient technique to pre-pattern substrates for subsequent site-controlled deposition of functional metal and oxide materials such as ZnO films and nanowires, and Ag or Ni films by electrodeposition, electroless deposition or solution phase deposition. Both interconnected patterns and isolated features were deposited. PDMS stamps with a connected channel structure provided the best results due to the fast diffusion of oxygen plasma that is possible in such structures. Channel diffused plasma etching is a time dependent process. During the etching process we observed a roughened Au film after plasma exposure, which stimulated the nucleation of ZnO during the subsequent electroless deposition process. The deposited ZnO thin films and nanowire micropatterns have semiconducting properties. The process could be more efficient and faster by engineering more plasma inlets from the sides and at the top of the PDMS channel mask.

6.5. References

1 . Carr, D.W.; Lercel, M.J.; Whelan, C.S.; Craighead, H.G.; Seshadri, K.; Allara, D.L. *J. Vacuum Sci. Technol. A* **1997**, *15*, 1446-1450.

2. Pesika, N. S.; Radisic, A.; Stebe, K. J.; Searson, P. C. *Nano Lett.* **2006**, *6*, 1023-1026.

3. Hsu, C.-H.; Yeh, M.-C.; Lo, K.-L.; Chen, L.-J. *Langmuir* **2007**, *23*, 12111-12118.

4. Maury, P.; Peter, M.; Mahalingam, V.; Reinhoudt, D.N.; Huskens, J. *Adv. Funct. Mater.* **2005**, *15*, 451-457.

5. Hoff, J.D.; Cheng, L.-J.; Meyhofer, E.; Guo, L.J.; Hunt, A.J. *Nano Lett.* **2004**, *4*, 853-857.

6. Dulcey, C. S.; Georger, J. H.; Krauthamer, V.; Stenger, D. A.; Fare, T. L.; Calvert, J. M. *Science* **1991**, *252*, 551-554.

7 Greg, G.; Scott, W.; Joe, B.; Michael, J. T. *Appl. Phys. Lett.* **1994**, *65*, 534-536.

8. Lercel, M.J.; Tiberio, R.C.; Chapman, P.F.; Craighead, H.G.; Sheen, C.W.; Parikh, A.N.; Allara, D.L. *J. Vac. Sci. Technol. B* **1993**, ***11***, 2823-2828.

9. Jeon, N. L.; Finnie, K.; Branshaw, K.; Nuzzo, R. G. *Langmuir* **1997**, *13*, 3382-3391.

10. Ginger, D. S.; Zhang, H.; Mirkin, C. A. *Angew. Chem. Int. Ed.* **2004**, *43*, 30-45.

11. Maoz, R.; Frydman, E.; Cohen, S. R.; Sagiv, J. *Adv. Mater.* **2000**, *12*, 424-429.

12. de la Rica, R.; Baldi, A.; Mendoza, E.; Paulo, Á. S.; Llobera, A.; Fernández-Sánchez, C. *Small* **2008**, *4*, 1076-1079.

13. George, A.; Blank, D. H. A.; ten Elshof, J. E. *Langmuir* **2009**, *25*, 13298-13301.

14. Xu, S.; Liu, G.-y., *Langmuir* **1997**, *13*, 127-129.

15. Biebuyck, H. A.; Larsen, N. B.; Delamarche, E.; Michel, B. *IBM J. Res. Dev.* **1997**, *41*, 159-170.

16. Delamarche, E.; Schmid, H.; Bietsch, A.; Larsen, N. B.; Rothuizen, H.; Michel, B.; Biebuyck, H. *J. Phys. Chem. B* **1998**, *102*, 3324-3334.

17. Dameron, A. A.; Hampton, J. R.; Smith, R. K.; Mullen, T. J.; Gillmor, S. D.; Weiss, P. S. *Nano Lett.* **2005**, *5*, 1834-1837.

18. Masuda, Y.; Kinoshita, N.; Sato, F.; Koumoto, K. *Cryst. Growth Design* **2006**, *6*, 75-78.

19. Masuda, Y.; Seo, W. S.; Koumoto, K. *Langmuir* **2001**, *17*, 4876-4880.

20. Masuda, Y.; Ieda, S.; Koumoto, K. *Langmuir* **2003**, *19*, 4415-4419.

21. Shirahata, N.; Masuda, Y.; Yonezawa, T.; Koumoto, K. *Langmuir* **2002**, *18*, 10379-10385.

22. Saito, N.; Haneda, H.; Komatsu, M.; Koumoto, K. *J. Electrochem. Soc.* **2006**, *153*, C170-C175.

23. Saito, N.; Haneda, H.; Sekiguchi, T.; Ohashi, N.; Sakaguchi, I.; Koumoto, K. *Adv. Mater.* **2002**, *14*, 418-421.

24. Lin, M.-H.; Chen, C.-F.; Shiu, H.-W.; Chen, C.-H.; Gwo, S., *J. Am. Chem. Soc.* **2009**, *131*, 10984-10991.

25. Izaki, M.; Omi, T. *J. Electrochem. Soc.* **1997**, *144*, L3-L5.

26. Greene, L. E.; Law, M.; Goldberger, J.; Kim, F.; Johnson, J. C.; Zhang, Y.; Saykally, R. J.; Yang, P., *Angew. Chem. Int. Ed.* **2003**, *42*, 3031-3034.

27. Khan, S. U.; Gobel, O. F.; Blank, D. H. A.; ten Elshof, J. E. *ACS Appl. Mater. Interfaces* **2009**, *1*, 2250-2255.

28. Gobel, O. F.; Blank, D. H. A.; ten Elshof, J. E. *ACS Appl. Mater. Interfaces* **2010**, *2*, 536-543.

29. ten Elshof, J. E.; Khan, S. U.; Göbel, O. F. *J. Europ. Ceram. Soc.* **2010**, *30*, 1555-1577.

30. Wang, Z. L.; Song, J. *Science* **2006**, *312*, 242246.

31. Huang, M. H.; Mao, S.; Feick, H.; Yan, H.; Wu, Y.; Kind, H.; Weber, E.; Russo, R.; Yang, P. *Science* **2001**, *292*, 1897-1899.

32. Liao, L.; Lu, H. B.; Li, J. C.; Liu, C.; Fu, D. J.; Liu, Y. L. *Appl. Phys. Lett.* **2007**, *91*, 173110-173110-3.

33. Law, M.; Greene, L. E.; Johnson, J. C.; Saykally, R.; Yang, P. *Nat. Mater.* **2005**, *4*, 455-459.

34. Huang, Y.; Zhang, Y.; Gu, Y.; Bai, X.; Qi, J.; Liao, Q.; Liu, J. *J. Phys. Chem. C* **2007**, *111*, 9039-9043.

35. Yeh, P. H.; Li, Z.; Wang, Z. L. *Adv. Mater.* **2009**, *21*, 4975-4978.

36. Maas, M.G.; Rodijk, E.J.B.; Maijenburg, A.W.; Blank, D.H.A.; Ten Elshof, J.E. *J. Mater. Res.* **2011**, DOI: 10.1557/jmr.2011.93

37. Veeco AFM manual, Application Modules, Nanoscope V7-B (004-1020-000).

Chapter 7

Micro- and nanopatterning of functional materials on flexible plastic substrates via site-selective surface modification using oxygen plasma

* A shortened version of this chapter is published in Journal of Materials Chemistry (DOI: 10.1039/C1JM14931H)

Abstract

A simple and cost effective methodology for large area micro and nanopatterning of a wide range of functional materials on flexible substrates is presented. A hydrophobic-hydrophilic chemical contrast was patterned on surfaces of various flexible plastic substrates using molds and shadow masks with which selected areas of the substrate surface were shielded from exposure to oxygen plasma. The exposed areas became hydrophilic and were then used as templates for site-selective adsorption, electroless deposition and solution phase deposition of functional materials like ZnO, Ag thin films, Au nanoparticles, conducting polymers, titania and ZnO nanowires. The patterned surfaces and functional materials were characterized by scanning electron microscopy, x-ray diffraction and atomic force microscopy.

7.1. Introduction

Flexible polymeric substrates are important in novel roll-to-roll manufacturing technologies. Plastic substrates are ideal candidates for ultra-light electronic devices, portable computers, personal health monitors and ultrathin foldable display screens due to their flexibility, low weight and inexpensiveness. In order to realize functional flexible devices, the controlled patterning of various materials such as conducting polymers, metals and metal oxides in the form of thin films, nanoparticle assemblies, or nanowire arrays is crucial. To ensure high yield and low cost production of flexible devices, the invention of cost-effective, low temperature patterning processes under mild chemical conditions is very important. Conventional device fabrication approaches such as photolithography, chemical vapour deposition or wet /dry etching often require a clean room and are not always suitable on plastic substrates due to the instability of organic polymers in these kinds of process environments.

More recent methodologies such as surface modification [1], material transfer [2] and self-assembly [3] are ideal in combination with plastic substrates, due to the technical simplicity, low temperature and mild chemical process conditions. Site-selective surface modification of flexible substrates, followed by local immobilization or growth of materials is an ideal strategy for patterning functional materials on flexible substrates. A similar strategy has been reported to achieve site-selective functionalization on plastic substrates by Langowski et al., who introduced plasma lithography on plastic substrates as a way to pre-pattern a wide range of plastic substrates with a hydrophobic-hydrophilic contrast prior to deposition of biomolecular inks [1]. The method provided an easy way to achieve site-selective chemical functionalization of plastics by confining plasma species inside the channels formed between the plastic substrate and a polydimethylsiloxane (PDMS) mold.

In the present paper we employed different templates such as soft lithographic PDMS moles and silicon-based micro/nano stencil shadow masks to prepattern flexible substrates such as PDMS, polycarbonate (PC) and polyethylene terephtalate (PET) site-selectively using oxygen plasma. The hydrophobic/hydrophilic contrasted substrate were used for area selective deposition of functional polymeric, metallic and ceramic materials. A schematic diagram of the patterning process is shown in

Figure 1. First conformal contact is made between the shielding template, i.e., a patterned PDMS mold with connected channel structure or a silicon-based shadow mask, and the flexible polymeric substrate. The substrate-shielding template assembly is then exposed to oxygen plasma. The oxidizing plasma diffuses reaches all non-shielded areas and oxidizes those parts of the substrate surface so that it is partly oxidized and becomes hydrophilic. The regions on the substrate that are in conformal contact with the protruding parts of the PDMS mold or the shadow mask are protected from surface modification and remain hydrophobic. After this prepatterning step, functional materials are selectively patterned onto the hydrophilic areas via electroless deposition, site-selective de-wetting, colloidal self-assembly and/or solution phase deposition. We demonstrate the versatility of our approach by patterning a wide range of functional materials such as ZnO, ZnO nanowires, TiO_2, silver, gold nanoparticles and the conducting polymer poly(2,3-dihydrothieno-1,4-dioxin)-poly(styrene sulfonate) (PEDOT: PSS) on length scales down to a few hundred nanometers.

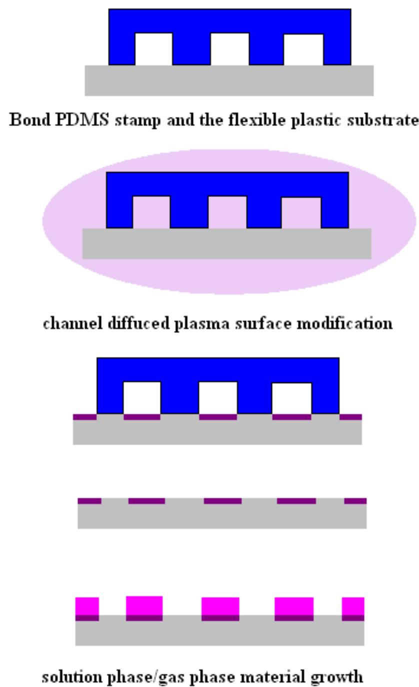

Figure 1: Schematic diagram of the channel diffused plasma patterning process and plasma modification.

7.2. Experimental

2.1. Preparation of PDMS molds and substrates: PDMS and curing agent (Sylgard 184) were purchased from Dow Corning Corporation and mixed in a mass ratio 10:1 and poured over the micro/nano-patterned silicon master that had been created by photolithography or e-beam lithography. For fabrication of planar PDMS substrates the mixture was poured over a silicone wafer functionalized with a monolayer of 1H,1H,2H,2H-perfluorooctylsilane . The PDMS was cured for 48 h at 70^oC. After curing, the PDMS molds were removed from the master or the silicon wafer and cut into pieces of required size.

2.2. Channel diffused plasma surface modification and surface modification through micro/nano stencils The PDMS molds with micro/nano-patterned features were gently pressed against the flexible substrates, so that the patterned side of the mold faced the substrate. The PDMS mold made conformal contact with the substrate via attractive Van der Waals forces. The substrate-mold assembly was transferred to an oxygen plasma cleaner (Harrick Plasma) operating at 25 W at a pressure < 1 mbar. The substrates were exposed to oxygen plasma for 10-15 minutes. After plasma etching the PDMS

mold was peeled off the substrate and the substrates were used immediately for further deposition of functional materials.

In addition to PDMS molds, patterning experiments were also performed with silicon and silicon nitride micro- and nanostencils with regular arrays of perforations. Silicon microstencils with 6 µm perforations were fabricated in the MESA+ cleanroom following a fabrication process that has been reported elsewhere [4]. Silicon nitride nanostencils with perforation diameters of 200, 400, and 800 nm were obtained from Aquamarijn BV, Netherlands. Planar PDMS substrates were brought into conformal contact with the stencils and were exposed to oxygen plasma for 5 min. After plasma treatment the PDMS substrates were peeled off the stencil and immediately used for further deposition of functional materials.

Patterning TiO_2: Ti(IV) isopropoxide ($Ti[OCH(CH_3)_2]_4$, >99.999%) was purchased from Sigma-Aldrich. Benzyl alchohol was purchased from Acros. The reactants were used as received and stored in a water-free environment. A solution of 0.2 M Ti(IV) isopropoxide in benzyl alcohol was prepared. 5 µL of the solution was spin-coated at a speed of 2000 rpm for 2 min on plasma patterned substrates that had been exposed to water vapor prior to spin coating. After spin coating the substrates were again exposed to water vapor to convert the precursor to amorphous titania. The substrates were then dried at 60 ^{o}C for 2 h.

2.3 Silver seeding for electroless deposition: Plasma-patterned substrates were dipped in a 1 mM aqueous solution of silver nitrate (Arcos Organics, Purity 99% for 1 h to attach silver ions to the modified regions. After removing the substrates from solution they were washed in a stream of absolute ethanol, dried in a stream of nitrogen and annealed at 80 ^{o}C for 20 min, and then exposed to light for 30 min to ensure complete photoreduction of Ag ions. Ag deposited in the hydrophilic regions acted as seed layer for the electroless deposition of Ag and ZnO.

2.4. Electroless deposition of ZnO: Electroless deposition of ZnO was carried out as described in ref. [5]. 1.5 g of zinc nitrate hexahydrate ($Zn(NO_3)_2{\cdot}6H_2O$, Sigma-Aldrich, purity 99%) and 0.058 g of dimethylamine borane (DMAB, Aldrich, purity 97%) were dissolved in 100 ml water. The solution was heated to 55 or 65 °C and the substrates were immersed in the solution for 15 min up to a few hours for ZnO thin film growth.

2.5. Deposition of silver: Ag deposition solutions (Silver enhancer A and Silver enhancer B) were obtained from Aldrich and mixed in equal proportions. The solution was diluted with water to 25%. The plasma patterned substrates were Ag seeded first and then placed in the solution for few minutes for Ag film growth.

2.6. Solution phase growth of ZnO nanowires: After the plasma surface modification process the substrates were immersed in a 0.2 M ethanolic solution of zinc acetate (Aldrich, purity 99.99%), taken out and allowed to dry at room temperature. The samples were kept in an oven at 80°C for 1 h. An oxygen plasma treatment was employed for 5 minutes to convert the zinc acetate to ZnO seed particles. After seeding, ZnO nanowires were grown on the substrate as described in more detail in ref. [14]. $Zn(NO)_2{\cdot}6H_2O$ (0.15 g) and 0.07 g of hexamethylenetetramine (HMTA, Fluka, purity 99.5%) were mixed in 100 ml water. The solution was heated to 70-85 °C. The substrates were then placed floating upside down on the surface of the ZnO growth solution. ZnO nanowires were grown for 2 to 15 h, depending on the desired length of the nanowires.

2.7. Conducting polymer micropatterns: PEDOT/PSS [Poly(2,3-dihydrothieno-1,4-dioxin)-poly(styrenesulfonate)] was purchased from Sigma Aldrich. 50 µL of PEDOT/PSS suspension was spin coated at a speed of 2000 rpm for 60 s on the plasma patterned substrates. After spin coating the PDMS substrates were heated to 70 ^{o}C for 15 min and stored for further analysis

2.8 Adsorption of gold nanoparticles: (3-Aminopropyl)triethoxysilane $(CH_3CH_2O)_3Si\text{-}C_3H_6\text{-}NH_2$ (APTES, 98% purity) was purchased from Sigma Aldrich. The stencil oxidized PDMS substrates were soaked in a 0.5 wt% solution of APTES in absolute ethanol for 10 min. The substrates were removed from the solution, washed several times with absolute ethanol, and blow-dried in pure nitrogen stream**.** A colloidal solution of gold nanoparticles was prepared as described in ref. [7]. The substrates were immersed in the gold nanoparticle solution for 12 h. The amine functional groups on the surface where protonated and electrostatically bound to the citrate ion coated gold nanoparticles.

2.9. Characterization: Prepatterned substrates and patterned materials were imaged using high resolution scanning electron microscopy (HR-SEM, Zeiss 1550) and tapping mode AFM. X-ray diffraction (XRD, Philips defractometer PW 3020, Software XPert Data Collector 2.0e, Panalytical B.V., Almelo, The Netherlands) was used for phase determination of the patterns.

7.3. Results and discussion

3.1. Plasma patterning of flexible substrates

Oxygen plasma treatment is commonly used as a technique to clean substrates [8, 9, 10] and chemically modify surfaces to promote the wetting properties [8]. In soft lithographic approaches like micromolding in capillaries (MIMIC) and microtransfer molding (µTM), oxygen plasma is used to increase the surface energy of the PDMS surface to improve the wetting and/or promote the flow of sol-gel precursor solutions in PDMS channels [28,29]. Exposure of plastic surfaces such as PET, PC, and poly-methyl-methacrylate (PMMA) to oxygen plasmas creates surface –CO and –COOH groups which are responsible for the increased hydropilicity of the exposed surface [11,12]. In the case of PDMS, plasma exposure yields a silica (SiO_x)-like surface [13]. In both cases the surfaces return to their previous hydrophobic state in the course of time [11,12,13].

Figure 2a shows an HR-SEM image of a microstencil that we used for our experiments and Figure 2b shows an HR-SEM image of a plasma-patterned PDMS substrate using the microstencil of Figure 2a. The stencil has perforations of 5 µm; the oxidized dots on the PDMS substrate have the same diameter. Figures 2c and 2d show plasma-patterned PDMS substrates using nanostencils of 400 and 200 nm, respectively. Nanostencil lithography was only possible on PDMS substrates since the elasticity of the PDMS allowed to make good conformal contact between stencil and substrate. The plasma diffusion process inside the channels is time and geometry-dependent [24]. A substantial degree of chemical modification could be achieved by plasma exposure over an area of 1x1 cm^2 within 10 min of exposure time. The same molds could be reused for many patterning cycles without loss of quality of the replicated patterns. We tested different PDMS mold pattern geometries, including straight lines and interconnected network-type channel structures such as square grids, circular grids and honeycomb-type channel arrays. Optical microscopy examination confirmed that surface modification occurs faster when connected channel structures (circular grid, square grid, honeycomb patterns, etc.) were used, when compared to pattern geometries derived from non-connected channel structures (straight lines, zigzag lines, etc.). We also examined PDMS molds with different height-to-width aspect ratios to determine the dependence of the plasma diffusion rate on aspect ratio. PDMS channels with a larger aspect ratio allowed faster diffusion of plasma, so that substantial diffusion distances could be accomplished in less time.

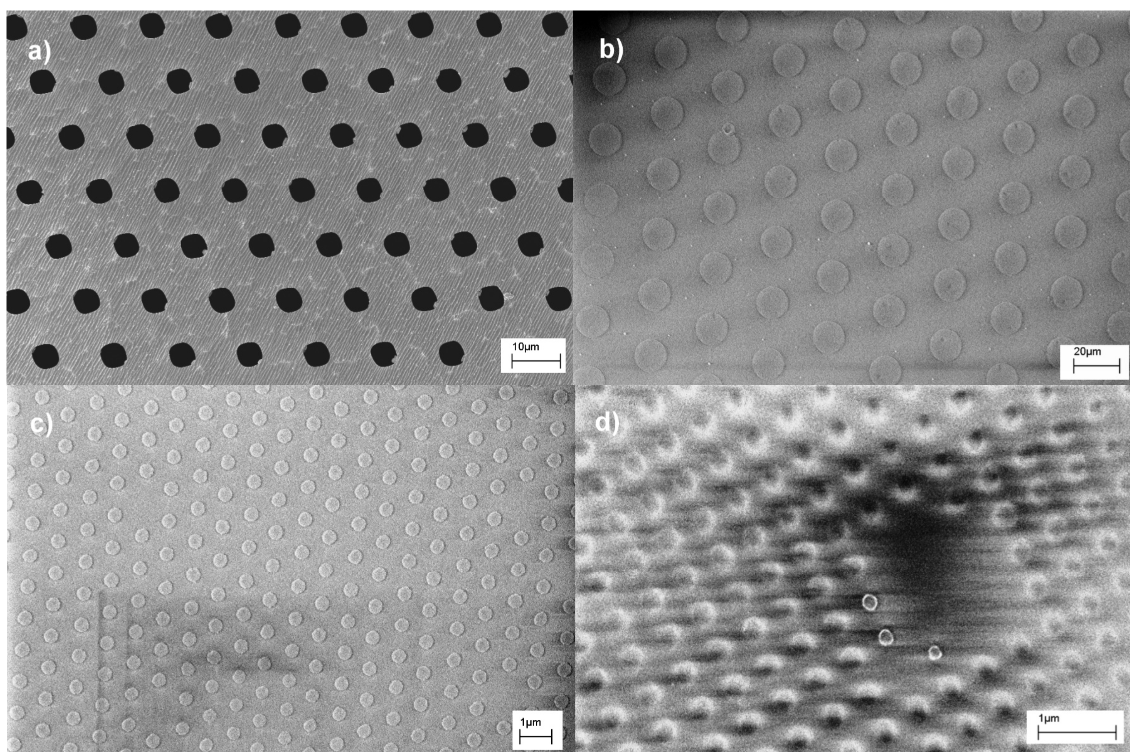

Figure 2: HR-SEM images of a) microstencil with 5 µm perforations; b) PDMS substrate plasma-patterned using microstencil of Fig. 2a; c) PDMS substrates with 400 nm wide oxidized dots; d) PDMS substrate with 200 nm wide oxidized dots.

3.2. Deposition Experiments

3.2.1. Electroless deposition of ZnO thin films

ZnO thin films were deposited on plasma patterned silver seeded regions of the substrate following the recipe of Izaki and Omi as explained in section 2.3 [5]. The film growth mechanism is explained in detail in ref. [5]. Figure 3a and 3b show honeycomb patterns of ZnO grown on plasma-modified Ag-seeded regions of a PDMS substrate. Figure 3c and 3d show a zigzag line pattern of ZnO formed on a PET substrate. The hydrophobic non-seeded regions of the substrates were almost free from ZnO. However, a few small particles of ZnO were found in the non-seeded areas. These were attributed to homogeneously nucleated particles from the growth solution. To illustrate the versatility of the technique we used different pattern geometries, including lines, dots, grids and honeycomb patterns. The SEM images in Figure 3 show that nucleation took place within the plasma modified and seeded regions of the substrate.

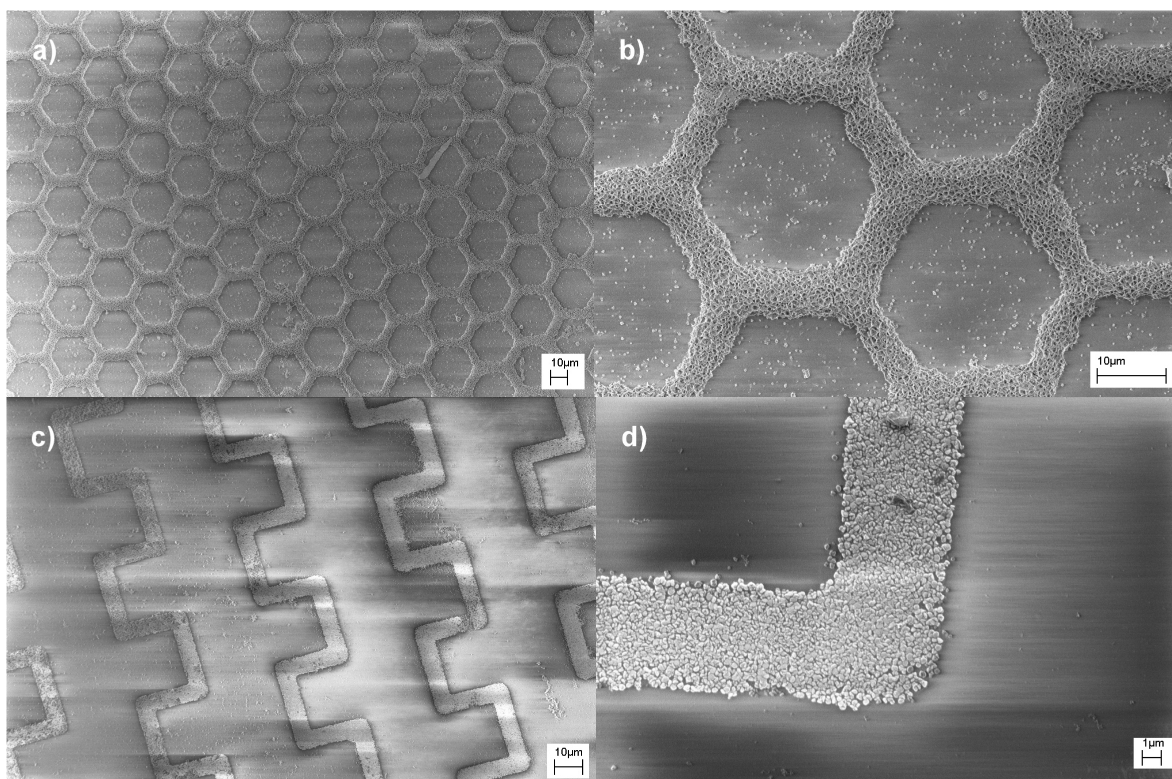

Figure 3: SEM images of ZnO patterns formed by area-selective electroless deposition on plasma-modified Ag-seeded regions of PDMS and PET substrates. a) Honeycomb pattern on PDMS substrate, line width 3.2 µm; b) Magnified view of image in Figure 3a; c) Zigzag line pattern of ZnO grown on PET substrate, line width 5.3 µm; spacing 2.8µm; d) Magnified image of the zigzag line pattern of Figure 3c.

Figure 4 shows the tapping mode 3D topography and height profile of a high aspect ratio ZnO pattern on PDMS substrate, corresponding to the SEM images of Figure 3a and 3b. A ZnO film of ~2 µm thickness formed on the plasma-modified silver seeded areas after 5 h of deposition time. The wurtzite phase of ZnO was confirmed by the xrd diffractogram in Figure 5. The rate of deposition was approximately 5–6 nm/min, independent of deposition time. However, the SEM images showed that during the initial 15-30 min of film growth the film density was not uniform. Longer deposition times yielded more uniformly covered films.

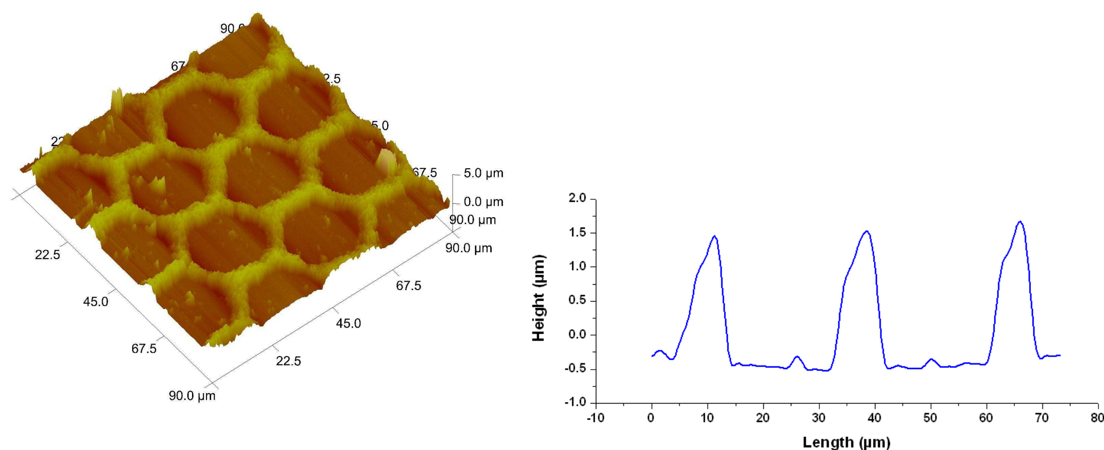

Figure 4: Tapping mode AFM 3D topography and height profile of high aspect ratio ZnO pattern shown in Figure 3a and 3b. The patterns grew to ~1.8 µm thickness in ~5 h time.

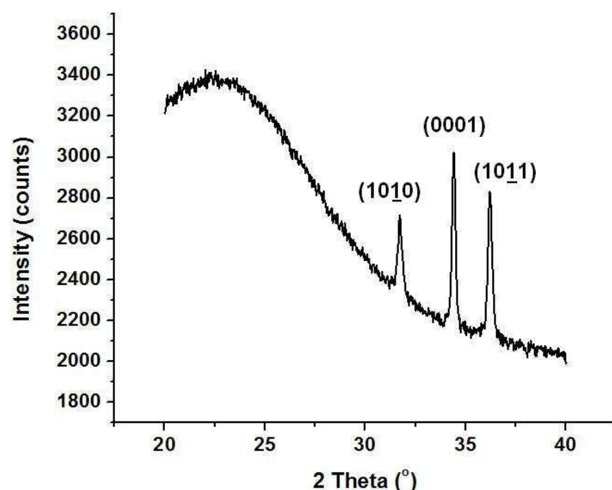

Figure 5: XRD spectrum of ZnO thin films grown at 55 °C.

3.2.2 Patterning ZnO nanowires

ZnO nanowires are one-dimensional nanostructures with potential applications in device fabrication of nanogenerators [14], nanophotonic devices [15], gas sensors [16], solar sells [17], field emission devices [18] and biosensors [19]. Patterning of ZnO nanowires on plastic substrates is very interesting due to their possible application in flexible devices. Figure 6 shows SEM images of ZnO nanowires deposited on plasma-patterned regions of the PDMS substrate. The ZnO nanowires were grown according to the method of Greene et al. [6]. First, a ZnO seed growth step was performed by immersing the plasma patterned substrates in a 0.5 M ethanolic solution of zinc acetate, followed by drying at 80°C for 1 h. A subsequent oxygen plasma treatment was employed to convert the zinc acetate phase to ZnO seed particles. Then the substrates were kept floating on the surface of the nutrient solution, with the ZnO-seeded side facing downward into the solution at 80°C. This was essential to avoid any deposition of homogeneously nucleated material on the substrate. The ZnO nanowires grew downwards, following the crystal orientation of the ZnO seeds. The XRD data confirmed the preferential [0001] growth direction of wurtzite ZnO. The growth rate of the nanowires was ~100-200 nm/h. We grew nanowires for periods of 1 to 24 h. In view of the considerable reduction of Zn^{2+} ion concentration in the solution due to consumption by growth, it was necessary to replace the nutrient solution after every 10 h to maintain a constant growth rate.

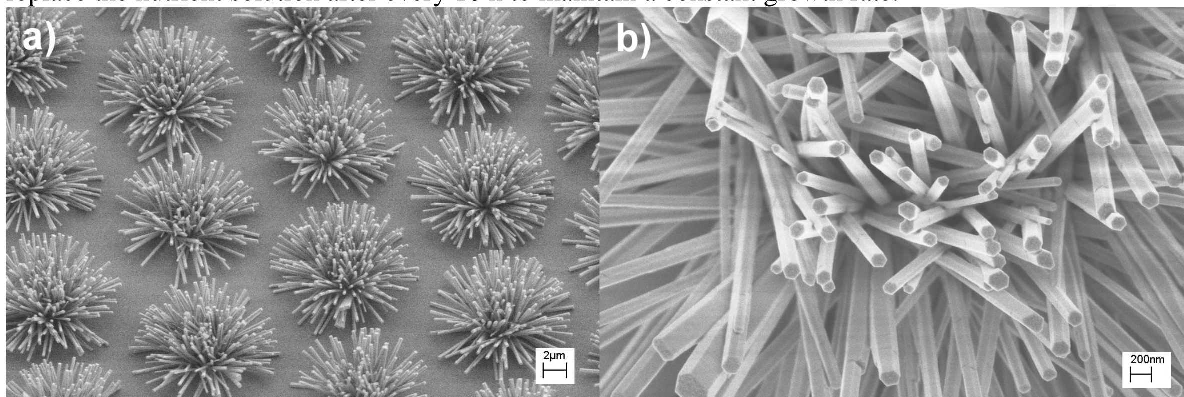

Figure 6: a-b) SEM images of ZnO nanowires grown on channel diffused plasma modified regions of PDMS substrate at different magnifications. Growth time was 15 h. The nanowires were ~3 μm long.

3.2.3 Patterning of amorphous TiO_2

Titania deposited onto conductive and/or transparent plastics can be utilized, among others, in solar-cell applications [20], optical humidity sensors [21], and photocatalysis [22]. Figure 7a shows HR-SEM image of titania patterns formed on a PET substrate. The tapping mode height profile of titania

pattern is shown in Figure 7b. The formation of titania was confirmed by EDX analysis. The patterns have an average height of 80 nm and a surface roughness of ~ 30 nm. Patterns of amorphous TiO_2 were obtained by a selective deposition and subsequent hydrolysis of titanium(IV) benzyloxy-isopropoxide. The precursor was synthesized by reacting titanium(IV) isopropoxide with benzyl alcohol yielding a 0.2 mol/dm^3 solution. The ^{1}H NMR measurements showed that at least 88 mol% of the isopropoxy ligands were directly exchanged by benzyl alcohol ligands during preparation [23]. By this means the overall reactivity of titanium(IV) precursor was significantly decreased, so that it can be handled relatively easily in a typical laboratory environment. Sol-gel processing of titanium(IV) alkoxide into titanium oxide gel follows through hydrolysis and condensation reactions [24]. Depending on hydrolysis ratio, used catalysts, and coordinating alcoholic ligands, different titania morphologies can be obtained [25]. The as-prepared titania is amorphous, but can be converted easily into crystalline rutile or anatase by mild hydrothermal treatment [26].

3.2.4. Electroless deposition of Ag

Metallic patterns on plastic substrates are important due to their application as interconnects and active components like sensing elements in flexible devices. We used silver-seeded plasma-treated regions of the plastic substrates for site-selective electroless deposition of Ag. Figure 7c and 7d show an HR-SEM image and tapping mode AFM height profile of Ag micropatterns formed over plasma-patterned silver-seeded PC substrates. The patterns have a line width of 8 µm and a line spacing of 1.2 µm. The deposition time was 15 min for a thickness of 150 nm. The growth rate can be controlled by dilution of the growth solution, and film thickness can be controlled by deposition time. Formation of Ag was confirmed by XRD and EDX analysis of the pattern grown on PC substrate.

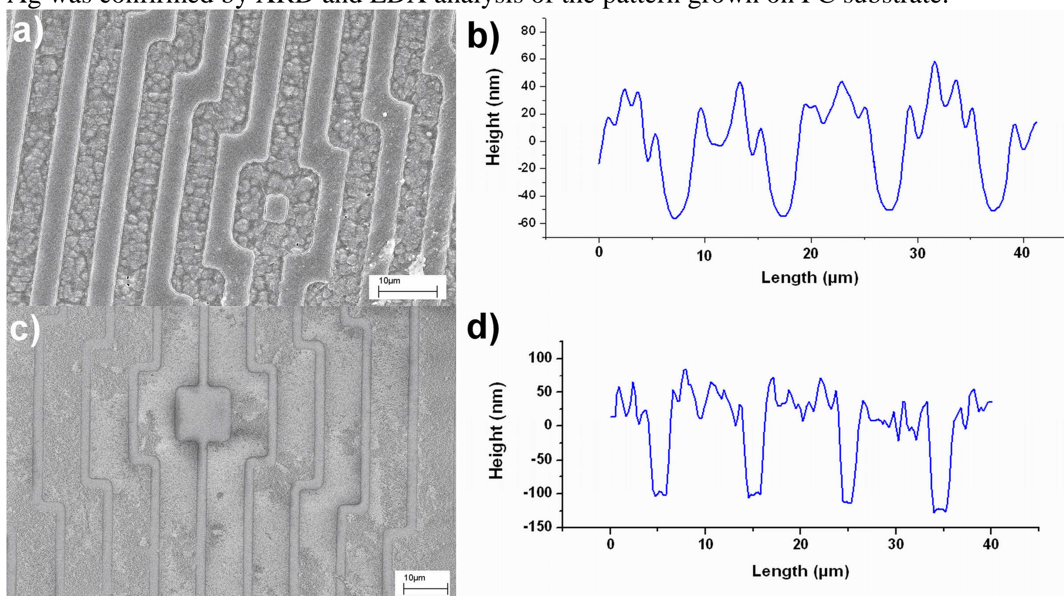

Figure 7. a) HR-SEM images of TiO_2 patterns on PET substrate. b) Tapping mode AFM height profile of TiO2 pattern; c) HR-SEM images of Ag micropatterns on PC substrate; d) Tapping mode AFM height profile of Ag pattern grown on PC substrate.

3.2.5. Patterning of PEDOT: PSS by site-selective de-wetting

Conducting polymers such as PEDOT: PSS and polyaniline (PANI) are important materials in the manufacture of flexible devices such as flexible displays. Figure 8a-c shows an HR-SEM image, a tapping mode AFM 3D topography image and an AFM height profile respectively of PEDOT: PSS patterns spin-coated over a plasma-patterned PDMS substrate made with a silicon stencil. The dot patterns have a diameter of 5 µm and a spacing of 5 µm between the dots. The height of each PEDOT:PSS dot is 65 nm.

3.2.6. Site-selective adsorption of Au nanoparticles

Figure 9e (5 µm dots) and 9f (800 nm dots) shows optical microscope images and figure 9g (5 µm dot) shows a HR-SEM image of Au nanoparticles that were selectively attached on an APTES-

patterned PDMS substrate. After plasma modification on PDMS substrates using micro and nanostencils, APTES molecules were selectively bonded to the modified areas. The hydroxyl groups on the oxidized areas of the substrate reacted with APTES and formed a self-assembled molecular thin film. Gold nanoparticles were deposited selectively on the aminosilane areas by immersing the patterned substrates in a colloidal solution of gold nanoparticles. The $–C_3H_6NH_2$ side chains in the film were protonated at a pH of 2.5 and formed $-NH_3^+$ end groups which selectively bonded to negatively charged citrate ion-coated Au nanoparticles.

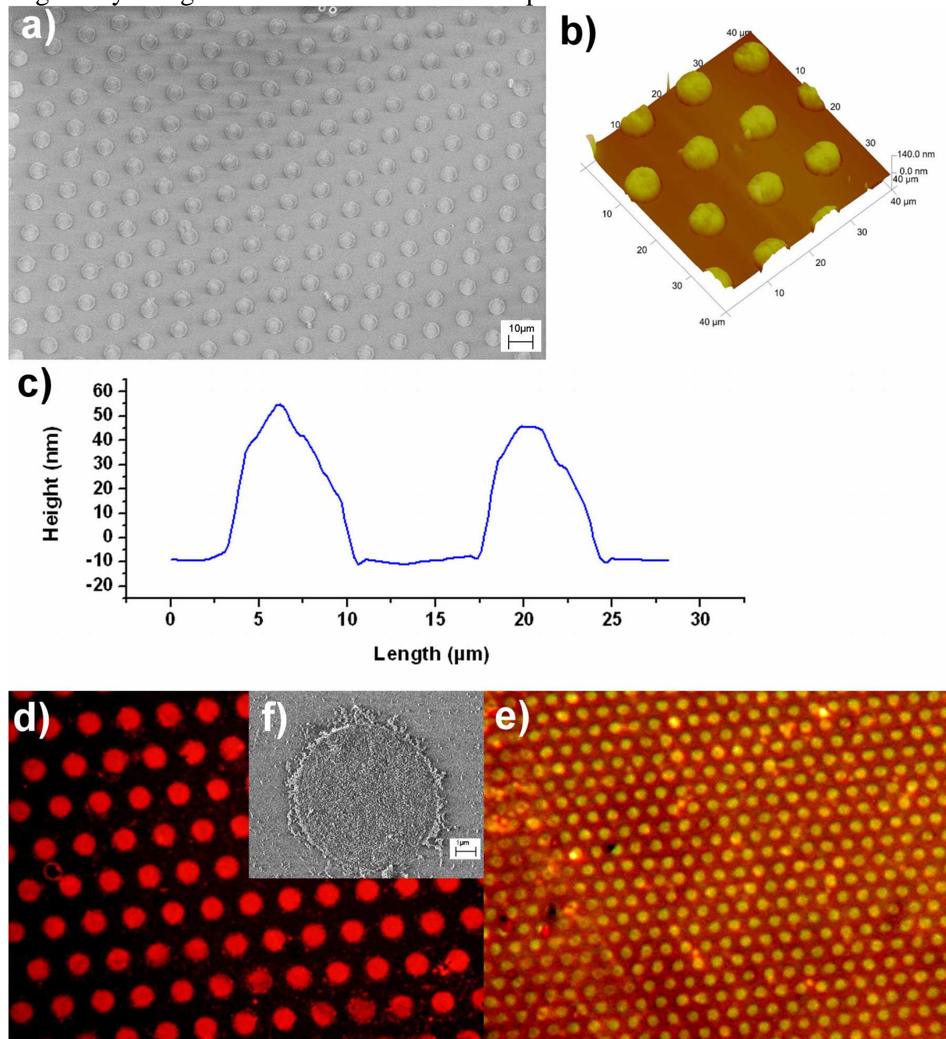

Figure 8: a) HR-SEM image of PEDOT: PSS dot array selectively spincoated on the hydrophilic regions of the substrate. b) Tapping mode AFM 3D topographic image of PEDOT:PSS dots. c) AFM height profile of PEDOT:PSS dots. d) Optical microscopic image of Au nanoparticle arrays of 5µm dots selectively adsorbed on the stencil patterned substrates; e) optical micrograph of 800 nm dots; f) HRSEM image of a 5µm dot with adsorbed Au nanoparticles.

7.4. Conclusions

We demonstrated a fast and easy approach to pattern a wide range of functional materials, including ZnO, ZnO nanowires, Au nanoparticles, Ag and PEDOT: PSS on flexible substrates like PDMS, PC and PET by oxygen plasma-modified patterning using PDMS molds or micro/nanostencil shadow masks. We made patterns of arbitrary complexity, with different geometrical features such as lines, anitidots, honey comb and isolated dot arrays. The patterns formed by this technique have feature

dimensions as small as 200 nm, up to a few micrometer. Plasma-patterned surface modification using shielding templates is a simple, cost effective and efficient technique to pre-pattern plastic substrates for subsequent site-controlled deposition of metal oxides, metals and organic materials via a range of methods, e.g. electroless deposition, solution phase deposition, site-selective adsorption and site-selective de-wetting.

7.5. References

1. Langowski, B. A.; Uhrich, K. E., Microscale Plasma-Initiated Patterning (μPIP). Langmuir 2005, 21, (23), 10509-10514

2 Y. Yang, Y. Hwang, H. A. Cho, J.-H. Song, S.-J. Park, J. A. Rogers, H. C. Ko, Small, 7, 484.

3. Kim, S. S.; Saeedi, E.; Etzkom, J. R.; Parviz, B. A.; Ieee, LARGE SCALE SELF-ASSEMBLY OF CRYSTALLINE SEMICONDUCTOR MICROCOMPONENTS ONTO PLASTIC SUBSTRATES VIA MICROFLUIDIC TRAPS. Ieee: New York, 2008; p 967-970.

4. Unnikrishnan, S.; Jansen, H.; Berenschot, E.; Mogulkoc, B.; Elwenspoek, M., MEMS within a Swagelok®: a new platform for microfluidic devices. Lab Chip 2009, 9 (13), 1966-1969.

5. Izaki, M.; Omi, T., Transparent Zinc Oxide Films Chemically Prepared from Aqueous Solution. Journal of The Electrochemical Society 1997, 144, (1), L3-L5.

6. Greene, L. E.; Law, M.; Goldberger, J.; Kim, F.; Johnson, J. C.; Zhang, Y.; Saykally, R. J.; Yang, P., Low-Temperature Wafer-Scale Production of ZnO Nanowire Arrays. Angewandte Chemie International Edition 2003, 42, (26), 3031-3034.

7. Frens, G., Controlled Nucleation for Regulation of Particle-Size in Monodisperse Gold Suspensions. Nature-Physical Science 1973, 241, (105), 20-22.

8. Khan, S. U.; Gobel, O. F.; Blank, D. H. A.; ten Elshof, J. E., Patterning Lead Zirconate Titanate Nanostructures at Sub-200-nm Resolution by Soft Confocal Imprint Lithography and Nanotransfer Molding. ACS Applied Materials & Interfaces 2009, 1, (10), 2250-2255.

9. Gobel, O. F.; Blank, D. H. A.; ten Elshof, J. E., Thin Films of Conductive ZnO Patterned by Micromolding Resulting in Nearly Isolated Features. ACS Applied Materials & Interfaces 2010, 2, 536-543.

10. ten Elshof, J. E.; Khan, S. U.; Göbel, O. F., Micrometer and nanometer-scale parallel patterning of ceramic and organic-inorganic hybrid materials. Journal of the European Ceramic Society 2010, 30, 1555-1577.

11. Chaudhury, M. K.; Whitesides, G. M., Direct measurement of interfacial interactions between semispherical lenses and flat sheets of poly(dimethylsiloxane) and their chemical derivatives. Langmuir 1991, 7, (5), 1013-1025.

12.Abenojar, J.; Torregrosa-Coque, R.; Martinez, M. A.; Martin-Martinez, J. M., Surface modifications of polycarbonate (PC) and acrylonitrile butadiene styrene (ABS) copolymer by treatment with atmospheric plasma. Surf. Coat. Technol. 2009, 203 (16), 2173-2180.

13. Vesel, A.; Mozetic, M.; Zalar, A., XPS study of oxygen plasma activated PET. Vacuum 2007, 82 (2), 248-251.

14. Wang, Z. L.; Song, J., Piezoelectric Nanogenerators Based on Zinc Oxide Nanowire Arrays. Science 2006, 312, (5771), 242-246.

15. Huang, M. H.; Mao, S.; Feick, H.; Yan, H.; Wu, Y.; Kind, H.; Weber, E.; Russo, R.; Yang, P., Room-Temperature Ultraviolet Nanowire Nanolasers. Science 2001, 292, (5523), 1897-1899.

16. Liao, L.; Lu, H. B.; Li, J. C.; Liu, C.; Fu, D. J.; Liu, Y. L., The sensitivity of gas sensor based on single ZnO nanowire modulated by helium ion radiation. Applied Physics Letters 2007, 91, (17), 173110.

17. Law, M.; Greene, L. E.; Johnson, J. C.; Saykally, R.; Yang, P., Nanowire dye-sensitized solar cells. Nat Mater 2005, 4, (6), 455-459.

18. Huang, Y.; Zhang, Y.; Gu, Y.; Bai, X.; Qi, J.; Liao, Q.; Liu, J., Field Emission of a Single In-Doped ZnO Nanowire. The Journal of Physical Chemistry C 2007, 111, (26), 9039-9043.

19. Yeh, P. H.; Li, Z.; Wang, Z. L., Schottky-Gated Probe-Free ZnO Nanowire Biosensor. Advanced Materials 2009, 21, (48), 4975-4978.

20.Miyasaka, T.; Ikegami, M.; Kijitori, Y., Photovoltaic Performance of Plastic Dye-Sensitized Electrodes Prepared by Low-Temperature Binder-Free Coating of Mesoscopic Titania. Journal of The Electrochemical Society 2007, 154 (5), A455-A461.

21. Yadav, B. C.; Pandey, N. K.; Srivastava, A. K.; Sharma, P., Optical humidity sensors based on titania films fabricated by sol-gel and thermal evaporation methods. Meas. Sci. Technol. 2007, 18 (1), 260-264.

22. Schmidt, H.; Naumann, M.; Müller, T. S.; Akarsu, M., Application of spray techniques for new photocatalytic gradient coatings on plastics. Thin Solid Films 2006, 502 (1-2), 132-137.

23. Stawski, T. M.; Veldhuis, S. A.; Göbel, O. F.; Ten Elshof, J. E.; Blank, D. H. A., Effects of Reaction Medium on the Phase Synthesis and Particle Size Evolution of BaTiO3. Journal of the American Ceramic Society 2010, 93 (10), 3443-3448.

24. Wright, J.D.; Sommerdijk, N.A.J.M. “Sol-gel Materials Chemistry and Applications”, Advanced Chemistry Texts, CRC Press, Boca Raton, 53-68, 2001.

25. U. Schubert, “Chemical modification of titanium alkoxides for sol-gel processing”, J. Mater. Chem., 15 3701-3715 (2005).

26. Wang, C.-C.; Ying, J. Y., Sol–Gel Synthesis and Hydrothermal Processing of Anatase and Rutile Titania Nanocrystals. *Chemistry of Materials* **1999,** *11* (11), 3113-3120.

Chapter 8

Electrodeposition in capillaries: Bottom-up micro and nanopatterning of functional materials on conductive substrates

* This chapter was published in *ACS Applied Materials & Interfaces* (**2011**, 3 (9), pp 3666–3672)

Abstract

A cost-effective and effective methodology for bottom-up patterned growth of inorganic and metallic materials on the micro and nanoscale is presented. Pulsed electrodeposition was employed to deposit arbitrary patterns of Ni, ZnO and FeO(OH) of high quality, with lateral feature sizes down to 200-290 nm. The pattern was defined by an oxygen plasma-treated patterned PDMS mold in conformal contact with a conducting substrate and immersed in an electrolyte solution, so that the solid phases were deposited from the solution in the channels of the patterned mold. It is important that the distance between the entrance of the channels, and the location where deposition is needed, is kept limited. The as-formed patterns were characterized by high resolution scanning electron microscope, energy-dispersive x-ray analysis, atomic force microscopy, and x-ray diffraction.

KEYWORDS soft-lithography, oxides, electrodeposition, micropatterning

8.1. Introduction

Fast and cost-effective realization of high resolution complex patterns of functional materials is crucial in future manufacturing technologies. Patterning techniques such as photolithography [1,2], electron beam lithography [3], ion beam lithography [4], nanoimprint lithography [5] and scanning probe lithographic methods [6,7] are used in industry and research for patterning functional materials. However all these techniques require either cleanroom processing conditions, or the use of resist materials often with complex processing steps of wet/dry etching. Some of these methods are slow due to their serial nature. Well-known alternatives developed by the Whitesides research group are the soft lithographic methods that use micro/nanopatterned polydimethylsiloxane (PDMS) molds and stamps in conformal contact with a substrate as a template for site-selective patterning with functional materials [8]. Interesting features of soft lithography are its technical simplicity, low capital investment cost, and effectiveness in producing large-scale functional patterns of arbitrary materials [8,9]. The soft lithographic techniques can be divided into printing and molding-based methods, and include microcontact printing [10], micromolding in capillaries (MIMIC) [11], micromolding [12,13], micro-transfer molding [14], edge lithography [15], solvent assisted micro-molding [16], nanotransfer printing [17], and gas phase pattern deposition [18]. These methods can be used for the fabrication of different functional patterns including self-assembling molecules, metals, metal oxides, nanoparticles, bio-molecules and polymeric materials.

Electrodeposition is a simple, scalable and cost effective tool for fabricating inorganic functional thin films of metals [19,20], metal alloys [21,22], metal oxides [23] and conducting polymers [24] on conductive substrates. Electrodeposition using templates such as patterned photoresist [1,2], polycarbonate membranes [25], anodic alumina membranes [26], colloidal crystals [27], and self-assembled monolayers [19,28] attracted a lot of research and industrial interest due to its ability to fabricate 2D and 3D patterns of inorganic functional materials [1,2,19], nanowires [25,26] and nanotubes [25]. As is shown below, a combination of soft lithography and electrodeposition can be

used as a tool for large area patterning of various functional materials on micrometer and nanometer scale. In comparison with other combinations of deposition and lithographic techniques to generate functional material patterns, the combination of electrodeposition and soft lithography is technically versatile and cost effective as it can be carried out under normal ambient conditions, without the use of complex patterning, etching and deposition steps.

In the present paper we demonstrate the possibility of a single step, bottom up, inexpensive and easy process for 2D nano and micropatterning of functional material on conductive substrates by electrodeposition using patterned PDMS molds as templates. A schematic diagram of the patterning process is shown in figure 1. A PDMS mold with micrometer or nanometer scale channels is gently pressed against a conductive substrate. A connected channel structure is formed between the substrate and the PDMS mold. The substrate-mold assembly is immersed in an electrolyte solution and used as working electrode to deposit functional materials like nickel, platinum, zinc oxide (ZnO) and iron oxohydroxide (FeO(OH)). We demonstrated patterns with a size range of 180 nm to few microns.

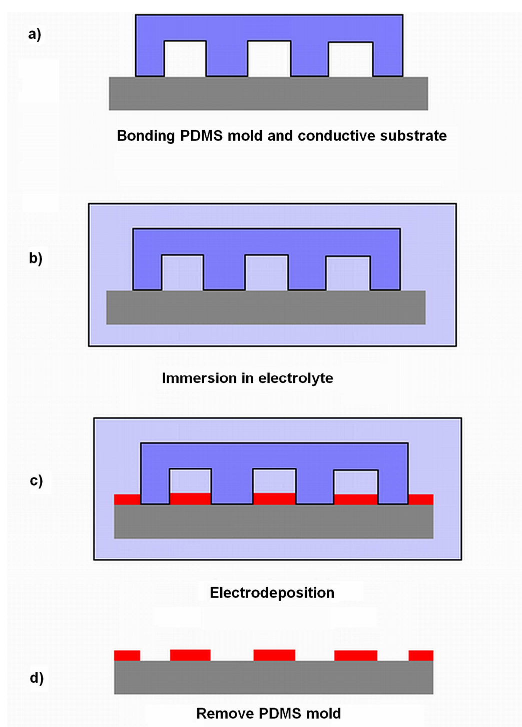

Figure 1: Procedure of electrodeposition in capillaries. a) Bonding the substrate and the patterned PDMS mold. b) Immersion in the electrolyte solution for several minutes to assure proper filling of the channels. c) Electrodeposition inside the capillaries to form the material patterns. d) Peeling off the mold from the substrate and washing in de-ionized water.

8.2 Experimental

Fabrication of PDMS templates: PDMS and curing agent (Sylgard 184) were purchased from Dow Corning Corporation, mixed in a mass ratio of 10:1 and poured over a patterned silicon wafer that was coated with a 1H,1H,2H,2H-perfluorooctylsilane monolayer as an anti-adhesion layer. The micrometer scale masters were patterned by standard photolithography and the patterns were transferred to the Si substrate by etching (Lionix BV, Netherlands). The nanometer scale masters were purchased from LightSmyth Technologies, Inc., USA. The PDMS was cured at a temperature of 70°C for 24 h. After curing, the PDMS substrates were removed from the master and cut into pieces of desired size.

Substrate preparation: P-type silicon wafers with a sputtered gold film of thickness ~75 nm, deposited with a Perking-Elmer sputtering machine, were used as substrates. A titanium film of ~10

nm thickness was used as an adhesion promotion layer between the silicon wafer and the gold thin film.

Electrodeposition in capillaries: The patterned PDMS molds were placed in an oxygen plasma cleaner (Harrick plasma, operating at 240 W) for 5 min prior to bonding with the substrate. The surface oxidation process increased the hydrophilicity of the mold to promote filling of the channels by the aqueous electrolyte. After plasma treatment, the patterned side of the molds was gently pressed against the substrate and the mold-substrate assembly was immersed in the electrolyte for 5 min to assure proper filling of the entire channels. The PDMS mold substrate assembly was placed vertically inside the electrodeposition cell. Good conformal contact is required to be able to obtain well-defined features.

Electrodeposition was carried out using a three-electrode potentiostat (Autolab PGSTAT 128N from Metrohm Autolab, Netherlands). The substrate-PDMS assemblies were used as working electrodes. A small Pt mesh was used as counter electrode. The reference electrode was Ag/AgCl in 3M KCl (Metrohm Autolab). Nickel patterns were formed from an electrolyte containing 0.23 M nickel sulphate hexahydrate ($NiSO_4 \cdot 6H_2O$, Sigma-Aldrch, purity 99%,) and 0.15 M boric acid (H_3BO_3, Aldrich, purity 99.99%). Deposition occurred at -1.00 V versus reference. Zinc oxide patterns were formed at 70°C at -1.00 V from an electrolyte containing 0.10 M zinc nitrate hexahydrate ($Zn(NO_3)_2 \cdot 6H_2O$, Sigma-Aldrich, purity 98%,). Iron oxohydroxide patterns were formed at -1.00V from an electrolyte containing 0.02 M iron nitrate nonahydrate ($Fe(NO_3)_3 \cdot 9H_2O$, Sigma-Aldrich), 0.430 M nitric acid (HNO_3, 65% solution, Arcos Organics) and 0.425 M sodium hydroxide (NaOH, pellets, Sigma-Aldrich). Further details can be found elsewhere [25].

In the deposition of Ni and ZnO, we applied pulsed potential electrodeposition. In most experiments, after every 5 s of deposition (T_{on}), the deposition was stopped for the next 120 s (T_{off}), by returning to open circuit potential (OCP), and these steps were repeated for any desired number of times. We also used other values for T_{on} and T_{off}, depending on the dimensions of the PDMS template and the electrolyte used for electrodeposition. In the case of FeO(OH) we used continuous potentiostatic electrodeposition for 5 min. Prior to electrodeposition the mold-substrate assembly was immersed in the electrolyte solution for 30 min to ensure complete filling of the channels. After deposition, the PDMS molds were removed from the substrate and the substrates were washed with de-ionized water, dried using a nitrogen stream and stored for further analysis.

Characterization: Patterned substrates were characterized using tapping mode Atomic Force Microscopy (AFM; Veeco Dimension Icon) to determine the surface morphology. Grown metal and oxide patterns were imaged using high resolution scanning electron microscopy (HR-SEM, Zeiss 1550) and tapping mode AFM. X-ray diffraction (XRD, Philips diffractometer PW 3020, Software XPert Data Collector 2.0e, Panalytical B.V., Almelo, The Netherlands) was used for phase determination of the patterns. Energy Dispersive X-ray Spectroscopy (EDX) mapping was performed using a NORAN EDS spectrometer.

8.3. Results and Discussion

Figure 2a shows the SEM image of a Ni pattern formed on an Au-coated silicon substrate by electrodeposition. Figure 2b, 2c and 2d show a tapping mode AFM image, a tapping mode 3D AFM image, and an AFM height profile, respectively. The PDMS molds of area ~5x5 mm^2 that were used in this experiment have an ordered array of pillars with a diameter of 1.5 µm, a height of 6 µm, and a repeat distance of 3 µm. Deposition was carried out in 5 intervals of 2 min each. After every 2 min of deposition, the deposition was stopped for the next 2 min without applying any potential. This time period allowed fresh Ni ions to diffuse into the channels to replace the deposited nickel ions. The patterns grew to a thickness of approximately 100 nm after 10 min of deposition.

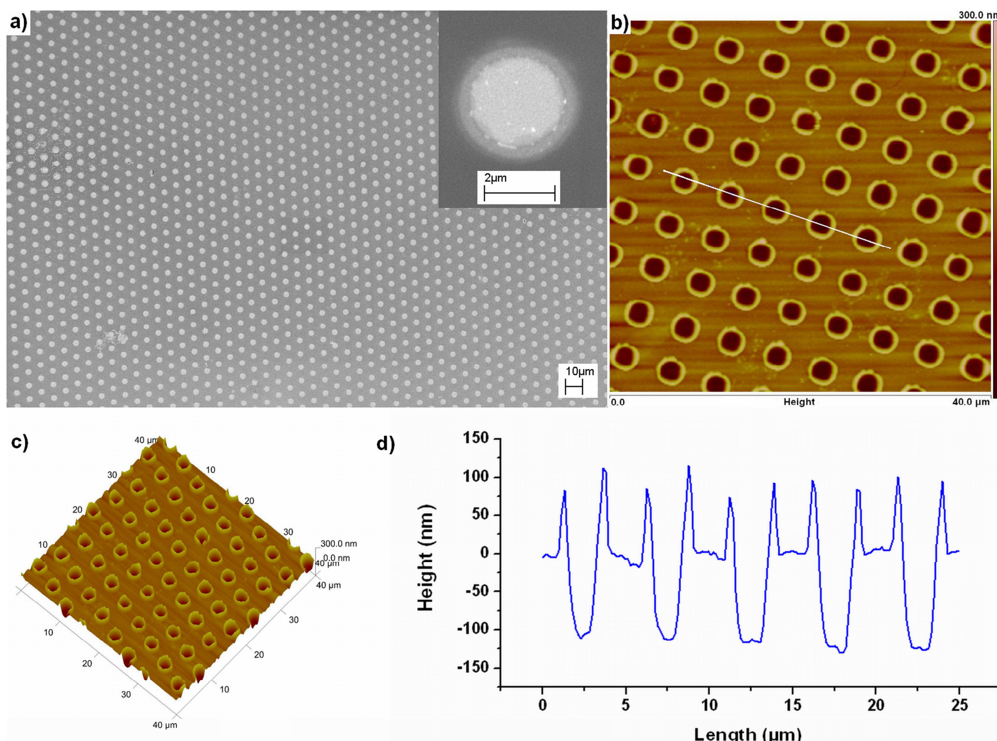

Figure 2: Images of Ni patterns formed on gold-coated silicon substrate after 10 min of electrodeposition. a) HR-SEM image; b) AFM height image; c) 3-D surface image; d) AFM height profile. The deposition was carried out in 5 intervals of 2 min, each separated by 2 min intervals in which no potential was applied.

The 3D AFM topography image and the AFM height profile show the sharp ring-like formation protruding at the periphery of every circular pit. Every ring has a width of approximately 200 nm at its base and a height of 80-100 nm. The ring formation is probably the result of an increased metal ion concentration at the surface of the PDMS molds. The oxygen plasma treatment of the PDMS mold prior to bonding with the gold substrate forms an amorphous SiO_x-rich surface layer on PDMS that becomes negatively charged in aqueous solutions above the isoelectric point (IEP) of silica at pH=2-3. Since we worked at pH 4, the negative ζ-potential of the surface oxide leads to an increased concentration of ions with a positive charge, in particular doubly charged ions, in the diffuse double layer near the surface. As a result, the local deposition rate of Ni is higher than further away from the PDMS walls, and ultimately forms ring-like structures.

The pulsed electrodeposition technique was employed due to the fact that the ion concentration inside the channels of the mold is depleted during the deposition process. In order to maintain a uniform concentration of ions throughout the channels, deposition was stopped for a period of time to allow fresh reactants to diffuse into the channels and to reach a uniform electrolyte concentration throughout the channels, before the next deposition pulse was initiated. The T_{on} and T_{off} times have to be carefully tuned in order to achieve uniform film thickness over the channels. The average diffusion distance L of ions over a given interval of time t is given by

$$L^2 = nDt \qquad (1)$$

where D is the self-diffusion coefficient of the ion, and n=6 in the case of unconstrained molecular movement in three dimensions. In aqueous solutions the self-diffusion coefficients of most ions are similar and have values in the range of 0.6×10^{-9} to 2×10^{-9} m^2/s at room temperature. In the experiments we employed PDMS templates with a total patterned area of 5x5 mm^2, and well

interconnected channel structures were employed. The maximum distance between the edge to the center of the template is approximately 2.5 mm. Considering that diffusional supply of reactant occurred from external openings at all sides of the PDMS mold, but is constrained inside the channels due to the presence of walls on a length scale of micrometers, the diffusion process is quasi-two-dimensional in this case, so that n is approximately 4. Then the time scale for replenishment t is of the order of ~100 seconds. The diffusion lengths can be reduced by engineering the PDMS mold, e.g. by constructing a few larger access channels between smaller channels, and/or by making access channels from the top side of the PDMS molds.

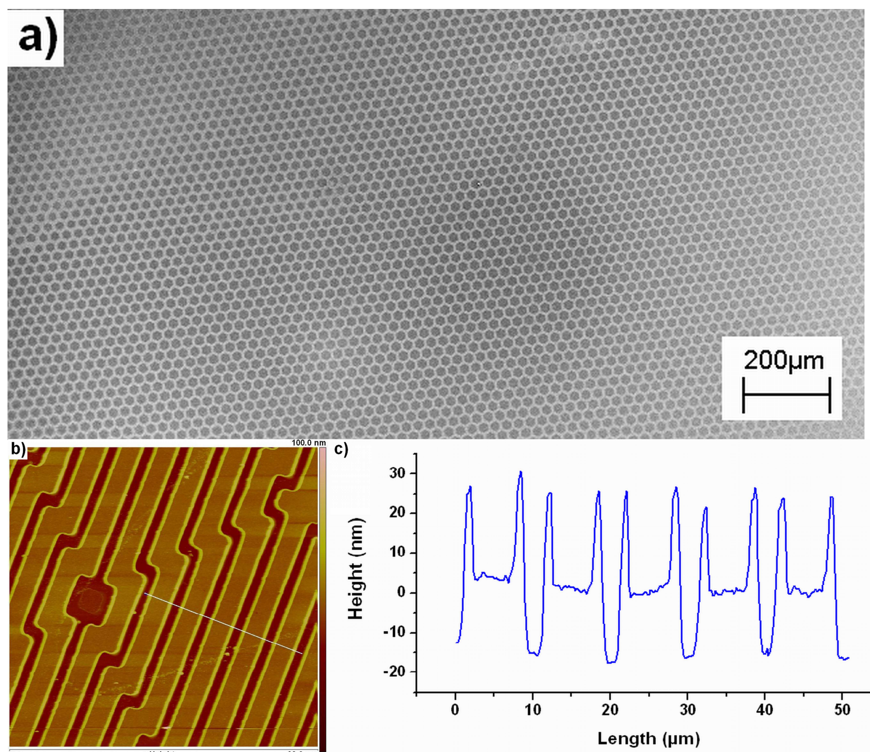

Figure 3: Ni patterns on gold-coated silicon substrate after 2 min of continuous electrodeposition. a) SEM image of honeycomb pattern. b-c) Tapping mode AFM image and AFM height profile of complex line patterns.

We also tested continuous potentiostatic electrodeposition of Ni. However, it did not result in high quality patterns when the PDMS molds did not have very well-connected channel structures. Probably in this case the diffusional supply of Ni^{2+} into the channels of the PDMS mold was smaller than the rate of consumption of nickel ions inside the channels. However, when a PDMS mold with well connected channel structure and large channel dimensions were employed, continuous potentiostatic reduction of Ni^{2+} also yielded high quality patterns, as illustrated in Figure 3 for a honeycomb pattern of Ni, fabricated by continuous deposition for 2 min at -1 V. The PDMS mold, with a patterned area of ~5x5 mm^2, had channels with a width of ~3.2 µm and a height of ~6 µm. The grown patterns have an approximate thickness of ~15 nm as measured by AFM. It was not possible to grow thicker layers by continuous deposition for longer periods of time, probably due to diffusional limitations. Longer deposition resulted in thicker films near the channel openings and thinner films in the central channels. This means that a concentration gradient of nickel ions is present in the channels, leading to a situation in which most metal ions were deposited on the substrate before reaching the middle of the channels.

We also used PDMS molds with smaller nanometer-scale features as templates. Figure 4 shows a tapping mode AFM image, an AFM height profile, and an AFM 3D topography image of a hexagonal array of Ni antidots on Au. The PDMS mold with an area of ~5 x 5 mm^2 contained a hexagonal array

of circular pillars with a diameter of 290 nm and a spacing of 200 nm between the pillars. The height of the pillars was 250 nm. The pattern was fabricated by pulsed electrodeposition, using 30 cycles with T_{on} = 5 s, and T_{off} = 120 s. The height profile shows that the resulting antidot pattern has a thickness of 65 nm. Figure 5a and 5b shows the chronoamperogram recorded during the deposition process. Figure 5a shows an example of a single 5 s deposition pulse. EDX analyses are provided in the Supporting Information file, showing that the areas where the PDMS mold was in conformal contact with the substrate, was isolated from deposition.

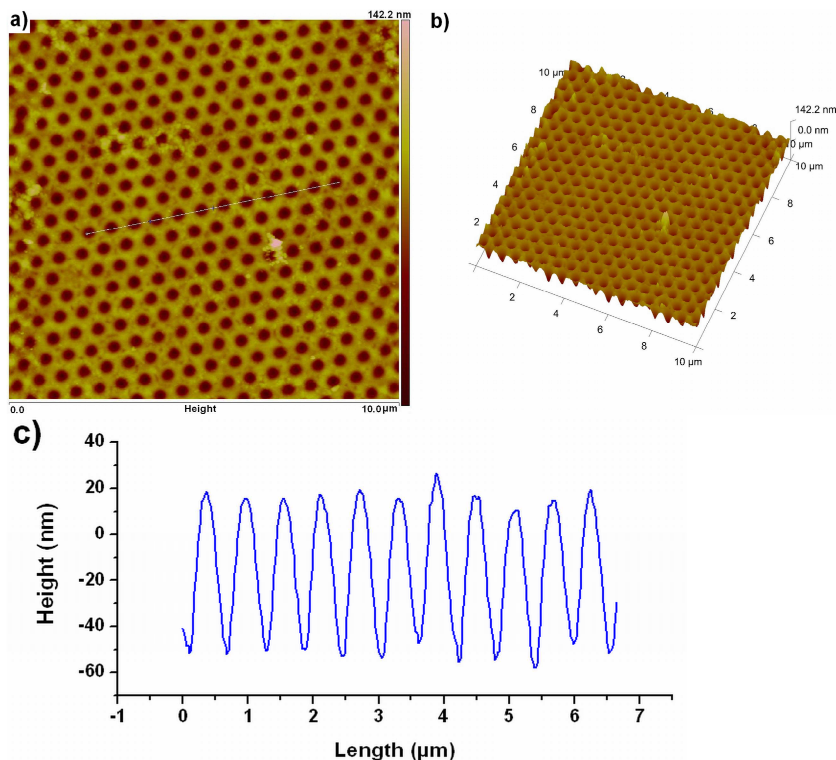

Figure 4: Nanoscale antidot Ni patterns on Au-coated silicon substrate after 150 s of deposition at -1.00 V. Deposition was carried out in 30 cycles of 5 s, with an interval of 2 min between cycles in which no current was applied. a) AFM height image; b) 3D surface image; c) AFM height profile.

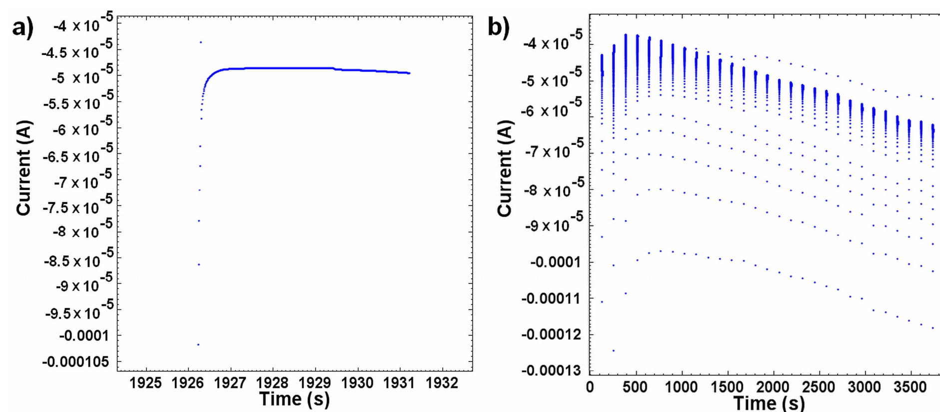

Figure 5: a) Chronoamperogram of pulsed Ni deposition inside nanoscale PDMS molds. Potentiostatic deposition lasted 5 s at -1.00 V. Waiting time between pulses was 2 min. b) Chronoamperogram of the complete deposition process.

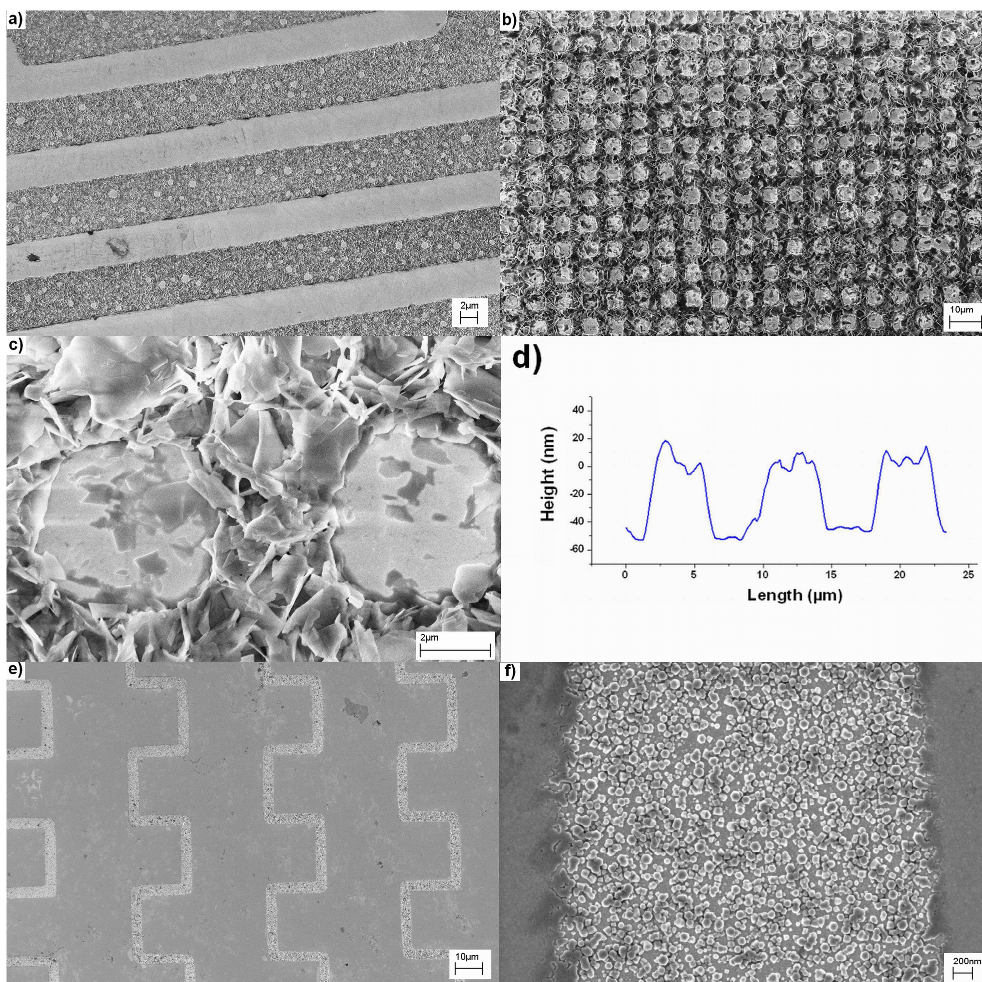

Figure 6: ZnO patterns on Au-coated silicon substrate. a-b) ZnO patterns formed after 5 cycles of cathodic deposition. T_{on} = 1 min, T_{off} = 2 min; c) Magnified view of ZnO pattern morphology of Figure 6b; d) AFM height profile of ZnO pattern of Figure 6b; e) ZnO nuclei on Au coated Si substrate after 10 deposition pulses. T_{on} = 1 sec, T_{off} = 1 min; f) Magnified view of ZnO pattern of Figure 5e.

Figure 6a-c shows HR-SEM images of ZnO patterns formed on a gold-coated silicon substrate by pulsed electrodeposition. Each deposition pulse was 1 min, and the interval between deposition cycles was 2 min. The pattern in Figure 6a was grown in 4 pulses to a thickness of ~20 nm. The PDMS mold used has lines of width 4.2 µm, spacing 5.8 µm and height 6 µm. The pattern in Figures 6b and 6c were grown in 10 pulses to a thickness of ~55 nm, as illustrated in the AFM height profile of ZnO shown in Figure 6d. The PDMS mold used has square pillars of width 4.25 µm, spacing 3.25 µm, and height 6 µm. The ZnO patterns formed has a flake-like porous surface morphology. Figure 6e and 6f shows ZnO nuclei formed as a result of applying very short deposition pulses during the deposition process. The PDMS mold used here has complex line features of width 25 µm, spacing 4 µm, and height 6 µm. Each deposition pulse was for 1 s, followed by a waiting time of 1 min. The total number of deposition pulses was 10. Due to the short duration of the entire deposition process, only isolated hexagonal ZnO nuclei had formed and no further growth occurred. ZnO deposition involves the reduction of nitrate and water to hydroxyl ions, followed by precipitation of zinc hydroxide, which is directly transformed into ZnO above 60°C via [25]:

$$NO_3^- + H_2O + 2e^- \rightarrow NO_2^- + 2\,OH^- \qquad (2)$$

$$Zn^{2+} + 2\,OH^- \rightarrow ZnO + H_2O \qquad (3)$$

The x-ray diffractogram of the patterned wurtzite film is shown in Figure 7. The strong (0002) peak is indicative of preferential (0001) growth of the ZnO phase, which is common under these growth conditions.

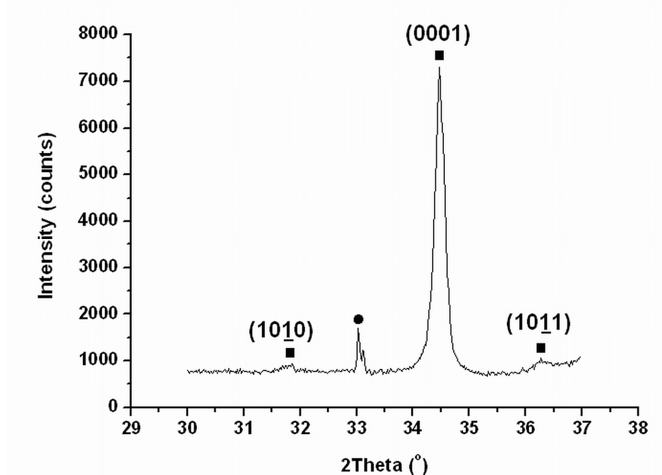

Figure 7: XRD pattern of ZnO grown on Au substrate. The peak at 2θ 34.4° corresponds to the (0002) reflection of the ZnO wurtzite structure. The squares represent ZnO pattern peaks and the circles represent substrate peaks. The split peak at 2θ 33° is from the silicon substrate. The splitting of the silicon peak is due to the presence of K_α and K_β radiation.

Figure 8 shows a SEM image of amorphous iron oxohydroxide FeO(OH) patterns formed on a Au coated silicon substrate after 5 min of continuous deposition. First an iron hydroxide gel formed inside the channels by precipitation of Fe^{3+} with OH^- that formed via reaction (4) at -1.00 V. The substrate-mold assembly was then dried on a hot stage at 60°C for 1 h. During drying, the iron oxohydroxide phase formed from the gel following [25].

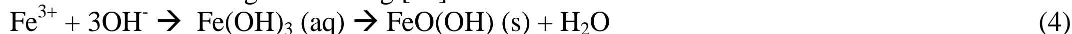

$$Fe^{3+} + 3OH^- \rightarrow Fe(OH)_3\,(aq) \rightarrow FeO(OH)\,(s) + H_2O \quad (4)$$

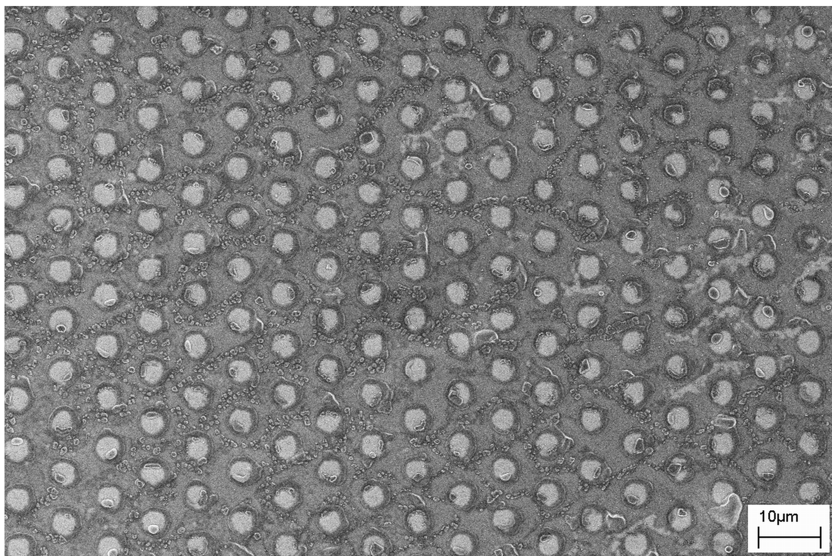

Figure 8: SEM image of FeO(OH) pattern on gold-coated silicon substrate after 5 min of continuous deposition at room temperature, and 1 h of drying at 60° C.

The process described here generated negative replicas of the patterns on the PDMS mold. Patterns with complex shapes such as sharp angles and curves can be prepared by this method. The process gives precise control of size and shape of the generated patterns, since the lateral dimensions are defined by the dimensions of the PDMS template used and the height is defined by the electrodeposition time. The process is a cost effective, bottom up patterning process in which metal, metal oxide and/or multilayered materials can be deposited. Electrodeposition is an old process which has proven its capacity to deposit a wide range of technologically important functional materials, such as metals (e.g. Ni, Au, Ag, Cu, Al), metal alloys (e.g. FePt), semiconducting oxides (e.g. ZnO, Fe_2O_3, TiO_2) and conducting polymers [24]. Due to low deposition temperature conditions, the process is suitable for any conductive substrate, including flexible plastic substrates with conductive coatings. We used conventional PDMS molds for the deposition experiments, but other materials could be used as well, provided that they make good conformal contact with the substrate. More research needed to design the molds with more access holes for the electrolyte from the sides as well as the top so that the process could be faster and even higher resolutions can be achieved.

8.4. Conclusions

Electrodeposition in capillaries is a promising tool for patterning nano and microscale structures on conducting substrates, especially for bottom up growth of metallic patterns which cannot be achievable easily by other soft lithographic patterning methods. We have patterned a wide range of functional materials including ZnO, Ni and FeO(OH) by the technique. A wide range of materials can be patterned in micro and nanometer scale by this technique. Further research is recommended with PDMS molds with engineered channels with more access channels for electrolyte for fast deposition over large areas of substrate.

8.5. References

1. Xiang, C.; Kung, S.-C.; Taggart, D. K.; Yang, F.; Thompson, M. A.; Güell, A. G.; Yang, Y.; Penner, R. M. *ACS Nano* **2008,** *2*, 1939-1949.
2. Menke, E. J.; Thompson, M. A.; Xiang, C.; Yang, L. C.; Penner, R. M. *Nat. Mater.* **2006**, *5*, 914-919.
3. Balaur, E.; Djenizian, T.; Boukherroub, R.; Chazalviel, J. N.; Ozanam, F.; Schmuki, P. *Electrochem. Commun.* **2004**, *6*, 153-157.
4. Rastei, M. V.; Meckenstock, R.; Bucher, J. P.; Devaux, E.; Ebbesen, T. *Appl. Phys. Lett.* **2004**, *85*, 2050-2052.
5. Ko, S. H.; Park, I.; Pan, H.; Grigoropoulos, C. P.; Pisano, A. P.; Luscombe, C. K.; Frechet, J. M. J. *Nano Lett.* **2007**, *7*, 1869-1877.
6. Ginger, D. S.; Zhang, H.; Mirkin, C. A. *Angew. Chem. Int. Ed.* **2004**, *43*, 30-45.
7. Xu, S.; Liu, G.-y. *Langmuir* **1997**, *13*, 127-129.
8. Xia, Y. N.; Whitesides, G. M. *Angew. Chem. Int. Ed.* **1998**, *37*, 551-575.
9. ten Elshof, J. E.; Khan, S. U.; Göbel, O. F. *J. Europ. Ceram. Soc.* **2010**, *30*, 1555-1577.
10. Kumar, A.; Whitesides, G. M. *Appl. Phys. Lett.* **1993**, *63*, 2002-2004.
11. Kim, E.; Xia, Y.; Whitesides, G. M. *J. Am. Chem. Soc.* **1996**, *118*, 5722-5731.
12. Göbel, O. F.; Blank, D. H. A.; ten Elshof, J. E., *ACS Appl. Mater. Interfaces* **2010**, *2*, 536-543.
13. Khan, S. U.; Gobel, O. F.; Blank, D. H. A.; ten Elshof, J. E. *ACS Appl. Mater. Interfaces* **2009**, *1*, 2250-2255.
14. Göbel, O. F.; Nedelcu, M.; Steiner, U. *Adv. Funct. Mater.* **2007**, *17*, 1131-1136.
15. Sharpe, R. B. A.; Titulaer, B. J. F.; Peeters, E.; Burdinski, D.; Huskens, J.; Zandvliet, H. J. W.; Reinhoudt, D. N.; Poelsema, B. *Nano Lett.* **2006**, 6, 1235-1239.
16. Shi, G.; Lu, N.; Gao, L.; Xu, H.; Yang, B.; Li, Y.; Wu, Y.; Chi, L. *Langmuir* **2009**, *25*, 9639-9643.
17. Lee, B. H.; Cho, Y. H.; Lee, H.; Lee, K. D.; Kim, S. H.; Sung, M. M. *Adv. Mater.* **2007**, *19*, 1714-1718.
18. George, A.; Blank, D. H. A.; ten Elshof, J. E. *Langmuir* **2009**, *25*, 13298-13301.
19. Pesika, N. S.; Radisic, A.; Stebe, K. J.; Searson, P. C., *Nano Lett.* **2006**, *6*, 1023-1026.

20. Zach, M. P.; Ng, K. H.; Penner, R. M. *Science* **2000**, *290*, 2120-2123.
21. Kleiman-Shwarsctein, A.; Hu, Y.-S.; Forman, A. J.; Stucky, G. D.; McFarland, E. W. *J. Phys. Chem. C* **2008**, *112*, 15900-15907.
22. Liu, R.; Vertegel, A. A.; Bohannan, E. W.; Sorenson, T. A.; Switzer, J. A. *Chem. Mater.* **2001**, *13*, 508-512.
23 Natter, H.; Schmelzer, M.; Hempelmann, R. *J. Mater. Res.* **1998**, *13*, 1186-1197.
24. Zhou, F.; Chen, M.; Liu, W.; Liu, J.; Liu, Z.; Mu, Z. *Adv. Mater.* **2003**, *15*, 1367-1370.
25. Maas, M. G., Rodijk, E. J. B., Maijenburg, A. W., Blank, D. H. A., ten Elshof, J. E. *J. Mater. Res.*, **2011**, (Available on CJO 16 May 2011) doi:10.1557/jmr.2011.93
26. Routkevitch, D.; Bigioni, T.; Moskovits, M.; Xu, J. M. *J. Phys. Chem.* **1996**, *100*, 14037-14047.
27. Yan, H.; Yang, Y.; Fu, Z.; Yang, B.; Xia, L.; Fu, S.; Li, F. *Electrochem. Commun.* **2005**, *7*, 1117-1121.
28. Azzaroni, O.; Schilardi, P. L.; Salvarezza, R. C. *Appl. Phys. Lett.* **2002**, *80*, 1061-1063.

8.6. Appendix to Chapter 8

EDX analysis of Ni patterns

Figure S1 shows an Energy Dispersive X-ray (EDX) spectrum recorded on a Ni patterned substrate. Figure S1a shows an EDX spectrum taken on the area where the PDMS stamp was in contact with the substrate. No significant Ni signal can be seen in the spectrum. Figure S1b shows an EDX spectrum recorded on areas where the PDMS mold was not in contact with the substrate, i.e. the areas where Ni was deposited. The presence of a strong Ni signal indicates in the patterned regions, and the near absence of a signal in the other areas indicates that the PDMS mold isolated the substrate completely from where it was in conformal contact with the substrate.

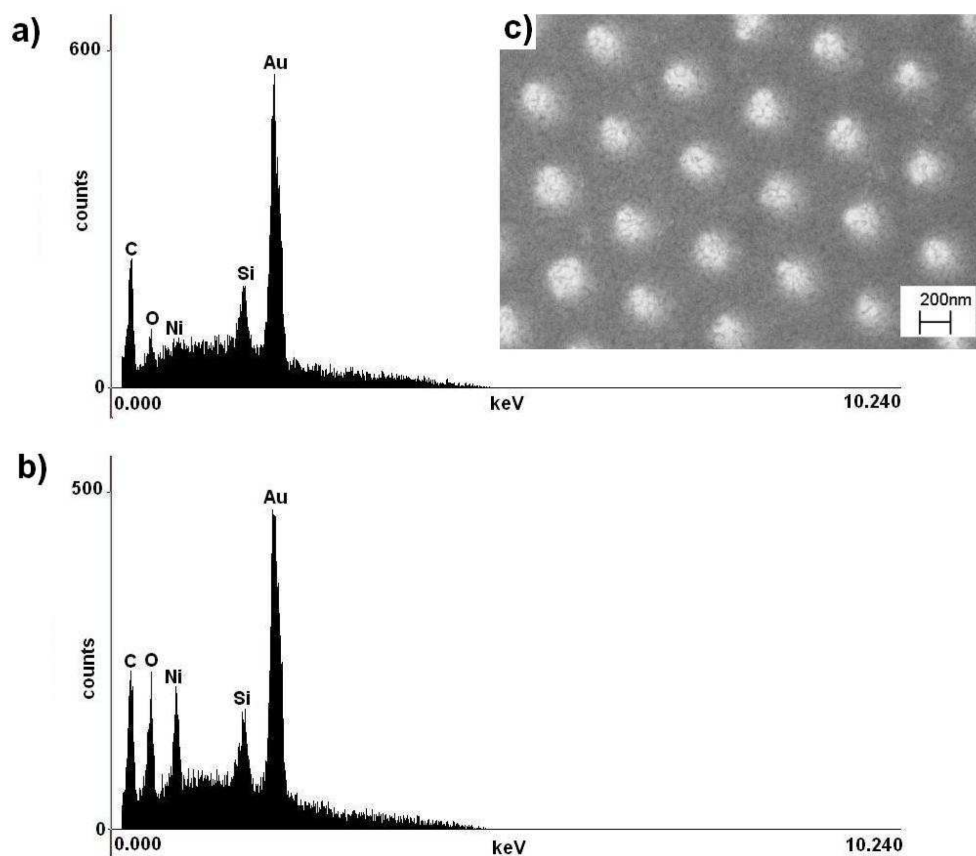

Figure S1: EDX analysis of Ni pattern. a) EDX spectrum taken at the place where PDMS mold was in conformal contact with the substrate during deposition. b) EDX spectrum taken out side the PDMS contact area during deposition. c) HR-SEM image of Ni pattern which correspond to the AFM images in Figure 4.

Chapter 9

Conclusions

Soft lithography is developed as a powerful tool for patterning functional materials in the micrometer and nanometer scale. The beauty of soft lithography is the degree of freedom it has. Researchers working on the field demonstrated soft lithography as a tool to pattern virtually any material (including, molecules, polymers, biomaterials, metal, semiconductor, oxides, nanowires, nanoparticles etc) on any arbitrary substrate (metallic, semiconducting, insulating, paper and plastic). Also the simplicity and cost effectiveness of the technique makes soft lithography as a powerful candidate for future manufacturing techniques.

This thesis demonstrates the potential applicability of soft lithography as a tool to pattern a wide range of fabricates functional materials on silicon, metallic and plastic substrates on sub-50 nm to micrometer length scale. It shows the possibility of combining soft lithography with various deposition techniques including electrodeposition, electroless deposition, sol-gel synthesis, atomic layer deposition and solution phase deposition. Also the thesis put forward novel ideas of gas phase patterning of organosilane molecules, edge transfer printing of water soluble polymers and electrodeposition in capillaries. The major findings of the thesis is concluded in the following table

	Materials can be patterned	**resolution**	**advantages**	**disadvantages**
Transfer printing of water-soluble polymers (Chapter 2)	Oxides (CuO,ZnO,Fe_2O_3,NiO) PDMS, metal nanoparticles, water-soluble polymers, complexes	Sub 50 nm	Simple, cost effective, parallel, fast procedure, micrometer scale stamps for nanopatterning, Large area direct patterning of simple oxides.	Requires high temperature annealing process.
Channel diffused plasma patterning **(Chapter 6 & 7)**	SAMs, plastic surfaces (subsequent templated deposition of ZnO, Nanowires,Ni, TiO_2, conducting polymer, Au nanoparticles and Ag)	Sub 300 nm	Cost effective, simple, parallel patterning, fast technique, Easy way to create templates for solution phase deposition ,electrodeposition, electroless deposition, ALD etc.	Only PDMS with connected channel structures or line features can be used, Process is slower when using nanometer scale low aspect ratio PDMS stamps.(takes ~ 40 min to pattern 5x5 mm^2 area with stamps 200 nm line width and hight)
Electrodeposition In capillaries **(Chapter 8)**	Metals, ZnO, Fe_2O_3	Sub 300 nm	Cost effective, simple bottom up, parallel approach, direct patterning	Relatively slow electrodeposition process (takes ~1h to ~2h) due

			of metallic structures.	to the waiting time for ion diffusion , more research is required to engineer PDMS stamps, Only PDMS with connected channel structures or line features can be used, Process is slower or inefficient when using low aspect ratio PDMS stamps.
Gas phase pattern deposition using PDMS masks **(Chapter 3, 4 & 5)**	Organosilanes, self assembling molecules (Subsequent deposition of ZnO, Ni, Au nanoparticles etc)	Sub 100 nm	Use of micrometer scale PDMS stamps for nanometer scale features, High quality organosilane self assembled thin films, cost effective, parallel approach, and fabrication of patterned multi-length scale, multifunctional surfaces. Large area patterning is possible.	The process takes 15 min to several hours to generate pattern in different pattern resolution.

Soft lithography has the potential of being the major device fabrication technology in future, especially in the area of flexible light weight devices. Considering the research efforts and findings from various research groups in the area of soft lithography, it could be a technology of the future for direct structuring of devices on various substrates. Moreover, soft lithography can be used in combination with the current well established technology of photolithography, which may give more dimensions to the current fabrication technologies.

Samenvatting

In dit proefschrift komen twee belangrijke kwesties ter sprake:

1) Het fabriceren van patronen van functionele materialen op nanometerschaal
2) Het uitbreiden van de toepasbaarheid van zachte lithografische processen voor een breed bereik aan functionele materialen op conventionele silicium substraten en flexibele substraten.

Dit proefschrift beschrijft nieuwe zachte lithografische processen, die het mogelijk maken om structuren van een breed bereik aan functionele materialen als metalen, nanodeeltjes, organosilaan moleculen, nanodraden, halfgeleidende materialen en geleidende polymeren op silicium en flexibele plastic substraten te maken met een lengteschaal van beneden de 50 nm tot micrometers.

Hoofdstuk 2 beschrijft het patroneren van oxide materialen over een lengteschaal van beneden de 50 nm tot micrometers met behulp van een printtechniek (transfer printing) waarbij gebruik wordt gemaakt van water oplosbare polymeren waaraan metalen zijn gebonden. Dit proces is een eenvoudige en goedkope manier om een groot bereik aan oxide materialen te patroneren op een schaal beneden 100 nm en vindt een potentiele toepassing in de fabricage van apparaat structuren.

Hoofdstuk 3 introduceert een methode om organosilaan moleculen te patroneren op silicium substraten op nanometer en micrometer schaal. Het proces is tijd-gecontroleerd en maakt gebruik van het fenomeen van geometrisch gedomineerde condensatie van organosilaan moleculen vanuit een gas fase om patronen te genereren met een hoge resolutie. PDMS stempels met grote dimensies kunnen gebruikt worden voor de fabricage van patronen met veel kleinere dimensies.

Hoofdstuk 4 breidt de toepasbaarheid van het proces dat beschreven staat in voorgaand hoofdstuk uit door het patroneren van anorganische functionele materialen op de nanometer tot micrometer schaal. Het hoofdstuk laat zien dat depositie van patronen vanuit de gas fase volledig controleerbaar is. Daarnaast werden zelf-geassembleerde moleculaire dunne lagen van mercaptosilaan moleculen gebruikt als dunne beschermlagen voor de elektrodepositie van metallische en halfgeleidende materialen.

Hoofdstuk 5 breidt verder uit of the toepasbaarheid van het proces dat beschreven staat in hoofdstuk 3. Sequentiële depositie van verschillende organosilaan moleculen op silicium substraten werd gebruikt om substraten met verschillende chemische functionaliteiten te fabriceren. Multifunctionele oppervlakten met verschillende lengteschalen werden gefabriceerd. De potentiële toepassing van organosilaan patronen als beschermlagen voor atomaire laag depositie (ALD) en als sjabloon voor plaats-selectieve adsorptie van nanodeeltjes wordt tevens in dit hoofdstuk gedemonstreerd.

Hoofdstuk 6 beschrijft een nieuw proces om patronen van SAMs van octadecaanthiol (ODT) op goud substraten te vormen met behulp van een kanaal gediffundeerde plasma ets techniek. De gepatroneerde SAMs werden gebruikt als sjablonen voor elektrodepositie, electroless depositie en depositie vanuit een oplossing van een breed bereik aan functionele materialen (Ni, Ag, ZnO en ZnO nanodraden) op nanometer en micrometer schaal.

Hoofdstuk 7 beschrijft de potentiële toepassing van kanaal gediffundeerde plasma oppervlakte modificatie op plastic substraten als polycarbonaat (PC), PDMS, en polyethyleentereftalaat (PET) om een hydrofiel-hydrofoob contrast op deze oppervlakten te creëren. Na oppervlaktemodificatie werden depositie processen als electroless depositie, depositie vanuit een oplossing, locatie selectieve opdroging en locatie selectieve adsorptie gebruikt om patronen te verkrijgen van functionele materialen als ZnO, ZnO nanodraden, Ag, TiO_2, geleidende polymeer (PEDOT:PSS) en zilver nanodeeltjes.

Hoofdstuk 8 beschrijft een nieuw proces van elektrodepositie in capillairen. Met behulp van elektrodepositie van een elektrolyt oplossing binnenin PDMS capillairen die contact maken met het substraat, werden micro- en nanopatronen van metallische en halfgeleidende materialen gevormd (bottom-up).

Acknowledgements

I would like to thank my daily supervisor and promoter Prof. Andre ten Elshof for having confidence in choosing me for this project and giving me the freedom to do whatever I want in the Lab. Without that freedom, this thesis would never have been possible. I always remember the encouragement and appreciation of Andre whenever I introduce some ideas to him. I also would like to thank my promoter Prof. Dave Blank for his support during my PhD period.

I express my thanks Prof. Yong Lei, Prof. Rob Lammertink, Prof. Jurriaan Huskens, Prof. Jos Benschop and Prof. Paul Kelly for being part of my PhD committee.

I would express my thanks to my friends and colleagues with whom I spend my time mostly in the lab/research; Wouter, Michiel, Sjoerd, Tomek, Minh, Sajid, Ole, Maarten, Eddy, Suresh, Nicholas, Rogier, Gerard, Nirupam, Peter Brinks, Brian Smith; I appreciate the scientific/non scientific discussions we had as well as the interesting research we did together.

I also would thank all IMS (past and present) members for the nice time we spend together; Matthijn, Mercy, Paul, Peter de Veen, Ruud, Gerwin, Indu, Arjen, Arjan de waal, Josee, Joska, Hajo, Jeroen, Willem, Rik, Brian, Sander Kommeren, Wouter Vijselaar, Daniel Hagedoorn, Enne Faber, Xin, Debakanta, Evert, Anuj, Gertjan, Mark, Guus, Bernard, Henk, Dominic, Josè, Marion, Bouwe, Gerrit, Michelle, Alim, Hans, Hein Verputten, Frank, Oktay, Gerard, Ronald ; I thank all of you for the nice time we had during my PhD. I would like to thank Mark Smithers for his help with HR-SEM imaging and fitting me in his schedule many times to meet my deadlines. Also the help of Gerard Kip, Frank Roesthuis and Dick Veldhuis is appreciated.

My special thanks to Dr. Mato Knez for the interesting research we did together as well as the continuing collaborations. I appreciate the fruitful collaboration and friendship I made with Raoul van Gastel and Gregor Hlawacek during the end period of my PhD. Even though I couldn't insert the work we did on graphene into this thesis, I would greatly appreciate their help which would result in at least a couple of interesting publications.

Outside research I have to thank many people who made my stay in Netherlands memorable and enjoyable. I thank Wouter Maijenburg, Eddy & Esther, Tomek & Kasia, Maarten Nijland, Michiel Mass, Sjoerd, Nirupam, Debakanta, Sajid, Mustafa, Shahina & Aditya, Shaji, Mercy& kids, Sekhar, Sandeep & Jalaja, Babu & Indu, Bernie Uncle & Kamala Aunty, Ole & family, Vijay & Ranjini, Deepak Pratap for being great friends always. I would thank Susanta da & family for their continuous support and encouragement. I also thank my friends Thomas Ravi Mathew, Sumith Sreedhar, Pradeep Yadav and Ajay Panwar for their support.

Thanks to Meegha for being such a great ambitious wife. Without her support I could never ever produced such a reasonable professional achievement. I didn't even have to think about anything

other than my study in the last two years of my PhD, since she managed everything else without complaining for being late from the office or about working in the weekends.

I thank my parents and sister for their never ending love and affection. I always remember their motivation to achieve big things in life. I remember the motivation from my grandfather for getting the best education. I also thank Meegha's parents and brother for their support and motivation.

I thank God Almighty for the blessings bestowed upon me and guiding me always in the right path throughout my life.